SKI Report 2006:10

Research

Models for MOX fuel behaviour

A selective review

Ali R. Massih

January 2006

ISSN 1104-1374
ISRN SKI-R-06/10-SE

SKI

SKI Perspective

Nuclear fuel containing mixed oxide (MOX) pellets have been used since the 1960´s. MOX fuel pellets are made from a mixture of uranium and plutonium oxide. MOX allows the large quantities of fissile isotopes produced and remaining in spent nuclear fuel from light water reactors to be recycled. Producing MOX fuel can be seen as a method to more efficiently use the natural uranium since most isotopes in natural uranium are the Pu-producing U-238. In fact, programs for using MOX were developed in the 1970´s to meet the feared or anticipated scarce supply of uranium at moderate prices. Although uranium prices have remained moderate, MOX is used in nuclear power reactors in for example Belgium, Germany, France and Switzerland, while other countries like Japan have programs for introducing MOX as part of their nuclear fuel cycle.

SKI has recently identified a need to gain knowledge about the in-reactor performance of mixed oxide nuclear fuel. Since issues regarding the properties, manufacturing and transportation of MOX fuel occasionally attract the attention of media it may be of public interest to gain knowledge of its utilisation as well. Small quantities of MOX fuel rods have been irradiated in Swedish reactors, but there exist plans for using limited quantities of MOX fuel in a Swedish power plant in the near future.

The present study covers basic physical properties and some models for fuel rods with MOX pellets and allows comparing the use of MOX with conventional UO_2 fuel in light water reactors in a general sense.

Responsible for the project at SKI has been Jan-Erik Lindbäck.
Project Identification Number: 200506022

SKI Report 2006:10

Research

Models for MOX fuel behaviour

A selective review

Ali R. Massih

Quantum Technologies AB
Uppsala Science Park
SE-751 83 Uppsala
Sweden

January 2006

Abstract

This report reviews the basic physical properties of light water reactor mixed-oxide (MOX) fuel comprising nuclear characteristics, thermal properties such as melting temperature, thermal conductivity, thermal expansion, and heat capacity, and compares these with properties of conventional UO_2 fuel. These properties are generally well understood for MOX fuel and are well described by appropriate models developed for engineering analysis. Moreover, certain modelling approaches of MOX fuel in-reactor behaviour, regarding densification, swelling, fission product gas release, helium release, fuel creep and grain growth, are evaluated and compared with the models for UO_2. In MOX fuel the presence of plutonium rich agglomerates adds to the complexity of fuel behaviour on the micro scale. In addition, we survey the recent fuel performance experience and post irradiation examinations on several types of MOX fuel types. We discuss the data from these examinations, regarding densification, swelling, fission product gas release and the evolution of the microstructure during irradiation. The results of our review indicate that in general MOX fuel has a higher fission gas release and helium release than UO_2 fuel. Part of this increase is due to the higher operating temperatures of MOX fuel relative to UO_2 fuel due to the lower thermal conductivity of MOX material. But this effect by itself seems to be insufficient to make for the difference in the observed fission gas release of UO_2 vs. MOX fuel. Furthermore, the irradiation induced creep rate of MOX fuel is higher than that of UO_2. This effect can reduce the pellet-clad interaction intensity in fuel rods. Finally, we suggest that certain physical based approaches discussed in the report are implemented in the fuel performance code to account for the behaviour of MOX fuel during irradiation.

Sammanfattning

Denna rapport undersöker grundläggande fysikaliska egenskaper hos blandoxid (mixed oxide, MOX) bränsle däribland dess nukleära egenskaper, termiska egenskaper såsom smälttemperatur, värmeledningsförmåga, termisk expansion och värmekapacitet, samt jämför dessa egenskaper med motsvarande egenskaper för konventionellt UO_2 bränsle. Materialegenskaperna för MOX bränsle är allmänt väl kända och beskrivs väl med lämpliga modeller som utvecklats för ingenjörsmässig analys. De viktigaste modellerna för att beakta beteendet hos MOX bränsle under reaktorförhållanden, dvs. förtätning, svällning, fissionsgasfrigörelse, heliumavgivning, bränslekrypning och korntillväxt utvärderas och jämförs med UO_2. Förekomsten av plutoniumrika områden (agglomerat) i MOX bränsle spär på komplexiteten i bränslebeteendet på detaljnivå. Vi granskar också de senaste erfarenheterna från drift och efterbestrålningsundersökningar på fyra typer tillverkningsprocesser för MOX bränsle. Vi diskuterar data från dessa undersökningar beträffande förtätning, svällning, fissionsgasfrigörelse och utvecklingen av mikrostrukturen under bestrålning. Resultaten från vår undersökning indikerar att MOX bränsle i allmänhet har högre fissionsgasafrigörelse och heliumavgivning än UO_2 bränsle. Denna ökning till en del beror på MOX bränslets högre driftstemperatur jämfört med UO_2 bränsle till följd av den lägre värmeledningsförmågan hos MOX material. Men denna inverkan verkar vara otillräcklig för att förklara den iakttagna skillnaden i fissionsgasfrigörelse mellan UO_2 och MOX bränsle. Vidare är den bestrålningsframkallade kryphastigheten i MOX bränsle högre jämfört med UO_2. Denna effekt kan minska intensiteten av växelverkan mellan kutsar och kapsling i en bränslestav. Avslutningsvis föreslår vi att vissa av de fysikaliskt baserade modellerna, som diskuteras i rapporten, implementeras i bränslestavprogram för att ta hänsyn till beteendet hos MOX bränsle under bestrålning.

List of contents

1 Introduction

A substantial amount of plutonium is produced by neutron transmutation of uranium-238 (^{238}U) in commercial light water reactors (LWRs). The spent fuel from low-enriched uranium-235 contains about 1 wt% plutonium, i.e., about 200 kg to 250 kg from the annual down-load of 20 to 25 tons from each reactor. The spent fuel can be reprocessed to recover the plutonium (and remaining enriched uranium) for recycling as new fuel. For example, the reprocessing plant at La Hague, France, operated by COGEMA has the capacity to process 1600 tons of spent fuel per year. Thus La Hague can separate 16 tons of so-called reactor grade plutonium per year. This is produced as plutonium oxide, a dry powder, which is then welded into small cylindrical containers (Garwin and Charpak, 2001). The reactor grade Pu is composed of some 60 wt% ^{239}Pu, 26 wt% ^{240}Pu, 9 wt% ^{241}Pu, 5 wt% ^{242}Pu and 1 wt% ^{238}Pu. Only the odd isotopes 239 and 241 (those with an odd number of nucleons) of Pu are fissile, meaning that, are subject to fission by slow thermal neutrons.

A number of these plutonium oxide containing cylinders are sealed into an outer steel cylinder for protection and storage. These are eventually transported to a special fuel fabrication plant, where the plutonium oxide is mixed with uranium oxide and fabricated into mixed-oxide (MOX) ceramic fuel pellets for use in LWRs. In order to provide, for the MOX fuel, a fissile content comparable with that in normal uranium, roughly 5 kg of spent uranium fuel must be reprocessed to give sufficient plutonium for 1 kg of MOX. The fabrication process of MOX fuel is considerably more costly and potentially more hazardous than for uranium fuel (Garwin and Charpak, 2001). We note that the half-life of plutonium-239 is 24000 years in comparison with 4.5 billion years for uranium-238 and 0.7 billion years for uranium-235, i.e., in a gram of ^{239}Pu there are roughly 200 000 as many disintegrations per second as in a gram of uranium.

When MOX fuel is loaded into a LWR and burned for four years, only part of the plutonium is consumed. The remainder can either be disposed as unprocessed spent fuel or reprocessed for further recycles. If it is reprocessed, this multi-recycle plutonium becomes a burden on the LWRs, because spent MOX fuel has a larger fraction of non-fissile plutonium isotopes and yield less energy per mass of fuel reprocessed. Only fast-neutron reactors (fast breeder reactors, FBRs) have the intrinsic capability of consuming all the reprocessed plutonium and to burn the minor actinides (Stacey, 2001).

There are much more experience with MOX fuel in pressurised water reactors (PWRs) than in boiling water reactors (BWRs). The number of reactors licensed for MOX fuel in Europe and Japan are 38 PWRs vs. 2 BWRs; commercial US LWRs do not use reactor grade MOX fuel (IAEA, 2003). A typical fuel assembly design average plutonium content in PWR MOX is 7.2 wt% and in BWR is 5.4 wt% Pu (see Figs. 1.1 and 1.2).

The intent of this report is to review the basic understanding on LWR MOX fuel behaviour during reactor operation in terms of theoretical approaches and relate them to experimental observations. The basic physical properties of MOX fuel comprising nuclear characteristics, thermophysical properties such as melting temperature, thermal conductivity, thermal expansion, enthalpy and heat capacity are briefly reviewed. These

properties are, in general, well understood for MOX fuel and are well described by appropriate models, which can be used for analyses of MOX fuel. The modelling approaches of MOX fuel behaviour (under normal operation and transients) namely, densification, swelling, fission product gas release, helium release, fuel creep and grain growth are discussed in more detail, since they are, as for UO_2 fuel, more complex and the models less precise compared to the aforementioned thermophysical properties. In MOX fuel the presence of Pu-rich agglomerates (heterogeneity) gives rise to additional complexity of fuel behaviour on the micro scale. We also survey recent fuel performance experience and post irradiation examinations on several types of MOX fuels that are fabricated with different routes.

The organisation of this report is as follows. Fabrication processes and structures for four types of MOX fuel experimented with and utilised in LWRs in the past decade or so are briefly discussed in section 2. Section 3 reviews the nuclear characteristics and thermophysical properties of MOX fuel. In section 4, which is the main section of the report, we analyse fuel behaviour models in more detail and carry out some calculations for the purpose of exposition. Fuel performance experience and post irradiation examination results are briefly reviewed in section 5 with special emphasis on the effects described in the preceding section. Finally, we end the report by some concluding remarks and provide suggestions for implementation of physically based concepts, discussed in section 4, in the computational software to be qualified for MOX fuel analysis. The appendices A to E offer the mathematical details and the parameters for the models discussed in the report.

2 Fabrication processes and fuel structure

In this section, three main fabrication processes of LWR MOX fuel and their structures, for which irradiation performance data and experience are reported in literature, are outlined. A more comprehensive overview of these and other processes can be found in the IAEA review report (IAEA, 2003). The MOX fuel is characterised by a spatially dependent plutonium concentration that locally ranges from almost zero to 100% (Hanus and Kleykamp, 1982), but typically to 20-30% for modern MOX fuel discussed below. The presence of plutonium rich zones (agglomerates) within the uranium rich zone (matrix) affects the oxygen behaviour in the fuel. At sufficiently high temperatures there is a tendency for oxygen atoms to migrate from the agglomerates toward the matrix so that the oxygen Gibbs free energy (potential) of the zones becomes equal. Nevertheless, since fuel temperatures and plutonium concentrations are relatively low in LWRs (compared to FBRs) the oxygen redistribution is too small to affect significantly the MOX fuel behaviour.

2.1 OCOM and AU/PuC processes

The OCOM (optimised co-milling) process, developed by Alkem in the early 1980s, applied intensive milling of UO_2 (70%) and PuO_2 (30%) to achieve plutonium particle homogeneity (Roepenack et al., 1987). A parallel route, also developed by Alkem, called the AU/PuC process (Ammonium Uranyl-Plutonyl Carbonate), achieved the desired homogeneity by means of precipitation of the AU/PuC complex and adding ammonia and carbon dioxide to a solution of uranium nitrate and plutonium nitrate followed by a calcination step. The two routes continue separately by mixing natural UO_2 in the specified proportion to the mixed oxide powders, after which pellets are produced in the conventional way by pressing, sintering and grinding to final size. Both processes produce pellets comprising UO_2/PuO_2 particles with Pu content of 30 wt% in a matrix of natural UO_2. Integral fissile Pu content is in the range of 2.0 to 3.5 wt% with a density of 10.32 to 10.45 g/cm^3. Regarding the heterogeneity of fuel, vendors show standard α-radiography pictures of polished sections of fuel (0.2 mm resolution) to emphasise that their products are homogeneous (Roepenack et al., 1987). However, observations using Electron Probe Micro Analyser (EPMA) indicate areas enriched in Pu of dimensions 50 to 100 μm equivalent diameters (Walker et al., 1991).

2.2 MIMAS process

The MIMAS (micronized master) MOX fuel process, which originally developed by Belgonucleaire in the 1980s (Deramaix et al., 1993), is an adaptation of the reference fabrication process developed earlier and utilized commercially in the 1970s at the Dessel fabrication plant in Belgium. The MIMAS fuel is designed so that even unirradiated fuel would be almost completely soluble in pure nitric acid solution. To attain this, the PuO_2 powder is *micronized*[1] with UO_2 powder to form a "master blend"

[1] To micronize is to blend mechanically UO_2 and PuO_2, and mill them together to obtain a fine powder where UO_2 and PuO_2 crystallites are well mixed together.

with a plutonium content in the range of 20 to 30%. In the subsequent step, this is mechanically mixed with free flowing AUC or ADU (Ammonium Di-Uranate) UO_2 to obtain the specific plutonium content required. The very close contact between UO_2 and PuO_2 aggregates allows for sufficient inter-diffusion during sintering and therefore results in the desired solubility. The final product is a fuel pellet in which Pu-rich particles are distributed in a UO_2 matrix which is similar to ex-AUC UO_2 microstructure regarding grain size and pore size distribution (average grain size is 7 to 10 μm and average pore diameter 2 to 4 μm).

Thus the characteristic size in the MOX fuel can be the plutonium agglomerate (particle) size. These agglomerates are nearly spherical and contain most of the plutonium isotopes. There are very few published data on the details of these agglomerates, which may influence the retention and/or release of fission product gases during irradiation, and also other properties of the fuel, which will be discussed in this report. Lippens and co-workers in a paper (Lippens et al., 1986) on MIMAS fuel note that plutonium is spatially distributed homogeneously on the pellet scale (millimetres), but is heterogeneous when is observed on the micron scale. According to Lippens et al. typical Pu particle size, determined by α-autoradiography, ranges from less than 1 μm to 100 μm with a frequency distribution centred at about 15 μm and an average size around 30 μm; and a much reduced population above 50 μm.

Garcia et al. (2000) have reported a more precise way to classify plutonium distribution in MOX fuel. In particular, using electron probe microanalysis three zones with different plutonium contents were distinguished: high, intermediate and low plutonium content regions. For MIMAS fuel, typically the high Pu content region associates with nearly spherical Pu-rich particles (about 20 heavy metal atom%, i.e., 100Pu/(U+Pu)). The low Pu content region also comprises spherical Pu-rich clusters with an average Pu content of 2.7 at%; and finally the intermediate region with a Pu content of 7.3 at%. This region is referred to as the *coating phase*, since it appears to coat the UO_2 rich region (Garcia et al. 2000). In Figure 2.1 the results of the analysis reported by Garcia et al. (2000) on un-irradiated ADU type MIMAS fuel vis-à-vis surface area fraction and fraction of total Pu content in each region is displayed.

Oudinet et al. (2004) have characterised three types of MIMAS fuel microstructures, especially regarding the Pu distribution, using X-ray microanalysis technique. The fuel specimens were type A, a standard MOX MIMAS fuel used by EDF (Electricitet de France) with a high Pu content of 7.2% (Pu/(U+Pu)); type B, an experimental MIMAS with Pu content of 7.1% elaborated so that the average Pu particle size is smaller than that of the standard MIMAS; and type C a MIMAS fuel with a Pu content of 11.1% but made in the standard way. Some of the characteristics of Pu agglomerates for these fuels are listed in Table 2.1.

MIMAS type	A	B	C
S, %	14	7	30
Pu, wt%	24	23.9	23.7

Table 2.1: Some characteristics of Pu-rich particles in MIMAS fuel. Here S is the surface area fraction of Pu-rich particles in fuel, after Oudinet et al. (2004).

In type B MIMAS, the population of small Pu-rich agglomerates (≤20 μm) constitutes about 29% of the total agglomerate surface, whereas in the case of type A this

population contains around 12% of that surface. Figure 2.2 shows typical size spectrum of Pu-rich particles determined by Oudinet et al. (2004). In another recent report, Vandezande (2000) using an advanced α-radiography technique characterised Pu-rich agglomerates in a MIMAS fuel. Figure 2.3 shows a typical micrograph of the fuel after so-called segmentation.

2.3 SBR process

The SBR (short binderless route), developed and produced by British Nuclear Fuels plc (BNFL), is a way for blending and conditioning of the MOX powder before pressing and sintering (Edwards et al., 1995). Homogenisation is attained by means of a high energy attritor mill, which blends the oxide powders and a spherodizer in order to condition the powder to granules prior to pressing and sintering. At the milling stage, lubricant and Conpore pore former are added in order to control the pellet density and obtain similar characteristics as those of the UO_2 pellets produced by BNFL from IDR (integrated dry route) UO_2 powder. The MOX produced by SBR has a mean grain size of about 7.4 μm with a standard deviation of 0.6 μm, and for pores with a diameter ≥ 5 μm the median pore size has never been observed to exceed 15.4 μm during the production as reported by Edwards et al. (1995). According to these authors, the homogeneity of the fuel with respect to plutonium agglomerates is excellent when measured by α-radiography, which is a coarse scale. Moreover, they showed some data, obtained by EPMA, which indicated that the SBR fuel with a mean Pu/(U+Pu) ratio of 5.5% had the highest plutonium rich region in the pellet with Pu/(U+Pu) ratio of 32%.

Ivison et al. (2000) used X-ray microanalysis techniques to obtain quantitative data on plutonium distribution in SBR MOX fuel. Figure 2.4 shows the results of their investigation vis-à-vis plutonium concentration and size distribution across unirradiated fuel pellet, respectively. They point out that the area of the largest plutonium agglomerate observed corresponds to an equivalent diameter of 30 μm. In another paper, Ivison and Fisher (1999), using again X-ray microanalysis techniques, reported that the largest agglomerates in the examined fuel specimen were 40-50 μm. Ivison and Fisher's measured plutonium concentration profiles for typical SBR fuel specimens are shown in Fig. 2.5.

3 Physical properties

3.1 Nuclear characteristics

Plutonium in reprocessed LWR fuel contains five principal isotopes, namely, ^{238}Pu, ^{239}Pu, ^{240}Pu, ^{241}Pu and ^{242}Pu. These isotopes have roughly the same probability of fission in fast reactors, however, in LWRs only the odd isotopes ^{239}Pu and ^{241}Pu fission and hence contribute to energy production (Stacey, 2001). Typical compositions of these isotopes plus the uranium isotopes in MOX fuel are presented in Table 3.1. From this table we can see that in a gram of ^{239}Pu, there are $4.5\times10^{9}/2.4\times10^{4}$=187500 times as many disintegrations per second as in a gram of ^{238}U.

The use of MOX fuel in LWRs changes the neutronics in several ways. The variation with energy of the cross sections of plutonium isotopes is more complex than uranium isotopes (Stacey, 2001). The absorption cross sections for plutonium are much larger than those for uranium isotopes in a thermal spectrum and are characterised by large absorption resonances in the epithermal (0.3 to 1.5 eV) range and by overlapping resonances (Stacey, 2001).

Isotope	Initial composition (wt%)	Half-life (year)
^{238}Pu	1	88
^{239}Pu	60	24400
^{240}Pu	25	6540
^{241}Pu	9	14
^{242}Pu	5	3.87×10^{5}
^{241}Am	1	433
^{234}U	0.003	1.58×10^{5}
^{235}U	0.25	7.04×10^{8}
^{236}U	0.001	2.39×10^{7}
^{238}U	99.74	4.48×10^{9}

Table 3.1: Typical isotopic composition (White, 1999) and half-life of principal heavy elements in MOX fuel.

It is worth mentioning that because the probability of fission of ^{242}Pu in LWRs is practically zero, the only way of its elimination is through neutron capture to higher actinides,[2] which evolves at a very slow rate (Hesketh, 1995). Consequently, in contrast to a fast reactor, the quantity of ^{242}Pu accumulates in each recycle and the fissile quantity, i.e., the fraction of ^{239}Pu and ^{241}Pu to total plutonium isotopes decreases and higher and higher concentrations of plutonium are required to sustain thermal fission (Hesketh, 1995).

[2] Actinides are in the group of 15 elements following actinium (atomic number 89) in the fifth period.

Isotope	σ_a (barns)	σ_f (barns)	L_a in oxide (cm)
^{239}Pu	1025	743	0.02
^{240}Pu	197	0.03	0.12
^{241}Pu	1377	1009	0.02
^{235}U	681	582	0.04
^{238}U	2.70	0.0	8.7

Table 3.2: Microscopic cross sections at 0.0253 eV and the neutron mean free path L_a (Glasstone and Sesonske, 1981). Subscripts a and f stand for absorption and fission. Visit also: www.atom.kaeri.re.kr

The thermal (0.0253 eV) microscopic nuclear cross sections of ^{235}U, ^{238}U, ^{239}Pu, ^{240}Pu and ^{241}Pu are listed in Table 3.2, from which the mean free path of thermal neutrons are estimated. The mean free path inside an agglomerate ^{238}U-^{239}PuO$_2$ with plutonium concentration 0.3=Pu/(Pu+U) is of the order of 0.07 cm, which is quite larger than the maximum size of the agglomerates (< 0.01 cm) in modern MOX fuel.

It is seen from Table 3.2 that the cross sections for plutonium are different than the ones for uranium isotopes. This dissimilarity leads to a different neutronic behaviour between MOX and UO$_2$ fuel. Oguma et el. (1995) and Hesketh (1995) have pointed out the special features of MOX, which require especial design consideration.

The void reactivity coefficient must be kept negative in MOX as in UO$_2$ fuel to ensure that formation of vapour bubbles in a LWR, leads to seizure of nuclear reaction, not the opposite. Hesketh (1995) states that (does not show any calculations or measurements for support) as long as the plutonium content is moderate, say less than 10 wt% of total Pu, a negative void coefficient is assured in all normal operating conditions. However, if the plutonium content is in excess of 10 wt%, a MOX fuel assembly can resemble a fast reactor, in which plutonium concentration is in the range of 15 to 25 wt%. Thus if the moderator gets voided, the neutron energy spectrum shifts toward that of a fast reactor, where all plutonium isotopes fission. Under these situations the void coefficient can be positive. Nevertheless, as pointed out by Demazière (2002), the effect of BWR MOX fuel on void coefficient is rather complex, since many competing effects are involved when the void content changes. The results of Demazière's analysis indicate that the void coefficient is more negative for MOX fuel than for UO$_2$, except at high void fractions, where the effect of the fast fission factor (due to increase of flux around the fission energies) becomes larger for MOX fuel than for UO$_2$.

The reactivity of MOX decreases more slowly with burnup than that of UO$_2$ fuel. As discussed by Hesketh (1995), this is partly due to the different neutron capture property of MOX fuel versus UO$_2$ and to a degree because ^{240}Pu, which is a neutron absorber in a LWR neutron energy spectrum, gets partially converted to ^{241}Pu, which is fissile. This implies that at high burnup, MOX fuel generates more power than UO$_2$ and also experiences a higher transient power for the same increase in neutron flux (Turnbull, 1995; Stacey, 2001).

The neutron spectrum of MOX fuel, in general, is harder than that of UO$_2$; meaning that, the neutron flux in the resonance region for MOX fuel is higher. This reduces the

reactivity worth of control rods, thereby decreasing the reactor *shutdown margin*.[3] Therefore to control reactivity and maintain satisfactory shutdown margin, modifications in control rod design and boron dilution management might be necessary (Demazière, 2002).

An important difference between MOX fuel and UO_2 fuel is the variations of the effective fraction of delayed neutrons, the prompt neutron lifetime and the reduction of the control rod efficiency. The effective fractions of delayed neutrons from ^{239}Pu and even ^{241}Pu are lower than from ^{235}U (see Table 5.1 in Stacey, 2001) and the prompt neutron life times are shorter in MOX. Moreover, the larger value for thermal cross-section of MOX fuel compared to UO_2 reduces the mean free path of the thermal neutrons in MOX fuel, thereby lowering the thermal absorption probability of the control rod.

The increase in the concentration of plutonium renders the MOX moderator temperature and the fuel temperature Doppler coefficient more negative (Demazière, 2002). The latter effect may be beneficial from the standpoint of the reactivity initiated accident (RIA), however, the more negative moderator temperature makes the core more vulnerable to accidents involving injection of cold water into the reactor core, e.g., steam-line break in PWRs and turbine trip in BWRs (Bairiot & Vanden Bemden, 1995).

There are very few detailed analyses of the aforementioned reactor physics characteristics of MOX fuel, especially for BWRs, published in literature. There are two detailed feasibility studies for MOX fuel in a BWR by C. Demazière (2000, 2002) which can be of interest to the reader. Table 3.3 summarizes some important parameters for MOX vs. UO_2 fuel from Demazière´s calculations (Demazière, 2002).

Parameter	Full UO_2 core		Mixed UO_2/MOX core	
	BOC	EOC	BOC	EOC
Moderator temperature (pcm/°F)	−55.44	−57.01	−57.69	−60.37
Uniform Doppler coefficient (pcm/°F)	−1.12	−1.08	−1.10	−1.15
Effective fraction of delayed neutrons (pcm)	604	532	536	491
Prompt neutron lifetime (μs)	39.6	41.4	34.1	35.9
Control rod worth (pcm)	35023	35965	32132	33251
Shutdown margin (%)	2.426	3.756	0.737	3.039
Average discharge burnup (MWd/kg)		28.3		29.9/35.6 (UO_2/MOX)

Table 3.3: The results of computations of the reactivity coefficients and the associated parameters for two types of BWR cores, from Demazière, 2002. *BOC (beginning of cycle), EOC (end of cycle).*

Another essential aspect in case of a BWR is the stability of the reactor, which e.g., is quantified in terms of a parameter called the decay ratio (DR). The *decay ratio* is defined as the ratio between two consecutive maxima of the impulse response of the normalized neutron density, i.e., it is a measure of the decay of the system. The larger is the decay ratio the less stable is the reactor. Demazière (2002) has evaluated this ratio for BWR using the March-Leuba model. The results of his calculations are summarized in Table 3.4. It is seen that DR is much smaller for full UO_2 core than for mixed

[3] See, e.g., www.tpub.com Nuclear Power Fundamentals for definition and description.

MOX/UO2 core. However, as burnup increases this difference gets smaller. The explanation for this appreciable difference in the stability of the UO_2 vs. MOX core is clearly discussed by Demazière (2002) and hence is not conferred here.

	Full UO_2 core	Mixed UO_2/MOX core
DR (%) at BOC	0.18	2.54
DR (%) at EOC	1.90	2.73

Table 3.4: The stability for two types of BWR cores calculated in terms of the decay ratio (DR), from Demazière, 2002. *BOC (beginning of cycle), EOC (end of cycle).*

It has been stated that MOX fuel has a higher radial flux depression at low burnups, however, equates to that of UO_2 around 30 MWd/kg (Turnbull, 1995). To examine this assertion, we used the TUBRNP model (Lassmann et al., 1994) to calculate the power distribution across fuel pellet for UO_2 and MOX fuel at different pellet average burnups for a fuel pellet with design data presented in Table 3.5. The number of radial nodes of the mesh used across the pellet is 50 in the calculations. The results of our calculations are depicted in Fig. 3.1, which shows that with increasing burnup the UO_2 and MOX fuel power distributions converge. We note that in the calculations for MOX, we assumed that the fuel is perfectly homogeneous.

Technical parameter	UO_2 fuel	MOX fuel
Pellet inner radius (mm)	0.0	0.0
Pellet outer radius (mm)	4.24	4.24
Porosity fraction (%)	5.0	5.0
U-235 content (wt%)	4	0.25
Pu-content (wt%)	0.0	5.4
Pu-composition	0.0	See Table 3.1

Table 3.5: Engineering as-fabricated data on fuel pellet used in the radial power distribution calculations.

3.2 Thermophysical properties

In this section, we briefly review the thermophysical properties of MOX fuel and compare them with those of UO_2 fuel. Especially, our deliberation is directed toward the recent upgrade of the FRAPCON-3 code with MOX fuel properties (Lanning et al., 2005). The properties discussed here comprise the melting temperature, thermal conductivity, thermal expansion and heat capacity. A recent state of the art review of these properties is available (Carbajo et al., 2001).

3.2.1 Melting temperature

Solidus and liquidus temperatures of uranium/plutonium dioxide data and correlations have been recently reviewed by Carbajo et al. (2001). Introduction of PuO_2 in UO_2 will reduce the melting temperature of fuel as a function of PuO_2 content. The data also show that burnup and/or deviation from stoichiometry lowers the melting temperature. Also burnup changes the stoichiometry of the fuel. An empirical correlation, based on curve fitting of the data (Adamson et al., 1985), is recommended for applications

(Carbajo et al., 2001). The FRAPCON-3.3 code (Lanning et al., 2005) includes this recommendation.

We do not repeat the solidus and liquidus correlation functions here, however we present these correlations graphically in Figs. 3.2 and 3.3 for the phase diagram and the melting point vs. local burnup (MWd/kg of heavy metal), respectively.

3.2.2 Thermal conductivity

The thermal conductivity of UO_2 and MOX fuels is a function of temperature, composition, density, oxygen content (oxygen-to-metal ratio, O/M) or the deviation from stoichiometry, and the fuel burnup. The thermal conductivities of these oxides are reduced with temperature up to around 2000 K and then rise with temperature. The addition of PuO_2 into the UO_2 matrix reduces the thermal conductivity. Moreover, the deviation of O/M from 2 reduces the thermal conductivity so does the fuel burnup. Carbajo et al. (2001) have reviewed the literature on thermal conductivity data and models for both UO_2 and MOX fuels, and then recommended correlations for their descriptions. We do not replicate that work here; the interested reader can turn to their published paper for more information.

We, however, point out that the FRAPCON-3.3 code utilises a modified version of the MOX thermal conductivity correlation proposed by Duriez et al. (2000) augmented with a burnup dependence and a slightly reduced high temperature electron contribution (Lanning et al., 2005). The burnup dependence modification is based on the work of Ohira and Itagaki (1997). For the sake of illustration we have used this correlation for a 0.95 dense (5% porosity) and O/M=1.98 MOX fuel together with the corresponding one for UO_2 fuel to plot the thermal conductivity as a function of temperature (Fig. 3.4) and the local burnup (Fig. 3.5). The MOX fuel correlation is documented in Appendix A for the interested reader, while the UO_2 thermal correlation can be found in Lanning et al. (2005). Figures 3.4 and 3.5 show the non-negligible effect of plutonium on thermal conductivity of fuel.

We note from the calculations presented in this and the foregoing subsection that MOX fuel has both lower thermal conductivity and lower melting point compared to UO_2 fuel. A quantity, which gauges the combined effect of conductivity and melting point is the conductivity integral, defined as (Ronchi et al., 1999)

$$L(E) = \int_{773}^{T_m(E)} k(T,E)dT, \tag{3.1}$$

where $k(T,E)$ is thermal conductivity at temperature T and burnup E, and $T_m(E)$ is the melting temperature, which is a function of burnup. This integral represents the linear power density at which the centreline of the fuel pellet, whose outer surface is kept at 773 K, melts. We have used the aforementioned correlation functions of $k(T,E)$ and the melting point $T_m(E)$ for UO_2 and MOX fuel to calculate $L(E)$ vs. burnup (Fig. 3.6). The results show a moderate fall of $L(E)$ for MOX fuel relative to UO_2, although the difference decreases with increase in burnup.

3.2.3 Thermal expansion

Carbajo et al. (2001) have systematically reviewed the data and models for the thermal expansion and density of UO_2, PuO_2 and MOX fuel. The thermal expansion of these fuel materials is quite similar. Based on their re-assessment, Carbajo et al. recommend the correlations developed by Martin (1988) for engineering calculations. They note that, however, the MATPRO correlation (Hagrman et al., 1981) results in lower thermal expansion than that of Martin (1988) for UO_2, for temperatures greater than 1700 K. This means that if we should employ the MATPRO correlation for UO_2 and MOX fuel, we would predict a smaller thermal expansion for these materials. The FRAPCON-3.3 code utilises the same MATPRO 11 correlation (Hagrman, 1981) for UO_2 and MOX fuel (Lanning et al., 2005).

3.2.4 Enthalpy and heat capacity

Fuel enthalpy and its temperature derivative, the heat capacity, are important quantities for fuel behaviour during normal operations and anticipated transients. The enthalpy and heat capacity for UO_2 and MOX fuel are functions of the temperature, fuel composition (UO_2 and PuO_2 fractions), O/M ratio and fuel burnup. However, the former two variables are the main influencing quantities. Both enthalpy and heat capacity are increasing functions of temperature. In UO_2, Hiernaut et al. (1993) have observed a λ-shaped phase transition at 2670±30 K prior to melting[4]. At this transition, the heat capacity increases very sharply in a narrow temperature interval. A similar kind of phase transition is expected in MOX fuel (Leibowitz et al., 1983).

The review of enthalpy and heat capacity data and models on UO_2 and PuO_2 by Carbajo et al. (2001) suggests that the equations and parameters of Fink (2000) and Fink (1982) are the best fit to all experimental data on solid UO_2 and PuO_2, respectively; and therefore should be used for engineering analysis. For MOX fuel the thermodynamic quantities can be combined according to a simple rule of mixture in proportion to its PuO_2 mole fraction. For example, the heat capacity for solid MOX fuel is expressed as

$$C_P(T,\mathrm{MOX}) = (1-x)\,C_P(T,\mathrm{UO_2}) + x\,C_P(T,\mathrm{PuO_2})\,, \tag{3.2}$$

where C_P stands for the heat capacity at constant pressure and x is the mole fraction of PuO_2. We have used the correlations of Fink (Carbajo et al., 2001) for $C_P(T,\mathrm{UO_2})$ and $C_P(T,\mathrm{PuO_2})$ to calculate $C_P(T,\mathrm{MOX})$ in solid state as a function of temperature for PuO_2 contents of 0, 5 mol% and 10 mol% (Fig. 3.7). It's seen from Fig. 3.7 that the MOX values for 5 mol% PuO_2 are very close to the UO_2 values. We have also plotted the difference between the heat capacity of UO_2 and MOX with 10 mol% PuO_2 in Fig. 3.8. It is noted that the deviation between the two fuels are greatest at very high temperatures just prior to melting. The difference between the enthalpy of UO_2 and MOX fuel in the range of up to 10 mol% PuO_2 is very small, i.e., in the order of the uncertainty band of UO_2 enthalpy.

It is worth remarking that Eq. (3.2) assumes that the solid solutions formed in the UO_2-PuO_2 system are ideal solutions. Carbajo et al. (2001) refer to relation (3.2) as the Kopp-Neumann rule and recommend that it should be used in the calculations of enthalpy and heat capacity of solid MOX fuel. We have used this relation, together with

[4] This phase transition is considered to be an *oxygen Frenkel disorder*, whereupon at certain temperature, for actinide oxides prior to melting, oxygen atoms are displaced from their ordered sublattice sites to disordered interstitial sites (Clausen et al., 1984).

Fink's correlations, to predict the heat capacity of MOX fuel as a function of PuO_2 content in a wide range of temperatures (Fig. 3.9). The diagrams illustrate the different linear dependence (slopes) of the heat capacity vs. content at different temperatures. However, calorimetric measurements by Beauvy (1992), in the temperature range of 400 K to 900 K and contents up to 20 Pu/(U+Pu)%, indicate that the Kopp-Neumann rule is incorrect, i.e., the solution is non-ideal and the dependence of heat capacity on PuO_2 content is nonlinear. We have not investigated this discrepancy further, but it requires some attention when extrapolating data or models using relation (3.2) for MOX fuel.

Carbajo et al. (2001) have compared the widely used MATPRO correlations (Hagrman et al., 1981) with the Fink correlations. They note that at temperatures $T < 2000\,\mathrm{K}$ for UO_2 and $T < 1000\,\mathrm{K}$ for PuO_2, the MATPRO correlations yield slightly higher values for the heat capacities than the corresponding correlations recommended by Fink (Carbajo et al., 2001); but at higher temperatures, MATPRO predicts appreciably lower values. These lower heat capacities can be optimistic for certain transients and pessimistic (conservative) for others. For more discussion on the heat capacities, the interested reader can consult the review paper of Carbajo et al. (2001). The fuel performance code FRAPCON-3.3 utilises the MATPRO 11 enthalpy/heat-capacity correlations (Hagrman, 1981) for UO_2 and PuO_2 and then combines them according to Eq. (3.2) for MOX fuel (Lanning et al., 2005).

Finally, we should bring to mind that fuel heat capacity and thermal conductivity determine the fuel time constant, which is a key parameter for reactor stability analysis. The time constant, τ_f, for heat transfer out of a fuel pin of radius r and density ρ is $\tau_f = \rho r^2 C_p / k$, where k is the fuel thermal conductivity.

4 Fuel behaviour models

4.1 Densification and swelling

Oxide fuels like UO_2 and MOX fuel are subjected to densification during the early stages of reactor irradiation, caused by disappearance of submicron pores, and then to swelling due to the accumulation of fission products. Modelling fuel pellet swelling and densification is essential for the prediction of the thermal-mechanical behaviour of fuel rod during irradiation. Maximum densification, although occurs at a low burnup (around 5-6 MWd/kg), it is at that burnup, in many situations, for which fuel temperature reaches its peak. Therefore densification is an important attribute for reactor safety evaluation.

The in-reactor densification is controlled by external fields, such as the fission rate, the temperature and burnup, where at a given burnup, the densification increases with the fission rate and temperature (Freshley et al., 1979). It is also known that the irradiation-induced densification of UO_2 sintered fuel pellet is dependent on a combination of grain size, mean pore size and pore size distribution (Freshley et al., 1979). In particular, Freshley et al.'s (1976) investigation on UO_2 fuel showed that the stable fuel types (with low densifications) were characterised by grain sizes greater than 10 μm and median volume pores larger than 1 μm. However, for grain sizes less than 10 μm and median pores smaller than 1 μm, the fuel types they studied exhibited a wide range of stabilities. They also observed the same general behaviour in MOX fuel, i.e., fuels with grain sizes greater than 10 μm and median pores larger than 6 μm were highly stable (Freshley et al., 1979.

Moreover, in MOX fuel because of the presence of Pu agglomerates one expects that Pu-rich zones give rise to high local fission rates and temperatures that affect fuel densification in MOX fuel relative to UO_2 fuel. Even in the case of co-precipitated fuel where the plutonium is in homogenous solid solution of UO_2 matrix, the pore migration and hence densification, can get affected by the presence of plutonium due to the Pu-U inter-diffusivity at sufficiently high temperatures (Lippens, 1979).

In spite of the expected differences between UO_2 and MOX fuel the comprehensive study made by Freshley et al. (1979) on a variety of MOX fuels indicated that:

- The in-reactor densification of MOX fuel, as in UO_2, is correlated to the density changes that occur under ex-reactor isothermal re-sintering tests, for a given fabrication process.
- Generally, the densification behaviour of MOX fuel is comparable with that of UO_2 fuel, i.e., the Pu-rich agglomerates have no apparent effect on the densification.
- The effects of fission rate and temperature on densification of MOX fuel are similar to those observed on UO_2 fuel.

The majority of models used to describe in-reactor densification in fuel performance codes are empirically based, correlating the change in density ρ_D to fuel burnup by a simple relation, for example,

$$\rho_D = p_D\left(1-\exp(-E/E_D)\right) \tag{4.1}$$

where p_D is the maximum densification (or unstable porosity) and E is the burnup and E_D is a densification-related burnup constant. We have fitted Eq. (4.1) to some data on in-reactor densification of very unstable UO_2 and MOX fuels given in (Freshley et al., 1979) representing temperatures in the range of 1210 to 1790 K and fission rates $\dot{F} = 9.9 - 16.9\times10^{12}$ fission/cm^{3}s (Fig. 4.1, upper panel) and temperatures in the range of 578 to 973 K and fission rates $\dot{F} = 3.3 - 8.3\times10^{12}$ fission/cm^{3}s (Fig. 4.1, lower panel). We observe that at lower temperatures and lower fission rates, the densification is considerably smaller. In order to describe these data with relation (4.1) again we need to find 4 sets of values for parameters p_D and E_D , since Eq. (4.1) is independent of fission rate and temperature. Moreover, the data in Fig. 4.1 indicate that UO_2 densification is lower than that of MOX fuel at low temperatures and may be vice versa. Therefore, it is simplistic to use an equation of the form (4.1) to describe fuel densification during irradiation.

The swelling of fuel has two components: solid fission product swelling and gaseous swelling. The former is commonly taken to be an increasing linear function of burnup, i.e., $\rho_S = -cE$, where ρ_S is the change in fuel density due to solid swelling and c is a parameter in the range $c = 0.6$ to 1.0 %/10MWd/kg of heavy metal. The gaseous swelling is more complex depending on temperature and fission product gas inventory in fuel pellet. The gaseous swelling kinetics may be different in MOX fuel than in UO_2 because of the difference in fission gas release of the two fuels.

A more precise kinetic model for densification and swelling should account for both fuel macrostructure (median pore size, grain size, and agglomerate size) and external fields (temperature and local fission rate). One noted model for in-reactor densification is the Lindman (1977) model, which was verified with Freshley et al. (1976) UO_2 data. This model can be easily extended to treat MOX fuel and verify the Freshley et al. (1979) MOX data (e.g., Fig. 4.1). In Appendix B we outline the basic relations of the original Lindman's model.

The FRAPCON 3.3 code (Lanning et al., 2005) uses the same MATPRO 11 correlations (Hagrman et al., 1981) for UO_2 and MOX fuel densification and solid swelling, based on the limited available in-reactor data on MOX fuel.

4.2 Thermal fission gas release

4.2.1 Background

Gases xenon and krypton, produced during fission of uranium and plutonium isotopes, have low solubility in MOX fuel; hence, after a relatively short irradiation period a large number of fission gas filled bubbles are generated within the fuel grain. Fission gas bubbles in grains remain small, less than 30 nm (Matzke, 1980), whereas lenticular bubbles up to a few microns can be observed at grain boundaries (Turnbull & Tucker, 1974). The process of irradiation-induced re-solution causes the destruction of intragranular bubbles (Turnbull, 1980), ensuing a large population of small bubbles and ample fraction of produced gas atoms in enforced solution. The gas atoms in the solution migrate to the grain boundaries unless the bubbles trap them. The re-solution process should also act on the intergranular gas bubbles; however, at the grain boundary

the abundance of vacancies allow bubbles to grow to larger sizes. When these bubbles interlink, they form a tunnel network (Tucker & Turnbull, 1975), through which a fraction of gaseous fission products is released into the free volume of fuel rod increasing the internal fuel rod pressure. The bubble interlinkage is a cyclic process, since the tunnel network can close again under the effect of surface tension when the outgoing flow of gas atoms offset their supply.

Several physical processes contribute to fission gas release (FGR) in UO_2 as well as MOX fuel. They are usually separated into athermal and thermal release mechanisms (Olander, 1976). Athermal release takes place by recoil and knockout of fission gas atoms by energetic fission fragments. Since these mechanisms generally result in release of less than 1% of the fission gas produced within the fuel pellets, athermal release alone has to date not been considered a potential problem for excessive fuel rod pressure build-up. However, there is concern that the restructuring of UO_2 at high burnup, the so-called rim zone formation, could enhance athermal FGR in high-burnup fuel.

Fission product gas release process in MOX fuel is to a certain extent similar to that of UO_2. However, there are certain particular structural differences between the two kinds of fuel, which makes MOX fuel release different in certain conditions; notwithstanding the fact that post irradiation examinations of fuel rod irradiated in light water reactors indicate that gas release from MOX fuel is higher than from UO_2 fuel under similar operating conditions (Fig. 4.2). For example, Lanning et al. (2005), when evaluating the recent MOX fuel gas release data using the FRAPCON-3 code, were compelled to enhance the fission gas diffusivity in UO_2 by 1.75 in order to capture the experimental data.

In the ensuing subsections, we outline certain attributes of MOX fuel which affect its gas release differently than that of UO_2. We also discuss other phenomena such as helium gas production/release and grain growth which can affect fission gas release.

4.2.2 Fission yields

As mentioned in section 3.1 the three principal fissile elements in LWR fuels are ^{235}U, ^{239}Pu and ^{241}Pu. In MOX fuel the content of the first element is negligible, while in both UO_2 as well as MOX fuel the latter two elements are generated from the neutron absorption of ^{238}U, which makes up the bulk of the nuclear fuel. Comparison of the thermal fission yields for the three isotopes indicates that the yields in the mass numbers 80 to 90, e.g., krypton isotopes, are less from plutonium fission than from uranium fission. Since the xenon yields for these three isotopes are similar, the Xe/Kr ratio gives an indication of the source of fission gas that is measured in post-irradiation examination (PIE). The values for the yields of the stable fission gases for thermal neutrons are listed in Table 4.1.

Isotope	^{235}U	^{239}Pu	^{241}Pu
^{83}Kr	0.005495	0.002878	0.002
^{84}Kr	0.010063	0.00474	0.0035
^{85}Kr	0.00287	0.0013	0.00085
^{86}Kr	0.019644	0.0077	0.00606
Sum	0.038072	0.016618	0.01241
^{131}Xe	0.028868	0.03867	0.030665
^{132}Xe	0.04273	0.052627	0.04078
^{134}Xe	0.077486	0.075619	0.075992
^{136}Xe	0.062704	0.069402	0.067141
Sum	0.211788	0.236318	0.214578
Xe/Kr	5.562828	14.2206	17.29073
^{135}Xe	0.0658	0.0723	0.07277

Table 4.1: Cumulative yield ratios of stable isotopes of Xe and Kr and the radioactive isotope ^{135}Xe. From OECD NEA database through White (2000).

Using the data in Tables 3.1 and 4.1, we estimate the overall plutonium fractional fission yield to be = 0.2987. Here the conversion of ^{135}Xe to ^{136}Xe by neutron capture is included, with the ratio of 0.68 (White, 2000). The equivalent yield of ^{235}U is 0.2946 including the isotope ^{85}Kr, which gives 29.7 cm^3 fission gas at STP per MWd of irradiation. The corresponding fission gas volume from plutonium is estimated to be 30.11 cm^3 at STP per MWd of MOX irradiation.

Moreover, as can be seem from Table 4.1, the Xe/Kr ratio for ^{235}U is 5.56, while the effective Xe/Kr ratio for the two plutonium isotopes is 14.62 (with proportionality factors 0.87 and 0.13 for ^{239}Pu and ^{241}Pu, respectively). The FRAPCON code uses the corresponding Xe/Kr ratios of 5.67 and 16 for ^{235}U and ^{239}Pu+^{241}Pu, respectively (Lanning et al., 2005).

4.2.3 Enhancement of fission gas release

As mentioned earlier, there is observational evidence indicating that the fission gas release rates are enhanced in LWR-MOX fuels compared with conventional UO_2 fuels under similar operating conditions (Fig. 4.2). This enhancement has been ascribed to the non-perfect mixing of plutonium in MOX fuel pellets. A number of pragmatic models have been proposed to account for the heterogeneity effect particular to MOX fuel (Billaux & van Vliet, 1986) and (Ishida & Korei, 1994). Here, we specify how this MOX heterogeneity can affect fission gas release. The theoretical framework for thermal release, where the considered heterogeneity attributes are applicable, is the equivalent sphere model of diffusional release. In this framework, the polycrystalline oxide structure is treated as a collection of spheres of uniform size represented by an equivalent sphere with radius R_{eq} defined by $R_{eq} = 3(V/A)_{eq}$, where $(A/V)_{eq}$ is the specific surface of area of this sphere. The fission gas atoms diffuse in this sphere until they reach the surface of the sphere, the grain boundary, whereupon they precipitate into gas bubbles. The gas bubbles grow in size and number; they interlink and saturate the boundaries upon which tunnel out of the oxide fuel to the external environment. The gas bubbles under irradiation are subjected to a re-solution process tending to dissolve their enclosed gas. The theoretical framework for this model was set by Speight (1969) and was amended for our applications (see Jernkvist & Massih, 2005 and references

therein). Our treatment here is focused on the heterogeneity effect of plutonium rich agglomerates. We set up an effective medium approximation of this fuel characteristic.

Suppose a MOX fuel pellet with randomly distributed Pu-rich agglomerates is placed under neutron irradiation. On a microscopic scale different fission rates in Pu-rich (PuO_2 spots) and in UO_2 matrix are effective. Following Ishida & Korei (1994), we define a fission rate heterogeneity factor in the manner

$$f_H = \frac{\dot{F}_A}{\dot{F}_P} \tag{4.2}$$

where $\dot{F}_A$ is the fission rate of the plutonium agglomerate and $\dot{F}_P$ is the pellet average fission rate. These fission rates are expressed as follows:

$$\dot{F}_A = \phi N_h \left[\sigma_f^U (1 - w_p) + \sigma_f^{Pu} w_p\right] \tag{4.3}$$

where ϕ is the total neutron flux (neutrons/m^2/s), N_h the atomic density of heavy metal (U+Pu), σ_f^U, σ_f^{Pu} the one-group, i.e., averaged over the neutron energy spectrum and isotope composition, effective microscopic fission cross sections (m^2/atom in SI unit) of nuclei U and Pu, respectively, and w_p the PuO_2 weight fraction in the Pu-rich agglomerate. The pellet average fission rate is defined by

$$\dot{F}_P = \phi N_h \left[\sigma_f^U (1 - w_0) + \sigma_f^{Pu} w_0\right] \tag{4.4}$$

where w_0 is the pellet average PuO_2 weight fraction. Note that here the neutron flux depression discussed in section 3.1 is not taken into account (see Fig. 3.1). Combining now equations (4.2), (4.3) and (4.4), the fission rate heterogeneity factor is expressed as

$$\begin{aligned} f_H &= \frac{w_p + \xi(1 - w_p)}{w_0 + \xi(1 - w_0)} \\ \xi &\equiv \sigma_f^U \big/ \sigma_f^{Pu} \end{aligned} \tag{4.5}$$

A typical value of $\xi \approx 2.71 \times 10^{-3}$ is estimated for LWR-MOX fuel from data listed in Tables 3.1 and 3.2. Figure 4.3 illustrates the fission rate heterogeneity (peaking) factor as a function of w_p for various mean PuO_2 contents w_0.

The local fission rate in MOX Pu-rich agglomerates is enhanced by multiplying the average fission rate by f_H. As noted by Billaux and van Vliet (1986) this approach may be appropriate when the fuel is very heterogeneous, with large agglomerates (≥100 μm) and low burnup. However, for very small agglomerates, a homogeneous model may be more representative, since agglomerates can rapidly dissolve in the UO_2 matrix. In the intermediate agglomerate size range, one may need to calculate the kinetics of dissolution of agglomerate (Billaux & van Vliet, 1986). We shall discuss this effect in the subsequent section. Nevertheless, it can be argued that practically all fission gas release emanates from the Pu-rich agglomerates, and also during irradiation, only a portion of fission products remains in the agglomerates, the inter-diffusion of fissile atoms and the recoil of fission products reduce the size of the intermediate agglomerate,

thereby lessen the fission rate in that region by a factor $\Phi_A < 1$. Hence, roughly speaking, the average fission rate should be scaled as $\dot{F} \Rightarrow f_H \Phi_A \dot{F}$.

Fission rate appears through two parameters directly apropos fission gas retention calculations in nuclear fuel: the gas production rate and the gas diffusivity in fuel. Here we carry out some cursory calculations to compare release behaviour of conventional UO_2 fuel and MOX fuel characterised by the effect of Pu-rich agglomerates. We use the thermal gas release model of Speight (1969), i.e., gas diffusion to grain boundaries, re-solution and grain boundary saturation in a mathematical setting described in (Forsberg & Massih, 1985). We choose the gas diffusivity parameters as suggested by Ishida and Korei (1994), based on the works of Turnbull et al. (1982) and Wood et al. (1980), which are listed in Table C.1 in Appendix C (see Fig. 4.4). We calculate the fission gas density (per unit area) within grain boundary N_g and the gas density upon saturation of the grain boundary N_s. We suppose that gas release occurs when $N_g = N_s$. The ideal gas equation of state is used to describe N_s (White & Tucker 1983). These parameters and other pertinent data used in our calculations are given in Tables C.1 and C.2 in Appendix C. The relationship that is employed to calculate N_g is a simplified version of equations in (Forsberg & Massih, 1985). We have presented this relationship in Appendix D.

The results of our calculations are presented in Fig. 4.5, which shows the evolution of N_g / N_s with fuel pellet burnup for UO_2 ($f_H = 1$) and MOX (with $f_H = 3$) at different temperatures. The impact of Pu heterogeneity is directly seen from these calculations, i.e., the release in MOX fuel with $f_H = 3$ occurs at lower burnup than in UO_2. The present theory allows us to calculate directly the temperatures versus burnup threshold for the onset of thermal gas release (Fig. 4.6). As can be seen from Fig. 4.6, in MOX fuel the thermal release threshold is lower than in UO_2 fuel.

4.2.4 Redistribution of plutonium by diffusion

As we remarked in the foregoing subsection, small Pu-rich agglomerates may dissolve during irradiation (Billaux & van Vliet, 1986). Plutonium and uranium atoms can migrate at sufficiently high temperatures and the migration rate gets enhanced under fission in nuclear fuel (Matzke, 1983). The diffusion mean free path can be estimated from Einstein's famous formula, viz.,

$$< R_D^2 >= 6 D_M t \tag{4.6}$$

where R_D is the diffusion length, D_M is the diffusion coefficient of heavy metal (Pu or U) and t is the time. Also the average center-to-center distance between the between agglomerate and its nearest neighbor is estimated by the Chandrasekhar relation (Bansal & Ardel, 1972):

$$R_A = 0.554 \left(\frac{4\pi}{3\varphi} \right)^{1/3} r_A \tag{4.7}$$

where φ is the volume fraction of the agglomerate with mean radius r_A. Considering a typical value of $\varphi = 0.10$, then $R_A \approx 1.92 r_A$.

Three regimes of interest with respect to the size of the Pu-rich agglomerate (d_A) can be distinguished:

i. $R_D << d_A/2$; the size of the Pu-rich agglomerate remains virtually unaffected during irradiation.

ii. $R_D \le d_A/2$; a portion of the agglomerate is dissolved and the apparent agglomerate size increases.

iii. $R_D \ge R_A$, agglomerate is dissolved and the UO_2-PuO_2 mixture is homogenised.

At high temperatures case (iii) prevails, while at low temperatures, typical of LWR conditions during normal operation where the irradiation enhanced diffusion is active, case (ii) can be operative.

Here we use a simple model, suggested by Ishida and Korei (1994), to calculate the redistribution of Pu caused by diffusion-induced dissolution of a spherical Pu-rich agglomerate. The model is a PuO_2/UO_2 spherical cell representation illustrated in Fig. 4.7, where the PuO_2 particle is embedded in a UO_2 spherical shell (matrix). If we denote the mean radii of the UO_2 and PuO_2 spheres by a and b, we have

$$\frac{b}{a} = \left(\frac{C_0}{C_p} \right)^{1/3} \tag{4.8}$$

where C_0 is the initial average Pu content in the MOX fuel and C_p is the initial Pu content in the agglomerate.

Suppose that initially all Pu resides in the PuO_2 agglomerate and then by employing the diffusion equation for Pu concentration $c(r,t)$ in the spherical coordinate, we can calculate the spatial evolution of Pu atoms during irradiation. The initial and boundary conditions imposed are:

$$\begin{aligned} &c(r, t=0) = C_p \quad \text{for} \quad 0 \le r \le b \\ &c(r, t=0) = 0 \quad \text{for} \quad b \le r \le a \\ &c(b,t) = 0 \end{aligned} \tag{4.9}$$

Analytical solution to this initial/boundary value problem is available (Carslaw & Jaeger, 1956). In our computations, we have used a constant diffusivity for Pu/U inter-diffusion, $D_M = 1.369 \times 10^{-18}$ $m^2 s^{-1}$ and $C_p = 0.30$.

The results of our computations are presented in Fig. 4.8 for different b/a ratios at pellet burnups of 23 and 47 MWd/kgU, corresponding to the irradiation times of 490 and 980 days, respectively. For example, b/a=0.6 corresponds to $C_0 = 0.064$, $C_p = 0.30$ and so on. For burnup calculations we have used the data in Table C.2 of Appendix C. The diffusion coefficient used (Verma, 1984) corresponds to the temperature of 1373 K enhanced with a factor of 15. Model calculations show that for the selected diffusivity good portions of Pu remains in the agglomerates after a long irradiation period. A more detailed and involved model, along the same lines, has been presented by Billaux and vanVliet (1986); unfortunately, these authors do not present the results of their model computations, and so we could not compare our results with

theirs. Also, Ishida and Korei do not specify the value of their used diffusivity; therefore we could not compare quantitatively our Fig. 4.8 with their figure 7. Nonetheless, the general trend of our results agrees with theirs.

Assuming that the fission products residing in the UO_2 matrix do not contribute to release, meaning that all release emanates from Pu-rich agglomerates, it is useful to know how much of the fission products remains in the agglomerate during irradiation. Let us define the fraction of fission products that remain in the agglomerate by

$$\Phi_A = \left(\frac{d_A}{d_A + 2\Re} \right)^3 \tag{4.10}$$

where $\Re$ is the diffusion radius of fissile atoms plus the recoil radius of fission product. Let us make an order of magnitude estimation of Φ_A Suppose that fuel temperature is sufficiently low so that diffusion process is athermal, we write

$$\Re^2 = 6D_{irr}t + \ell^2 \tag{4.11}$$

where D_{irr} is the irradiation induced diffusivity of heavy metals directly proportional to the fission rate, i.e., $D_{irr} = k\dot{F}$ (Höh & Matzke, 1973) and ℓ is the fission fragment range. For an agglomerate of size $d_A = 50$ μm using the data in Table 4.2 after 490 days of irradiation, we find that about 50% of the fission products can remain in the agglomerates.

Parameter	Unit	Value
Irradiation time	S	4.23E+07
Agglomerate size	M	5.00E-05
Fission rate	fission/m^3/s	1.26E+19
Fission fragment range	M	6.00E-06
Diffusivity coefficient, *k*	m^5	1.50E-39
Calculation		
Diffusivity	m^2/s	1.89E-20
Diffusion mean free path	M	2.19E-06
Diffusion + recoil distance	M	6.39E-06
FFP in agglomerate, Φ_A	-	0.51

Table 4.2: Calculation of the fraction of fission products (FFP) in a Pu-rich agglomerate after irradiation.

4.3 Helium production and release

MOX fuel generates (and therefore releases) more helium than UO_2 fuel, which will results in higher rod internal pressure at high burnup. In a fuel pellet, helium is produced by α decay, ternary fission of heavy nuclides and (n,α) reaction of light elements in MOX fuel (Fig. 4.9). The α decay of curium is reported to be the main contributor to helium production (Katsuyama et al., 1998).

Kamimura et al. (1999) have evaluated helium generation and release in MOX in BWRs by measurements and calculations. The MOX fuel rod was irradiated to 30.4 MWd/kg in Tsuruga Unit 1 and the UO_2 rod to 36.5 MWd/kgU in Fukushima Daini Unit 2. The fission product (FP) gas release from these fuels to the rod free volume had been measured in an earlier examination and their fractional release amounted to 8% for the MOX fuel and 3.5% for the UO_2 fuel rod.

Six samples were selected by Kamimura et al. from the post-irradiation examination archives for the retained helium and FP gas analyses. Three samples were taken from the MOX rod and the other three from the UO_2 rod, from 3 axial levels of fuel column having 3 local burnups for each fuel type (Table 4.3).

Fuel rod type	Sample No.	Local burnup (MWd/kg)	Helium production (cm^3/g-fuel)	
			calculated	measured
MOX	M1	25	0.06	0.05
	M2	31	0.08	0.06
	M3	36	0.10	0.07
UO_2	U1	28	0.02	0.02
	U2	36	0.02	0.02
	U3	42	0.02	0.02

Table 4.3: Helium generation in BWRs calculated/measured as a function of burnup (Kamimura et al. 1999).

Kamimura et al. using the ORIGEN code calculated the helium production in the samples. Their calculation results are summarized in Table 4.3. It is seen that the production of helium in MOX fuel is substantially larger than in UO_2 during irradiation. Moreover, by a careful and involved procedure, they measured the gas production in each sample (Table 4.3). From the average released helium gas that had been determined in the earlier investigation, they could deduce the release fraction locally for the MOX and the UO_2 fuel (Table 4.4). From Tables 4.3-4.4 one can readily calculate the helium partial pressures in the two types of fuel, which are substantially larger for MOX fuel than UO_2.

Fuel rod type	Sample No.	Local burnup (MWd/kg)	Helium release (%)	
			average	local
MOX	M1	25	40	71
	M2	31		67
	M3	36		60
UO_2	U1	28	50	52
	U2	36		52
	U3	42		58

Table 4.4: Helium fractional release in BWRs determined as a function of burnup (Kamimura et al. 1999). Note that the average refers to rod average helium release not the sample average.

As mentioned before, the average fractional FP gas release of the MOX fuel rod in the puncturing test amounted to 8%, whereas Kamimura et al.'s analysis showed that the

average helium release was 40% in that rod. That is, in the MOX fuel rod the average helium release was five time times larger than that of the FP gas release. Also, in the UO_2 fuel rod the respective fractional releases were 3.5% (FP) and 50% (He), respectively, i.e., helium release was roughly 14 times larger the FP release. These data were similar to the earlier studies reviewed by Kamimura et al. (1999).

It is recalled by Kamimura et al. (1999) that helium has a diffusion coefficient about 1000 times larger than that of xenon. Since in the standard diffusion theory of fission gas release, the release fraction is proportional to the square root of diffusivity, one expects that in both MOX and UO_2 fuels the helium release rate should be about 30 times larger than that of xenon. It is argued that, since the concentration of helium in fuel is small relative to the concentration of the fission product gases, helium atoms do not form their own gas bubbles. Instead, the generated helium atoms diffuse to grain boundary and get trapped into the inter-granular fission product gas bubbles. These bubbles eventually grow and interlink; and then tunnel through the fuel structure and transfer to the free volume of the fuel rod.

Kamimura et al.'s analysis indicates that the similarity between the helium release fraction of MOX fuel and UO_2 implies that in both fuels the released helium volume is strongly proportional to their helium production. The proportion of helium production to the FP gas production is about 0.1 for MOX fuel and 0.025 for UO_2. This difference between MOX and UO_2 fuel justifies greater consequence of helium release in MOX fuel. As mentioned earlier, if the helium release in MOX is five times larger than the FP release (according to Kamimura et al.'s study), the proportion of released helium to the released fission product gases is about 0.5 to 0.125 for MOX and UO_2 fuel, respectively. Therefore, the helium pressure increase in BWR MOX fuel rod can reach 30% or more of the total pressure increase. Because this value is significant, from the standpoint of fuel performance, further investigations on the impact of helium is worthwhile.

We should also point out that the production and release of helium continues after irradiation through the chain of actinides (Fig. 4.9), which contributes to rod internal pressure build-up long after fuel discharge from reactor. The ORIGEN code computations can provide such data.

4.4 Fuel creep

The creep rate of oxide fuel is an important quantity for fuel rod performance. For example, the contact pressure between fuel and cladding and the cladding strain depend on the ratio of fuel swelling rate to creep rate under cladding restraint. Therefore, a quantitative evaluation of MOX fuel creep behaviour relative to UO_2 provides a way to assess the differences between the pellet-cladding interaction properties of the two kinds of fuel.

The creep rate in oxide fuel is considered to be a manifestation of two mechanisms, namely thermal creep and radiation-induced creep. It has been observed that the radiation-induced creep becomes progressively more temperature dependent at $T > 800$ K (Solomon, 1973). Thermal creep becomes predominant in the central region of fuel pellet where temperature can be above 1300 K. The creep in the thermal regime has been studied in the laboratory (ex-reactor) for UO_2 by Burton and Reynolds (1975).

Their results indicate a strong dependence of temperature and stoichiometry on the creep rate (Fig. 4.10). Routbort and company observed similar behaviour for $(U,Pu)O_{2-x}$ (Routbort et al., 1972; Routbort and Voglewede, 1973).

The in-reactor creep behaviour of UO_2 has been studied by a number of investigators: Sykes and Sawbridge (1969), Solomon and Gebner (1972) and by Solomon (1973) used helical springs, in compression and tension; Brucklacher and Dienst (1970) employed disks under compression; Clough (1977) used bars in three point bending, and Perrin (1971) utilized hollow cylinders in compression. These results were appraised and modelled by Solomon et al. (1971) and Solomon (1973) and we display them here in a similar fashion in Fig. 4.11.

The in-reactor creep of MOX fuel has been studied by Perrin (1972) using hollow cylinders in compression. Dienst (1976) investigated the creep rate of FBR MOX fuel pellets (natural uranium dioxide mixed mechanically with 15 % PuO_2) with densities 86% and 93.5% of the theoretical density (TD) and an O/M ratio of 1.985. The specimens' temperatures were between 573 and 1273 K, the applied compressive stresses were at 15 and 50 MPa and the fission rates between 2.5 and 5.0×10^{-9} fissions /(U+Pu) atom/s. We have included in Fig. 4.11 Perrin's (Pluses) and Dienst's (Diamonds) data on MOX with the density 93.5% TD. It is seen that the creep rate of MOX fuel is higher than UO_2 in particular for the Dienst data. The creep rate for the 86% TD MOX fuel examined by Dienst was much higher than the 93.5% TD fuel.

The results of these studies indicate that in-reactor creep of oxide fuel comprises (i) an elevated temperature regime in which normal thermal creep is enhanced, and (ii) a low temperature regime in which the fission process induces athermal creep. Moreover, they suggest that in-reactor creep has two stress domains: a low stress realm, where the steady state creep rate is linearly proportional to stress, and a high stress domain with a power law dependence on stress. An empirical correlation based on these data (UO_2) were deduced by Solomon, Routbort and Voglewede (SRV) in 1971, which describes the creep strain rate as a function of the stress, temperature, fission rate, grain size and density (Lambert and Strain, 1994). To illustrate the dependence of temperature and fission rate, we have used the SRV correlation to calculate creep rate for fixed values of grain size, 10 μm, density, 95%TD, and stress, 24 MPa for several values of fission rate, which may be regarded as different degrees of heterogeneity in MOX fuel (Fig. 4.12). We did not find an equivalent correlation for MOX fuel in literature. The equation used to generate the plots in Fig. 4.12 is given in Appendix E. The MOX fuel creep correlation given in the MATPRO 11 handbook (Hagrman et al., 1981) gave unsatisfactory results. Our recommendation is to apply or fit the SRV correlation to evaluate MOX data, and if necessary, adjust the parameters therein in order to validate the correlation.

4.5 Grain growth

Grain growth of polycrystalline materials such as UO_2 and $(U,Pu)O_2$ is a thermally activated process. Here, we only gloss over the so-called *equiaxed normal* grain growth. Normal grain growth is dissimilar to abnormal grain growth in which a few large grains extend and consume a matrix of smaller ones, eventually interrupting the normal grain growth. For a more detailed review and analysis of grain growth in UO_2 fuel we refer to an earlier report (Jernkvist & Massih, 2005) and references therein.

Sari (1986) employed direct electric heating to study grain growth of unirradiated $(U_{0.8}Pu_{0.2})O_{2-x}$ in a temperature gradient and found the following relationship between the final grain size G and the initial grain size G_0

$$G^3 - G_0^3 = Kt \ , \tag{4.12}$$

where $K = k_0 \exp(-Q/RT)$, k_0 a constant and Q the activation energy for the process. Sari found grain growth to be much faster in $(U,Pu)O_{1.97}$ than in $(U,Pu)O_2$. More precisely, $k_0 = 1.11\times10^{12}$ and 2.55×10^{9} μm^3/min, respectively, and the corresponding activation energies of 446 and 319 kJ/mol. Sari did not observe any significant grain growth below T=1473 K.

Bainbridge et al. (1990) measured grain growth of an irradiated MOX fuel. The MOX fuel material studied had a composition $(U_{0.68}Pu_{0.32})O_2$ and was irradiated in the Materials Testing Reactor at Harwell, UK to a burnup of 0.46 at% (≈ 4.4 MWd/kg). These researchers found a cubic grain growth kinetics according to Eq. (4.12), however, with $k_0 = 7.56\times10^{6}$ and $Q = 209.5$ kJmol^{-1}. In addition, a limiting grain size G_m above which grain growth ceases was found. Their results are different than the analysis presented by Jernkvist and Massih (2005) for UO_2 fuel. In particular, their data show that G_m is a decreasing function of temperature, contrary to the Jernkvist and Massih (2005) result and the earlier investigations (Ainscough et al., 1973), which show an opposite trend. Moreover the grain size evolution in Jernkvist and Massih (2005) obeys a transcendental equation (see equation (2.27) of this reference) rather than a simple cubic relation according to Eq. (4.12).

The plutonium concentration of the fuel examined by Bainbridge et al. (1990) was quite high compared to that of LWR MOX fuel; nevertheless, their results may be representative for the grain growth of Pu-rich agglomerates, especially if grain growth is used for the evaluation of fission gas release by grain boundary sweeping under power transients. However, we should mention that there are several competing mechanisms involved during temperature transients, e.g., the U/Pu inter-diffusion, which tends to homogenise the fuel at high temperatures. The characteristic times of fission gas diffusion, heavy element diffusion and grain growth will decide which mechanism is predominant.

5 Fuel performance experience

In this section we briefly survey some important in-reactor behaviour of commercial MOX fuels irradiated in PWRs, based on post-irradiation examinations (PIEs). The MOX fuel surveyed here were manufactured with the processes described in section 2. We place the emphasis on fuel densification and swelling, fission gas release and microstructure evolution.

5.1 MOX/OCOM and MOX/AUPuC fuel

An early comprehensive irradiation performance evaluation of MOX fuel fabricated with OCOM and AUPuC processes (see section 2.1) in PWRs was made by Goll et al. (1993). The MOX fuels examined consisted of UO_2/PuO_2 agglomerates with a plutonium content of 30 wt% dispersed in UO_2. The integral fissile plutonium content of pellets ranged from 2.0 to 3.5 wt%. The fuel densities were in the range of 10320 to 10450 kg/m^3. These authors report the results of PIE on MOX fuel rods with burnups ranging from 6 to 47 MWd/kg of heavy metal. Their study includes fuel densification and swelling, fission gas release and some structural features of irradiated MOX fuel.

The densities were measured on pellet size pieces by immersion in mercury and by buoyancy technique using tetrabrominethan (Goll et al., 1993). Their data show that the differences between the two MOX types are small. The density increased, due to sintering, up to a burnup of around 20 MWd/kg, after which it started to decrease as fission product swelling became predominant. Hence, as compared to UO_2 fuel experience, there was a delay of roughly 5 MWd/kg where the maximum densification occurred. The swelling rate of UO_2 was about 1% per 10 MWd/kgU, whereas the MOX swelling rate was observed to be at 0.78-0.87 per 10 MWd/kg (Turnbull,1995).

The amount of fission gas release in the rod free volume were determined by puncturing the rods and measuring the total content of gas using mass spectroscopy (Goll et al., 1993). The fractional gas release under steady PWR operating condition ranged from 0.1% to 17% for rod burnups of up to 43 MWd/kg. MOX/OCOM fuel released more fission gas than MOX/AUPuC fuel in similar operating conditions. In general, release fraction as a function of burnup was higher in the MOX fuels than UO_2. Goll et al. also reported the release of fission gas and caesium on a microscopic scale using micro-gamma scanning and analysis of "micro-samples". The results of micro-gamma scanning and micro-sample analysis indicated that most of the fission product gases were released from the central part of the pellet in accordance to radial temperature distribution.

Goll et al. (1993) also reported the results of transient tests (power ramping) done on MOX/OCOM (2 rods) and MOX/AUPuC (7 rods). The tests were performed in the Petten test reactor in Holland on rods pre-irradiated in commercial PWRs. The ramp maximum power (RMP) levels for the MOX/OCOM rods were around 40 and 43 kW/m at a burnup of 23 MWd/kg, while for the MOX/AUPuC rods, RMPs were between 40 to 47 kW/m in the burnup range of 27 to 43 MWd/kg. None of the rods failed the ramp testing. Goll et al. noted that the mechanical interaction between MOX fuel and

cladding was comparable and even smaller than UO_2 fuel. After power ramp tests, the rods were examined destructively in hot cells. For fission gas release measurement the rods were punctured and the amount of gases was determined. The highest transient fractional fission gas release was measured on two-cycle (27 MWd/kg) MOX/AUPuC fuel (46%) which had a RMP level of about 46 kW/m. In general, the fission gas release of the MOX rods were higher than that of the UO_2 fuel rods of standard design. This could partly be attributed to the larger radial pellet-cladding gap size of 105 μm in the MOX/AUPuC compared with 80 to 95 μm in the UO_2 fuel rods. Considerable grain growth had occurred during ramping; however the grain size values were not reported by Goll et al. (1993).

Electron probe microanalysis and quantitative image analysis were carried out at the European Institute for Transuranium Elements by C. T. Walker and co-workers to distinguish between the UO_2 matrix and Pu-rich agglomerates regarding fission products and plutonium distribution across fuel pellet. These of measurements were reported earlier by Walker et al. (1991) for MOX/OCOM fuel. The MOX agglomerates of the un-irradiated specimens were less than 100 μm in size and occupied 15 vol% of the fuel. Their average grain size varied between 5 and 6 μm. Three fuel rods were base irradiated in a commercial PWR to rod burnups of 23, 26 and 39 MWd/kg, with average linear powers of 23, 26 and 25 kW/m, respectively. One of the rods (2^{nd} rod) was subsequently subjected to a ramp test in the Petten reactor to an RMP level of 42 kW/m. The ramp tested rod released 43% of the total amount of gas generated. For the other two rods (1^{st} and 3^{rd}), the fractional release results after base irradiation were 2% and 9%, respectively.

Walker et al. (1991) main findings were as follows. Under a steady state reactor operation the U/Pu inter-diffusion between the MOX agglomerates and the UO_2 matrix was negligible. In the fuel irradiated to 23 MWd/kg, a small amount of Pu may have diffused into the UO_2 matrix at the centre of the pellet. Furthermore, for the fuel irradiated to 39 MWd/kg, the concentration of Pu in the UO_2 matrix did not exceed 1.5 wt% at the pellet centre. Under transient conditions, considerable U/Pu inter-diffusion can occur in the central region of the pellet and at sufficiently high temperatures the MOX agglomerates can get completely dissolved in the UO_2 matrix. For example, for the fuel that was ramped to 42 kW/m, Walker et al. observed that the MOX agglomerates had disappeared completely in the region between $r/r_0 = 0.3$ and pellet centre (r_0 = pellet radius), thereby producing a completely homogeneous solution containing 3% Pu.

Walker et al. (1991) determined the burnup in the irradiated agglomerates. In the fuel irradiated to 39 MWd/kg, the burnup in the agglomerates was in the range of 130 to 200 MWd/kg in the interval of $r/r_0 = 0.82$ and 0.32. Consequently, the plutonium content of the agglomerates had decreased appreciably during irradiation from about 27 wt% to around 11 wt%.

Walker et al. (1991) observed that the MOX agglomerates become highly porous in the course of irradiation and that the appearance of the porosity changes across fuel pellet as a result of temperature gradient. The MOX agglomerates in the outer region of the fuel contained a high concentration of small pores (≤ 3 μm), whereas those in the centre of the fuel included only a few large pores. In the outer region of the pellet, a large portion of fission gas was produced in the MOX agglomerates. For this case, in the outer region

of the fuel, irradiated to 39 MWd/kg, more than 50% of the Xe produced was included in the agglomerate pores.

During irradiation, the MOX agglomerates lose Xe and Cs to the UO_2 matrix (Walker et al., 1991). Depending on the fuel temperature the main mechanism of transport is either recoil or thermal diffusion. Walker et al. (1991) identify that the release process consists of two steps. First, the transfer of Xe and Cs atoms to the UO_2 matrix; second, diffusion of Xe and Cs atoms to the UO_2 grain boundaries through which release occurs. Under power ramp conditions, thermal diffusion is the chief mechanism for the transport of Xe and Cs from the MOX agglomerates to the UO_2 matrix.

The effect of heterogeneity on the level of fission product release from OCOM/MOX fuel during irradiation and fuel microstructure in the vicinity of pellet rim were examined by Walker and co-workers (Walker et al., 1996, 1997) using EPMA. In one fuel (OCOM30), the MOX agglomerates contained 18 wt% fissile plutonium and had a low volume fraction of 0.17; in the other (OCOM15) the agglomerates contained 9 wt% Pu and a high volume fraction (0.34). The fuels had a duplex structure consisting of Pu-rich agglomerates up to 200 μm in size, randomly dispersed in a matrix of natural UO_2 (with 0.72 wt% ^{235}U). Both fuels had been irradiated in a commercial PWR to a rod burnup of about 44 MWd/kg. During the irradiation the average linear power was 19.4 kW/m (OCOM15 segment) and 20.4 kW/m (OCOM30 segment).

Walker et al. (1996) did not observe any U/Pu inter-diffusion during irradiation, i.e., both fuels remained heterogeneous on a microscopic scale after irradiation. However, they noted that the Pu concentration in the MOX agglomerate decreased by about 50% as a result of fission, whereas the Pu content of the UO_2 matrix increased ten-fold to around 2 wt% due to neutron capture of ^{238}U. The agglomerates in the OCOM15 fuel, by and large, revealed a finer structure due to their lower burnup than those of the OCOM30. More than 80% of the fission gases had been transported from the oxide lattice to the pore structure of the agglomerates in both fuels. As a result, rod puncturing revealed that for both fuels the fractional fission gas release to the rod free volume increased from 0.5% at 10 MWd/kg to a maximum of 3.5% at 45 MWd/kg. Walker et al.'s conclusion was that the gas release fraction in MOX fuel is essentially unaffected by the degree of inhomogeneity of the fuel. Walker et al. (1996) also presented the rod puncturing results for the percentage of fission gas release from the OCOM15 and OCOM30 fuel irradiated in a PWR to show that there is no impact of the degree of the as-fabricated Pu inhomogeneity on fission gas release (Fig. 5.1). Comparing the data in Fig. 5.1 with that of other kinds of MOX fuel irradiated in PWRs (Fig. 4.2), we notice that the fission gas release level is comparable to other modern LWR MOX fuels and in effect higher than the conventional UO_2 fuel under similar operating conditions.

One noted finding of Walker et al. (1997) was that the MOX agglomerates in the outer low temperature region of OCOM fuel share several common attributes with the high burnup structure at the rim of the conventional UO_2 fuel (Matzke, 1995). These common features include a small grain size, a high density of small faceted pores and strong xenon depletion. In Table 5.1 we reproduce their results for the sake of exposition. Such similarities offer compelling indication that in both cases the mechanism for producing the characteristic microstructure is the same. This mechanism is considered to be due re-crystallisation induced by the accumulation of irradiation damage and increase in the strain energy of the lattice.

Attribute	Agglomerate in MOX/OCOM30 fuel	High burnup structure in UO_2 fuel
Mean grain size (μm)	1.5±.0.7	0.3±0.2
Porosity (%)	20-30	15-17
Pore size (μm)	1.3-1.5	1.1-1.2
Xe retention (wt%)	≤ 0.5	0.25
Cs retention (wt%)	100	100

Table 5.1: Comparison between MOX agglomerates in the outer low temperature of OCOM and the high burnup structure at the rim of conventional UO_2 fuel, after Walker et. al. (1997).

5.2 MOX/MIMAS fuel

The post irradiation examination data presented for MOX/MIMAS fuel (cf. section 2.2) are not as careful and systematic as the data provided for the OCOM and AUPuC processed MOX fuel presented in the forgoing subsection. For fuel densification, Deramaix et al. (1993) mention that measured stack shrinkage of MIMAS fuel after one or two cycles of irradiation corresponds to a densification of 1 to 1.5%. They claim that these are consistent with 0.4 to 1.4% obtained with standard 24 hours/1700°C re-sintering tests, which are typical for fuels fabricated from ex-AUC powder. Alas, Deramaix et al. do not provide any burnup dependent data on densification, which could be compared with other types of MOX fuel or with UO_2 fuel.

Garcia et al. (2000) have presented a more detailed report on the in-reactor densification of MOX/MIMAS fuels relating to their initial microstructures. They present data on fuel density as a function of burnup measured by the hydrostatic technique for both MIMAS/AUC and MIMAS/ADU type fuels. Their data indicate that densification ceases at burnups of about 15 to 20 MWd/kg, after which the fission product swelling becomes effective. Their data show that fuel swelling proceeds linearly at a rate of about 6×10^{-4} per MWd/kg. Garcia et al. point out that during densification the fractional volume of pores levels off at a value ranging from about 0.5% to 1% for UO_2 fuel and 1.2% to 2.2% for MIMAS/AUC fuel. They also note that the maximum in-reactor densification occurs at around 10 MWd/kg for the MIMAS fuel types they have examined. Moreover, they mention that the standard laboratory re-sintering test (24h/1700°C) underestimates the maximum densification relative to the in-reactor densification. Using Garcia et al.'s data, we have compared the densification of MIMAS/ADU fuel after re-sintering and irradiation (10 MWd/kg) in Table 5.2. We note a factor two difference between re-sintering test and irradiation results.

Method of analysis	After re-sintering (%)	After irradiation (%)
Density measurement	0.48	0.97
Image analysis (IA)	0.76	1.43
Pu-agglomerate (IA)	0.65	1.8
UO_2 matrix (IA)	0.76	1.38

Table 5.2: Densification of MIMAS/ADU fuel after re-sintering (24h/1700℃) and in-reactor irradiation (10 MWd/kg), Garcia et al. (2000).

A summary of Garcia et al.'s porosity measurements after irradiation (MIMAS/ADU) and re-sintering (MIMAS/AUC) is presented in Fig. 5.2. The authors did not report the corresponding data on porosity measurements of the AUC fuel after irradiation.

Fission product gas release of MIMAS fuel and its microstructure evolution during irradiation have been presented by Guérin et al. (2000). The MOX fission release data presented in Fig. 4.2 are from MIMAS/AUC fuel according to Guérin et al. (2000). Gurin et al. also presented additional data on MIMAS/ADU fuel irradiated to burnups below 40 MWd/kg. We should note that for burnups below 38-40 MWd/kg, under normal PWR conditions, the difference between the fission gas release of UO_2 and MOX fuel is small (cf. Fig. 4.2).

MOX/MIMAS fuel microstructure after irradiation was examined by Guérin et al. (2000) using optical microscopy. The large Pu-rich agglomerates were revealed to be very porous. For example, optical micrographs in Fig. 5.3 show sections of fuel pellet after 4 cycles of reactor operation (4 effective years of irradiation). It is seen that the MOX agglomerates situated in the central part of the pellet contains a large cavity and a small number of fission product gas filled bubbles.

Guérin et al. (2000) used EPMA to determine plutonium distribution in MOX/MIMAS fuel. They found that the plutonium content in large agglomerates (≥ 30 μm) decreased with burnup from the initial value of 24 wt% to 10 wt% after 3 cycles of reactor operation. The isotope composition was not identified. Guérin and co-workers did not observe significant Pu/U inter-diffusion during irradiation in agreement with the earlier finding by Walker et al. (1995). They determined xenon content by EPMA and found that Xe gets concentrated around the Pu-rich agglomerates reaching values of 0.6 to 0.8 wt%, as compared to the values in the UO_2 matrix which were around 0.5 wt%. Figure 5.4 shows the X-ray images presented by Guérin et al. (2000) showing the landscape of agglomerate (containing Pu and Xe) in the MIMAS/AUC fuel irradiated to 55 MWd/kg.

Guérin et al.'s (2000) EPMA measurements of caesium and the examination of the local Cs/Nd ratio in the MIMAS/AUC fuel revealed that after and beyond two irradiation cycles, Cs migrates out of the Pu-rich agglomerates toward the UO_2 matrix. In the pellet periphery, they report that the Cs/Nd ratio is lower by 10 and 20% from the U rich matrix, whereas in the central region of fuel pellet, 30 to 40% of the created Cs migrates out of the agglomerates.

By rod puncturing, Guérin et al. measured Xe/Kr ratios for several MIMAS/ADU fuel rods (irradiated up to 3 reactor cycles) and found values between 16 and 18, which are representative of the fission yields of plutonium isotopes. Helium release also was measured from the MIMAS fuel. They found that up to burnup of about 45 MWd/kg no helium release had occurred in the PWR rods. In view of the high diffusivity of helium atoms in oxide fuel (compared to Xe and Kr) this is surprising; however it might be due to the high backfill pressure of the PWR rods which contains helium gas in the oxide fuel and also that helium release may come about at higher burnups. Other micro-structural features found by Guérin et al. (2000) were similar to the earlier investigations of Walker and co-workers on MOX fuel, discussed in the foregoing section.

Finally a number of MOX/MIMAS fuel pins have been subjected to reactivity initiated accident (RIA) simulation tests in the CABRI test reactor in Cadarache, France (Schmitz & Papin, 1999). The fuel pins tested were PWR 17×17 fuel types, which were irradiated to various fuel burnups. Among the four MOX fuel pins tested, one failed at the fuel enthalpy of 503 kJ/kg (120 cal/g). This pin had a burnup of 55 MWd/kg. Schmitz and Papin (1999) point out that since the cladding for this failed pin was not oxidised excessively, i.e., it did not show any sign of oxide layer spalling or hydride blisters, the rupture mechanism could chiefly be due to transient fuel gaseous swelling, which for MOX fuel could be more prominent than for UO_2 fuel. This is because, they argue, for the MOX fuel the plutonium agglomerates act similarly as the pellet rim in UO_2 fuel at high burnup, but occupying about five times the volume fraction of the UO_2 pellet rim. Consequently, the loading of the cladding for MOX rods is substantially higher than in UO_2 rods. Therefore, MOX rods may have a lower failure threshold than UO_2 rods for the same fuel burnup. A summary list of both UO_2 and MOX pins tested in CABRI regarding their burnups, enthalpies, reactor pulse widths and failure thresholds are presented in Table 5.3.

Test ID	Fuel type	Peak pellet burnup MWd/kg	Peak fuel enthalpy J/g	Pulse width ms	Failure enthalpy J/g	Fuel dispersal
Na 1	UO_2	63.8	482	9.5	126	Yes
Na 2	UO_2	33	880	9.5	No	-
Na 3	UO_2	52.8	524	9.5	No	-
Na 4	UO_2	62.3	415	64	No	-
Na 5	UO_2	64.3	482	9	No	-
Na 6	**MOX**	**47**	620	35	No	-
Na 7	**MOX**	**55**	629	40	**503**	Yes
Na 8	UO_2	60	457	75	344	No
Na 9	**MOX**	**28**	880	34	No	-
Na 10	UO_2	62	461	31	331	No
Na 11	UO_2	63.4	461	31	No	-
Na 12	**MOX**	**65**	457	63	No	-

Table 5.3: PWR 17×17 pins pre-irradiated in French PWRs then RIA tested in the sodium loop reactor CABRI with coolant temperature of 280°C and pressure of 0.5 MPa (Papin et al. 2003 and Schmitz & Papin, 1999).

5.3 MOX/SBR fuel

The PWR performance of MOX/SBR fuel (cf. section 2.3) has been presented by BNFL and company in a number of recent conferences (e.g., Cook et al., 2000, 2003, 2004) and publications (White et al., 2001; Fisher et al., 2002). Judging from these publications, the results have been favourable. Cook et al. (2000) report on PIE of seven SBR fuel rods irradiated in a commercial PWR to an assembly average burnup of 33 MWd/kg with rod burnups varying from 32.5 to 35.6 MWd/kg. The PIE included, among other things, isotopic γ-scans which provided data on the increase of fuel stack length due to solid fission product swelling. The evaluated swelling rate was reported to be 5.24% per 10 MWd/kg, however no fuel densification data were presented to deduct the contribution of that effect. The fission gas release of 7 rods was measured by rod puncturing, for which the fractional release values were below 1.1%. These data are presented in Fig. 5.5 (square symbols).

Following gas puncturing measurements, samples were taken from some rods for ceramography and EPMA for microstructural observations. Some typical as-fabricated fuel micro-characteristics data on SBR fuel (White et al., 2001), along with data on the previously discussed fuels are presented in Table 5.4. As an example, Cook et al. (2000) presented a typical optical micrograph of a section of the pellet edge region revealing the microstructure of irradiated SBR fuel (Fig. 5.6). The micrograph shows a number of small intragranular as-fabricated pores that had not been sintered during irradiation. Conspicuous in this image is the presence of two dense clusters of fission products and fission product precipitates, which are the hallmark of plutonium rich agglomerates. On the other hand, Cook et al. (2000) did not observe any clusters of fission gas bubbles or sub-micron grain structure associated with plutonium rich agglomerates in the *optical* examination of any of the specimens between the mid-radius and pellet centre.

Electron probe microanalysis of fission concentrations within plutonium rich agglomerates had been made at different pellet radial positions and the results were presented in Cook et al. (2000). Figure 5.7 depicts data which show the burnup, xenon and caesium distribution. The local burnup was derived from the neodymium content of the agglomerate, whereas the release fractions of Xe and Cs are the differences between the quantity of Xe or Cs measured and the amount produced, based on the Nd content. Also presented in Fig. 5.7 is the variation of Pu content (area%) along a pellet radius using Energy Dispersive X-ray Analysis. The total area of analysis was 2.75 mm^2. The bottom right panel shows that less than 1% of the analysed area from the sample has plutonium content greater than 20%. The area fraction of Pu concentrations greater than 30 wt% was almost nil (Cook et al., 2000). In the pellet rim zone the local burnup in the agglomerate is fairly high due to low self-shielding (cf. Fig. 3.1). From the bottom right panel of Fig. 5.7, it may be seen that the area fraction of Pu concentrations greater than 20 wt% was reduced in the rim zone. In this region, the temperature is too low for any significant inter-diffusion of U/Pu atoms (Walker et al., 1991).

Cook et al. (2003) presented four additional fission gas release data, obtained by rod puncturing, from the MOX/SBR fuel irradiated to four cycles of PWR operation (Fig. 5.5, diamond symbols). We note that the release fraction exceeds 2% for the rod with a burnup of 44 MWd/kg. Comparing the fission gas release of MOX/SBR rods with the more extensive data of MOX/MIMAS fuel rods (cf. Fig. 4.2) at the comparable burnup levels, the values are in the same order or lower, although this may be may be the artefact of the paucity of MOX/SBR data.

[a] Discrete areas more than 20 wt% Pu.

	MIMAS AUC	OCOM 15	OCOM 30	SBR
Fuel density (%TD)	95	95	95	95
Grain size (μm)	5-10	5-6	5-6	7.5-8
Pu-content (wt%HM)	2.9-6.7	5.03	5.07	2.9-5.5
$^{235}U/^{238}U$ (%)	Depleted	0.72	972	0.3
Pu-rich spots (vol%)	24.6	34	17	1-2
Spot Pu content (wt%)	12.5	13.2	26.5	25-35
Max size of Pu-rich spot (μm)	150	200	200	25-35
Stoichiometry (O/M)	2.00	1.994	1.992	2.00
Area fraction of phases (%)				
Matrix	75.4	66	83	98-99
Pu-rich spots	24.6	34	17	1-2[a]
Distribution of input Pu (%)	39	3	3.5	96
Matrix	39	3	3.5	96
Pu-rich spots	61	97	96.5	4

Table 5.4 Comparison between certain characteristics of various modern LWR MOX fuels (unirradiated), after Fisher et al. (2002) and White et al. (2001).

BNFL workers also have conducted ramp tests in the Petten test reactor on 8 MOX/SBR fuel rodlets, which were refabricated from a high enrichment and medium enrichment parent rods. These parent rods were irradiated to three cycles in a commercial PWR (Cook et al., 2003, 2004). The burnup for the rodlets were in the range of 33 to 37 MWd/kg. No re-fabrication rod design data are provided in (Cook et al., 2003, 2004). The ramp maximum powers varied from 39 to 51 kW/m. All the rods survived the ramp tests. Post ramp examinations included rod puncturing for fission gas release measurements, helium release, grain size measurements and ceramography (Cook et al., 2004).

Fission gas release after ramp was reported to vary from 2 to 9%, however the release fraction value for one of the rods was not reported in (Cook et al., 2004); it is alluded that the rod produced a high fission gas release, presumably due to a long (60 h) pre-conditioning at 30 kW/m prior to the ramp. The puncture measurements also showed a significant volume of helium (about 5 cc) was released from the rodlets during the ramp test. Grain size measurement in the central part of the pellet showed an equiaxed growth of 20 μm for the rod ramped to 50 kW/m, i.e., an almost three times the size of the as-fabricated value (5-7 μm). At the pellet edge, no grain growth was detected, whilst modest grain growths of 2-3 μm were measured at the mid-pellet radius. Since these tests did not include conventional UO_2 PWR fuel as a reference specimen, it is difficult to draw definite conclusions regarding the transient gas release behaviour of UO_2 vs. MOX/SBR fuel.

6 Concluding remarks

In this report, we first reviewed the basic physical properties of MOX fuel comprising nuclear characteristics, thermophysical properties such as melting temperature, thermal conductivity, thermal expansion, enthalpy and heat capacity. These properties are, in general, well understood for MOX fuel and are well described by appropriate models, which can be used for analyses of MOX fuel. The FRAPCON3.3 code includes these properties. We also reviewed the main modelling approaches of MOX fuel behaviour, namely, densification, swelling, fission product gas release, helium release, fuel creep and grain growth. The models for these effects are not, as for UO_2 fuel, so well established as the models for thermophysical properties. In MOX fuel the presence of islands of Pu-rich agglomerates adds to the complexity of fuel behaviour on the micro scale. Finally, we surveyed the recent fuel performance experience and post irradiation examinations on four types of MOX fuel, namely OCOM, AU/PuC, MIMAS and SBR. We discussed the data from these examinations, regarding densification, swelling, fission product gas release and the evolution of microstructure during irradiation. The available data discussed here were from examinations made on fuel rods irradiated in commercial pressurised water reactors. Very few equivalent data are reported in literature from rods irradiated in commercial boiling water reactors.

The results of our review indicate that in general MOX fuel has a higher fission gas release and helium release than UO_2 fuel. Part of this increase is due to higher operating temperatures of MOX fuel relative to UO_2 fuel due to the lower thermal conductivity of MOX material. However, as it discussed by Lanning et al. (2005), the differences in thermal conductivity and power history are not sufficient for the fuel performance code to capture the analysed MOX fuel fission gas release data. The diffusion coefficient of the fission gas in UO_2 fuel was scaled by 1.75 for MOX fuel in order to obtain comparable predictive capability (Lanning et al., 2005). In a different evaluation, Bernard et al. (2002) argued that, since fission gas release is typically a non-linear function of burnup, the volume average fission gas release for MOX/MIMAS fuel is larger than the fission gas release for the average burnup. These workers modelled this effect by using an incubation burnup (in their model) that is lower for MOX fuels than for UO_2 fuels depending on the degree of heterogeneity of the MOX microstructure. Irradiation induced creep rate of MOX fuel is higher than UO_2 fuel, i.e., the Pu-rich agglomerates may act as porosity, enhancing the creep rate. This effect can alleviate the pellet-clad interaction intensity of fuel rod.

Nevertheless, we suggest that physical based approaches discussed in section 4 of this report should be implemented in the fuel performance code to account for the behaviour of MOX fuel during irradiation. In particular, we recommend that a fuel densification model, fission product gas and helium release model (important for BWR rods) are implemented in the FRAPCON3.3 computer code SKI version (Jernkvist, 2005). These models and the code outcome should then be verified with available relevant measured data. The FRACON3.3 fission gas release computation has been verified with only 6 MOX fuel rods, three under normal operations and the rest subjected to ramp tests. This database is substantially smaller than that used for UO_2 fuel.

7 References

Adamson, M.G., Aitken, E.A. and Caputi, R.W., 1985.
Experimental and thermodynamic evaluation of the melting behavior of irradiated oxide fuels, Journal of Nuclear Materials, 130, pp 349-365.

Ainscough, J.B., Oldfield, B.W. and Ware, J.O., 1973.
Isothermal grain growth kinetics in sintered UO_2 pellets,
Journal of Nuclear Materials, 49, pp 117-128.

Bainbridge, J.E., Forty, C.B.A., and Martin, D.G., 1990.
The grain growth of mixed-oxide fuel during irradiation,
Journal of Nuclear Materials, 171, pp 230-236.

Bairiot, H. and Vanden Bemden, 1995
Could weapon-grade plutonium be an asset for managing Pu inventories?
Recycling of Plutonium and Uranium in Water Reactor Fuel,
International Atomic Energy Agency, IAEA-TECDOC-941, pp 57-67, Vienna.

Bansal, P. P. and Ardell, A. J., 1972.
Average nearest-neighbor differences between uniformly distributed finite particles,
Metallography 5, pp 97-111.

Beauvy, M., 1992.
Nonideality of the solid solution n $(U,Pu)O_2$ nuclear fuel,
Journal of Nuclear Materials, 188, pp 232-238.

Bernard, L.C., Jacoud, J.L. and Vesco, P., 2002.
An efficient model for the analysis of fission gas release,
Journal of Nuclear Materials, 302, pp 125-134.

Billaux, M. and van Vliet, J., 1986.
Impact of fuel heterogeneities on fission gas release for LWR U-Pu mixed oxide fuels,
Res Mechanica, 17, pp 41-47.

Blanpain, P., Brunel, L., Thibault, X., and Trotabas, M., 2000.
MOX fuel performance in the French PWRs: status and development,
Proc. ANS Topical Meeting on Light Water Reactor Fuel Performance, Park City, Utah, April 10-13, 2000.

Burton, A. and Reynolds, G.L. 1975.
Physical Metallurgy of Reactor Fuel Elements,
The Metal Society, London, pp 87-98.

Brucklacher, D. and Dienst, W., 1970.
Continuous measurement of irradiation creep of UO_2,
Journal of Nuclear Materials, 36, pp 244-247.

Carbajo, J.J.Yoder, G. L., Popov, S. G. and Ivanov, V. K., 2001.
A review of thermophysical properties of MOX and UO_2 fuel,
Journal of Nuclear Materials, 299, pp 181-198.

Carslaw, H. S. and Jaeger, J. C., 1959.
Conduction of Heat in Solids, *2nd Edition*,
Oxford University Press, Oxford, England.

Clausen, K. et al., 1984.
Observations of oxygen Frenkel disorder in uranium dioxide above 2000 K by use of neutron-scattering techniques,
Physical Review Letters, 52, pp 1238-1241.

Clough, D. J., 1971.
Irradiation-induced creep of ceramic nuclear fuels,
Meeting on fast reactor fuel and fuel elements, GFK, Karlsruhe, cited in Solomon et al., 1971.

Clough, D. J., 1977.
Creep properties of oxide and carbide fuels under irradiation,
Journal of Nuclear Materials, 65, pp 24-36.

Cook, P., Stratton, R. and Walker, C.T., 2000.
Post irradiation examination of BNFL fuel,
Proc. ANS Topical Meeting on Light Water Reactor Fuel Performance, Park City, Utah, April 10-13, 2000.

Cook, P. et al., 2003.
Performance of BNFL MOX fuel,
Proc. of the ENS Top Fuel 2003 Meeting, Wurzburg, Germany, March 16-19, 2003.

Cook, P. et al., 2004.
Post irradiation examination and testing of BNFL SBR MOX fuel,
Proc. of the 2004 International Meeting on LWR Fuel Performance, Orlando, Florida, September 19-22, 2004.

Demazière, C., 2000
Analysis of the reactivity coefficient and the stability of a BWR loaded with MOX fuel,
Proc. of the PHYSOR 2000, ANS International Topical Meeting on Advances in Reactor Physics and Mathematics and Computation in the Next Millennium, May 7-12, 2000, Pittsburgh, PA, USA.

Demazière, C., 2002
Reactor physics calculations on MOX fuel in boiling water reactors,
Proc. of the 7th Information Exchange on Partitioning and Transmutation (IEMPT7), October 14-16, 2002, Jeju, S. Korea, OECD NEA.

Deramaix, P., Haas, D. and van de Velde, 1993.
In-pile performance of mixed-oxide fuel with particular emphasis on MIMAS fuel,
Nuclear Technology, 102, pp 47-53.

Dienst, W., 1976.
Irradiation-induced creep of mechanically blended porous UO_2-PuO_2 fuel,
Journal of Nuclear Materials, 61, pp 185-191.

Duriez, C., Alessanderi, J-P, and Gervais, T., 2000.
Thermal conductivity of hypostoichiometric low Pu content $(U,Pu)O_{2-x}$ mixed oxide,
Journal of Nuclear Materials, 277, pp 143-158.

Edwards, J. et al., 1995.
BNFL supply of MOX fuel assemblies to the Beznau 1 PWR of NOK,
Recycling of plutonium and uranium in water reactor fuel,
International Atomic Energy Agency, IAEA-TECDOC-941, pp 57-67, Vienna.

Fink, J.K., 1982.
Enthalpy and heat capacity of the actinide oxides,,
Int. Journal of Thermophysics, 3, pp 165-200.

Fink, J. K., 2000.
Thermophysical properties of uranium dioxide,
Journal of Nuclear Materials, 279, pp 1-18.

Fisher, S.B., et al., 2002.
Microstructure of irradiated SBR MOX fuel and its relationship to fission gas release,
Journal of Nuclear Materials, 30, pp 153-172.

Forsberg, K. and Massih, A.R., 1985.
Diffusion theory of fission gas migration in irradiated nuclear fuel UO_2,
Journal of Nuclear Materials, 135, pp. 140-148.

Freshley, M.D., Brite, D.W., Daniel, J.L. and Hart, P.E., 1976.
Irradiation-induced densification of UO_2 pellet fuel,
Journal of Nuclear Materials, 62, pp 138-166.

Freshley, M.D., Brite, D.W., Daniel, J.L. and Hart, P.E., 1979.
Irradiation-induced densification and PuO_2 particle behavior in mixed-oxide fuel,
Journal of Nuclear Materials, 81, pp 63-92.

Garcia , P., Boulore, A., Guérin, Y., Trotabas, M. and Goeuriot, P., 2000.
In-pile densification of MOX fuels in relations to their initial microstructure,
Proc. ANS Topical Meeting on Light Water Reactor Fuel Performance, Park City, Utah, April 10-13, 2000.

Garwin, R. L. and Charpak, G., 2001.
Megawatts and Megatons,
Alfred A. Knopf, New York.

Glasstone, S. and Sesonske, A., 1981.
Nuclear Reactor Engineering,
Reprint Edition, Krieger Publishing Company, Malabar, Florida.

Goll, W., Fuchs, H-P, Manzel, R. and Schlemmer, F.U., 1991.
Irradiation behavior of UO_2/PuO_2 fuel in light water reactors,
Reactor Technology, 102, pp 29-46.

Guérin Y., et al., 2000.
Microstructure evolution and in-reactor behaviour of MOX fuel,
Proc. ANS Topical Meeting on Light Water Reactor Fuel Performance, Park City, Utah, April 10-13, 2000.

Hagrman, D. L., Reymann, G.A. and Mason, G.E., 1981.
A handbook of materials properties for use in the analysis of light water reactor fuel rod behavior, MATPRO Version 11 (Revision 2), NUREG/CR-0479 (TREE-1280), prepared by EG&G Idaho, Inc., Idaho Falls, Idaho for the U.S. Nuclear Regulatory Commission, Washington, D.C., 1981.

Hanus, D. and Kleykamp, H., 1982.
Uran- und Plutonium Verteilung in unbestrhlten Mischoxid-Brennstoff aus der Industriellen Fertigung, Journal of Nuclear Materials, 106, pp 199-210.

Hesketh, K., 1995.
A review of multiple recycle of plutonium in LWRs.
Recycling of Plutonium and Uranium in Water Reactor Fuel,
International Atomic Energy Agency, IAEA-TECDOC-941, pp 57-67, Vienna.

Hiernaut, J.P., Hyland, G. J. and Ronchi C., 1993.
Pre-melting transition in uranium oxide,
Int. Journal of Thermophysics, 14, pp 609-612.

Höh, A. and Matzke, Hj., 1973.
Fission enhanced self-diffusion of uranium in UO_2 and UC,
Journal of Nuclear Materials, 48, pp 157-164.

IAEA, 2003.
Status and Advances in MOX fuel technology,
International Atomic Energy Agency, Technical Reports Series-415, Vienna, Austria.

Ishida, M. and Korei, Y., 1994.
Modeling and parametric studies of the effect of Pu-mixing heterogeneity on fission gas release from mixed oxide fuels of LWRs and FBRs,
Journal of Nuclear Materials, 210, pp 203-215.

Ivison, P. K. and Fisher, S. B., 1999.
Quantitative plutonium mapping using energy dispersive X-ray analysis,
Proceedings of TopFuel99, Avignon, France , 13-15 September 1999.

Ivison, P. K. et al., 2000.
Quantification of the homogeneity of BNFL SBR MOX fuel using compositional X-ray mapping, in Nuclear fuel behaviour modelling at high burnup and its experimental support, International Atomic Energy Agency, IAEA-TECDOC-1233, pp 239-246, Vienna, 2000.

Jernkvist, L.O., 2005.
The FRAPCON-3.3 Computer code SKI-version,
SKI report to be issued (TR 05-008).

Jernkvist, L.O. and Massih, A.R., 2005.
Models for fuel rod behaviour at high burnup,
Swedish Nuclear Power Inspectorate (SKI) research report 2005:41.

Kamimura, K., Kobayashi, Y., and Nomata, T., 1999.
Helium generation and release in MOX fuel,
Proc. of the IAEA International Symposium in MOX Fuel Cycle Technologies for Medium and Long Term Deployment, 17-21 May, 1999, Vienna.

Katsuyama, K., Mitsugi, T. and Asaga, T., 1998.
Evaluation of helium release behavior in MOX fuel,
Proc. of the 1998 ANS Winter meeting, Washington, D.C.
Material Science and Technology session, pp 115-116.

Lanning, D.D., Beyer, C.E. and Cunningham, M.E., 2000.
FRAPCON-3 fuel rod temperature predictions with fuel conductivity degradation caused by fission products and gadolinia additions, Proc. ANS Topical Meeting on Light Water Reactor Fuel Performance, Park City, Utah, April 10-13, 2000.

Lanning, D. D., Beyer, C. E. and Geelhood, K. J., 2005.
FRAPCON-3 updates, including mixed-oxide properties,
NUREG/CR-6534, PNNL-11513, Vol. 4, prepared for the U.S. Nuclear Regulatory Commission by Pacific Northwest Laboratory, Richland, Washington, 2005.

Lambert, J. D.B. and Strain, R., 1994.
Oxide Fuels,
Materials Science and Technology, Vol. 10A, Nuclear Materials Part I (Editor B.R.T. Frost) VCH, Weinheim, Germany.

Lassmann, K., O'Carroll, C., van der Laar, J. and Walker, C.T., 1994.
The radial distribution of plutonium in high burnup UO_2 fuels,
Journal of Nuclear Materials, 208, pp 223-231.

Leibowitz, L. and Fink, J.K. and Slagle, O.D., 1983.
Phase transitions, creep, and fission gas behaviour in actinide oxides,
Journal of Nuclear Materials, 116, pp 324-325.

Lee, B.H., Koo, Y.H. and Sohn, D.S., 2001.
Rim characteristics and their effects on the thermal conductivity in high burnup UO_2 fuel, Journal of Nuclear Science and Technology, 38(1), pp 45-52.

Lindman, N., 1977.
On the rate of in-reactor UO_2 densification,
Journal of Nuclear Materials, 71, pp 73-77.

Lippens, M., 1979.
Densification of UO_2-PuO_2 fuel,
Journal of Nuclear Materials, 81, pp 99-105.

Lippens, M., Van Loon, C., Ketels, J., 1986.
Ceramographic techniques and microprobe micro-analysis applied to uranium-plutonium oxides,
Proc. of the IAEA Technical Meeting on Properties of Materials for Water Reactor Fuel Elements and Methods of Measurement, 13-16 October, 1986, Vienna.

Martin, D. G., 1988.
Thermal expansion of solid UP2 and (U,Pu) mixed oxides-a review and recommendations,
Journal of Nuclear Materials, 152, pp 94-101.

Matzke, Hj., 1980.
Gas release mechanisms in UO_2- a critical review,
Radiation Effects, 53, pp 219-242.

Matzke, Hj., 1983.
Radiation enhanced diffusion in UO_2 and $(U,Pu)O_2$,
Radiation Effects, 75, pp 317-325.

Matzke, Hj., 1995.
The rim-effect in high burnup UO_2 nuclear fuel,
In P. Vincenzini (ed), Ceramics: Charting the Future, Proc. World Ceramics Congress, Florence, Italy, June 28 - July 4, pp 2913-2920.

Oguma, M., Mochida, T., Nomata, T. and Asahi, K., 1995.
Technology developments for Japanese BWR MOX fuel utilization,
Recycling of Plutonium and Uranium in Water Reactor Fuel,
International Atomic Energy Agency, IAEA-TECDOC-941, pp 57-67, Vienna.

Ohira, K. and Itagaki, N., 1997.
Thermal conductivity measurements of high burnup UO_2 pellet and a benchmark calculation of fuel centre temperature,
Proc. ANS Topical Meeting on Light Water Reactor Fuel Performance, Portland, Oregon, March 2-6, 1997, pp 541-549.

Olander, D.R., 1976.
Fundamental Aspects of Nuclear Reactor Fuel Elements,
TID-26711-P1, National Technical Service, U. S. Department of Commerce, Springfield, Virginia, USA.

Oudinet, G. et al., 2004
On the characterization of plutonium distribution in MIMAS MOX by image analysis,
Advanced fuel pellet materials and designs for water cooled reactors, International Atomic Energy Agency document, IAEA-TECDOC-1416, pp 221-233, Vienna, 2004.

Papin, J., Lemoine, F. and Federici, E., 2003.
Main outcomes from the CABRI test results
Proceedings of NEA CSNI topical meeting on RIA fuel safety criteria, Aix-en Provence, France, May 13-15, 2002, Report NEA/CSNI/R(2003)8/Vol 2, pp 61-81.

Perrin, J.S, 1971.
Irradiation creep of uranium dioxide,
Journal of Nuclear Materials, 39, pp 175-182.

Perrin, J.S, 1972.
Effect of irradiation creep of UO_2-PuO_2,
Journal of Nuclear Materials, 42, pp 101-104.

Ronchi, C., Scheindlin, M., Musella, 1999.
Thermal conductivity of uranium dioxide up to 2900 K from simultaneous measurement of the heat capacity and thermal diffusivity,
Journal of Applied Physics, pp. 776-789.

Roepenack, H., Schlemmer, F. U., Schlosser, G. J., 1987.
Development of thermal plutonium recycling,
Nuclear Technology, 77, pp 175-186.

Routbort, J.L., Javed, N.A. and Voglewede, J.C., 1972.
Compressive creep of mixed-oxide fuel pellets,
Journal of Nuclear Materials, 44, pp 247-259.

Routbort, J.L. and Voglewede, J.C., 1973.
Creep of mixed-oxide fuel pellets at high stress,
Journal of the American Ceramic Society, 56, pp 330-333.

Sari, C., 1986.
Grain growth kinetics in uranium–plutonium mixed oxides,
Journal of Nuclear Materials, 137, pp 100-106.

Schmitz, F. and Papin, J., 1999.
High burnup effects on fuel behaviour under accident conditions: the tests CABRI REPNa
Journal of Nuclear Materials, 270, pp. 55-64.

Solomon, A.A., 1973.
Radiation-induced creep of UO_2,
Journal of the American Ceramic Society, 56, pp. 164-171.

Solomon, A.A. and Gebner, R. H., 1972.
Instrumented capsule for measuring fission-induced creep of oxide fuels,
Nuclear Technology, 13, pp. 177-184.

Solomon, A. A., Routbort, J.L., and Voglewede, J.C., 1971.
Fission-induced creep of UO_2 and its significance to fuel element performance,
Argonne National Laboratory Report, ANL-7857.

Speight, M.V., 1969.
Calculation on the migration of fission gas in material exhibiting precipitation and re-solution of gas atoms under irradiation,
Nuclear Science & Engineering, 37, pp 180-185.

Stacey, W.M., 2001.
Nuclear Reactor Physics,
John Wiley & Sons, Inc., New York.

Sykes, E.C. and Sawbridge, P.T., 1969.
Irradiation creep of uranium dioxide,
Central Electricity Generating Board Report RD/BN/1498.

Sykes, E.C. and Sawbridge, P.T., 1971.
Private communications cited in Solomon et al., 1971.

Tucker, M.O. and Turnbull, J.A., 1975.
The morphology of interlinked porosity in nuclear fuels,
Proceedings of Royal Society of London, 343, pp 299-314.

Turnbull, J.A. and Tucker, M.O., 1974.
Swelling in UO_2 under conditions of gas release,
Philosophical Magazine, 30, pp 47-63.

Turnbull, J.A., 1980.
A review of irradiation induced re-solution in oxide fuels,
Radiation Effects, 53, pp 243-250.

Turnbull, J.A., 1995.
A review of MOX fuel and its use in LWRs,
OECD Halden Reactor Project Report HWR-435, Halden, Norway.

Turnbull, J.A., Friskney, C.A., Findlay, J.R., Johnson, F.A. and Walter, A.J., 1982.
The diffusion coefficient of gaseous and volatile species during the irradiation of uranium dioxide,
Journal of Nuclear Materials, 107, pp 168-184.

Vandezande, J, 2000.
Microscopic determination of PuO_2 grain size and pore distribution of MOX pellets with an image analysis system,
Advanced methods of process/quality control in nuclear fuel manufacture, International Atomic Energy Agency, IAEA-TECDOC-1166, pp 59-63, Vienna, 2000.

Verma, R., 1984.
Study of homogenization and cation inter-diffusion in mixed UO_2-PuO_2 compacts by x-ray diffraction,
Journal of Nuclear Materials, 120, pp 65-73.

Walker, C.T., Coquerell, M., Goll, W., and Manzel, R., 1991.
Irradiation behaviour of MOX fuel: results of an EPMA investigation,
Nuclear Engineering and Design, 131, pp 1-16.

Walker, C.T., Goll, W. and Matsumura, T., 1995.
MOX fuel irradiation behaviour; results from X-ray microbeam analysis
International Atomic Energy Agency, IAEA-TECDOC-941, pp 301-318, Vienna.

Walker, C.T., Goll, W. and Matsumura, T., 1996.
Effect of inhomogeneity on the level of fission gas release and caesium release from MOX OCOM fuel during irradiation, Journal of Nuclear Materials, 228, pp 8-17.

Walker, C.T., Goll, W. and Matsumura, T., 1997.
Further observation on OCOM MOX fuel: microstructure in the vicinity of the pellet rim and fuel-cladding interaction, Journal of Nuclear Materials, 245, pp 169-178.

White, R.J. and Tucker, M.O., 1983.
A new fission-gas release model,
Journal of Nuclear Materials, 118, pp 1-38.

White, R.J., 1999.
The re-irradiation of MIMAS-MOX fuel in IFA 629.1,
OECD Halden Reactor Project Report, HWR-589.

White R.J., 2000.
Fission gas release,
OECD Halden Reactor Project Report, HWR-632.

White R.J., et al., 2001.
Measurement and analysis of fission gas release from BNFL's SBR MOX fuel,
Journal of Nuclear Materials, 288, pp 43-56.

Wood, M. H., Matthews, J.R., Johnson, F.A and Walter, A.J., 1980.
Some predictions from the ORGES gas release code and comparison with experiment,
Journal of Nuclear Materials, 92, pp 354-356.

Acknowledgments I thank J-E Lindbäck, L-O Jernkvist and Tero Manngård for comments and discussions. The work was supported by the Swedish Nuclear Power Inspectorate (SKI) under SKI contract 2005/1089/200506022.

Appendix A:
Fuel thermal conductivity correlation for MOX fuel

The correlation for thermal conductivity of MOX fuel applied in FRAPCON-3.3 is a modified version of the model proposed by Ohira and Itagaki (1997) for UO_2 and Duriez et al. (2000) for MOX fuel. The modifications made to this model in FRAPCON-3.3 relate to the phonon heat conduction term, where for fuel burnup $E < 45$ MWd(kgU)$^{-1}$ the correlation proposed by Ohira and Itagaki underestimated the thermal conductivity (Lanning et al., 2000) and the high temperature electron heat transport term, in which the constant multiplying factor of Duriez et al. was reduced in order to comply with measurements by Ronchi et al. (1999), see Lanning et al., 2005.

In the FRAPCON-3.3 model, the thermal conductivity of MOX fuel is correlated to fuel temperature and burnup through

$$k_{95} = \frac{1}{A(x) + B(x)T + 2.46 \cdot 10^{-4} T + h(E,T)} + \frac{1.5 \times 10^{9} e^{-13520/T}}{T^2} \quad \text{(A.1)}$$

where k_{95} [W(mK)$^{-1}$] is the thermal conductivity of fuel with 5% porosity, T [K] is the fuel temperature, and $h(E,T)$ is a burnup/temperature dependent factor, given by

$$h(E,T) = 1.87 \cdot 10^{-3} E + \frac{3.8 \cdot 10^{-2} \left(1 - 0.9 e^{-0.04E}\right) E^{0.28}}{1 + 396 e^{-6380/T}} \quad \text{(A.2)}$$

Here, E is the local fuel burnup in MWd(kg)$^{-1}$.

$$\begin{aligned} A(x) &= 2.85x + 0.035 \\ B(x) &= 2.86 \times 10^{-4} - 7.15 \times 10^{-4} x \\ x &= 2.00 - O/M \end{aligned} \quad \text{(A.3)}$$

A porosity correction factor according to Maxwell and Euken is finally used for application of the above correlation to materials with porosity volume fractions, p, other than 0.05. Hence, the thermal conductivity of MOX with porosity p is

$$k(p) = 1.0789 k_{95} \frac{1 - p}{1 + 0.5p} \quad \text{(A.4)}$$

Porosity p is defined, in terms of fully dense fuel ρ_{TD} and the actual density ρ, viz.,

$$p = \frac{\rho_{TD} - \rho}{\rho_{TD}} \quad \text{(A.5)}$$

Appendix B:
Lindman in-reactor fuel densification/swelling model

The basic assumption of Lindman (1977) was that during densification, (i) grain size is nearly constant, (ii) the densification rate parameter denoted by M is a decreasing function of burnup (irradiation time). Adapting Cobel's model for final-stage sintering the densification rate is expressed by

$$\frac{d\rho}{dt} = \frac{MD}{G_0^3} \tag{B.1}$$

where D is the diffusivity, G_0 is the initial grain size and ρ is the density (% Theoretical Density). Lindman assumes an exponentially decreasing function for the densification rate, i.e., $M = M_0 \exp(-B\dot{F}t)$, where $\dot{F}$ is the fission rate ($m^{-3}s^{-1}$), t the time and B, M_0 are empirically determined constants.
Adding the contribution of fuel solid swelling rate, which is proportional to the density and fission rate, we write

$$\frac{d\rho}{dt} = \frac{M_0 D}{G_0^3} \exp(-B\dot{F}t) - \rho S\dot{F} \tag{B.2}$$

where S is the fractional volumetric swelling rate (m^3/fission). Integrating Eq. (B.2) in the range $0 \le \rho \le 100\%\,\mathrm{TD}$, one obtains:

$$\rho = e^{-S\dot{F}t}\left[\rho_0 + \frac{M_0 D}{G_0^3}\frac{\left(1 - e^{-(B-S)\dot{F}t}\right)}{(B-S)\dot{F}}\right] \tag{B.3}$$

The diffusivity parameter is assumed to be the sum of two components: irradiation and thermal, i.e., $D = D_{irr} + D_{th}$ with the irradiation component taken to be a constant and the thermal component obeying an Arrhenius relation:

$$D_{th} = D_{oth} \exp(-E_D / RT) \tag{B.4}$$

All the constants appearing in equations (B.3) and (B.4) are given in (Lindman, 1977) for UO_2 fuel, which he obtained by evaluating Freshley et al. (1976) experimental data. We note that Lindman's densification/swelling model has the basic elements (fission rate, temperature, grain size) that can be adapted for MOX fuel behaviour analysis, using the data of Freshley et al. (1979) on MOX fuel and other recent data published in literature (e.g., Garcia et al., 2000).

Appendix C:
Fission gas diffusivity in fuel

Correlations/parameters/constants	Unit	Definition
$D_{eff} \equiv \nu_g D/(\nu_g + g)$	m^2s^{-1}	Effective gas diffusion coefficient
$D = C_1 e^{-Q_1/T} + C_2 \dot{F} e^{-Q_2/T} + C_3 \dot{F}$	m^2s^{-1}	Gas diffusion coefficient in trap free media
$\nu_g = 3.03\pi \ell \dot{F}(\overline{R}_b + \delta)^2$	s^{-1}	Intragranular bubble gas re-solution rate
$\overline{R}_b = 1.453\times10^{-10} \exp(1.023\times10^{-3} T)$	m	Mean intragranular bubble radius
$g = 4\pi \overline{R}_b C_b^{tot} D$	s^{-1}	Fission gas captured rate by intragranular bubble
$C_b^{tot} = 1.52\times10^{27}/T - 3.3\times10^{23}$	m^{-3}	Total gas bubble density
$\ell = 6\times10^{-6}$	m	Fission fragment range
$\delta = 10^{-9}$	m	Damage radius of fission fragment
$\dot{F} = N_A \dot{f}$	$m^{-3}s^{-1}$	Fission density
$\dot{f} = 5.189\times10^{-14} q_v$	$mol.m^{-3}s^{-1}$	Fission density
q_v	Wm^{-3}	Power density
$N_A = 6.022\times10^{23}$	atom/mol.	Avagadro number
$C_1 = 7.6\times10^{-10}$	-	-
$C_2 = 4.5\times10^{-35}$	-	-
$C_3 = 2.0\times10^{-40}$	-	-
$Q_1 = 3.5247\times10^4$	K	-
$Q_2 = 1.38\times10^4$	K	-

Table C.1: Relations and constants used for calculation of the fission gas diffusion coefficient in UO_2 fuel. Here, T is the absolute temperature, confer (White & Tucker 1983) and (Ishida & Korei, 1994) for diffusivity.

Parameter	Unit	Definition
$d_{pellet} = 8.48$	mm	Fuel pellet diameter
$\rho_{TD} = 0.960$	-	Relative (to T.D.) pellet density
$\nu_b \lambda / \beta(t) = 5.7 \times 10^{-8}$	$\mathrm{ms}^{-1} / \left(\mathrm{mol.m}^{-3}\mathrm{s}^{-1}\right)$	Ratio of gas re-solution rate to gas production rate
$\beta(t) = 0.3\dot{F}$	Atom $\mathrm{m}^{-3}\mathrm{s}^{-1}$	Fission gas production rate
$N_{sat} = \frac{8.72 \times 10^{-9}}{T}\left(\frac{2\gamma}{r_f} + P_{ext}\right)$	mole m^{-2}	Intergranular gas density at saturation
$2\gamma / r_f = 2.4 \times 10^6$	Pa	Bubble surface tension to radius of curvature
P_{ext} =0.0	Pa	External gas pressure acting on intergranular gas bubbles
$q_L = 25$	kWm^{-1}	Linear power density

Table C.2: Input parameter values used in fission gas release computations.

Appendix D:
Evolution of gas concentration in grain boundary

In (Forsberg & Massih, 1985), we developed a mathematical model for calculation of fission gas release accounting for gas diffusion to grain boundaries, irradiation-induced re-solution and grain boundary saturation. Here a simplified expression for the gas content of fuel in grain boundaries as a function of time for *isopotent (*constant power*)*, used in the calculations presented here, is outlined. We only present the short time solution of the governing equations, which is of practical interest here. The area density of intergranular gas atoms is described by:

$$N_g(\tau) = \frac{2\beta_e}{h_1}\left[\tau + (h_2 h_3)^{-1} - \frac{h_2 \exp(h_3^2\tau)\operatorname{erfc}(h_3\sqrt{\tau}) + h_3 \exp(h_2^2\tau)\operatorname{erfc}(-h_2\sqrt{\tau})}{h_2 h_3 (h_2 + h_3)}\right] + O(\tau^\infty)$$

$$\frac{Dt}{R^2} < \frac{1}{\pi^2}. \qquad \text{(D1)}$$

where

$$\beta_e = \frac{\beta}{D}; \quad \tau = Dt$$

$$h_1 = \frac{\nu_b \lambda}{D}$$

$$h_2 = -\frac{h_1}{2} + \sqrt{\frac{h_1^2}{4} + \frac{h_1}{R}}$$

$$h_3 = \frac{h_1}{2} + \sqrt{\frac{h_1^2}{4} + \frac{h_1}{R}}$$

Here t is the time, ν_b the re-solution rate, λ the re-solution distance, and all the other parameters are defined in Appendix C.

Appendix E:
In-reactor fuel creep correlation

The combined results of laboratory thermal creep and in-reactor creep of UO_2 (Fig. 4.11) suggest that the creep deformation comprises (i) an elevated temperature regime in which thermal creep is enhanced and (ii) a low temperature regime in which the fission process induces athermal creep. Solomon et al. (1971) supposed that in-reactor creep includes two stress regions, namely, a low-stress region where the steady-state creep strain rate is $\dot{\varepsilon} \propto \sigma$ and a high-stress region, $\dot{\varepsilon} \propto \sigma^{4.5}$, where σ is the stress. Solomon et al. recommended an expression for the creep rate related to the fission rate $\dot{F}$ and stress and temperature according to the relationship

$$\dot{\varepsilon} = A_1(\dot{F})\sigma^{4.5} \exp(-Q_1 / RT) + \frac{A_2(\dot{F})\sigma}{G^2} \exp(-Q_2 / RT) + C\sigma\dot{F} \qquad \text{(E1)}$$

where

$$A_1(\dot{F}) = \frac{1.38\times10^{-4} + 4.6\times10^{-17}\dot{F}}{-90.5+\rho}$$

$$A_2(\dot{F}) = \frac{9.73\times10^{6} + 3.24\times10^{-5}\dot{F}}{-87.7+\rho}$$

$Q_1 = 552.3$ kJ/mol

$Q_2 = 376.6$ kJ/mol

$C = 7\times10^{-23}$

$\dot{\varepsilon}$ is the total creep rate (1/h), $\dot{F}$ the fission rate (fissions/cm^3 s), σ the uniaxial stress (psi), G the grain size (assumed constant 10 μm), ρ the density (%TD), above 92; if less, then 92%, T the temperature (K) and R the gas constant.

Equation (E1) was used to generate the plots depicted in Fig. 4.12. The constants appearing in this equation may be re-adjusted to fit the data displayed in Fig. 4.11.

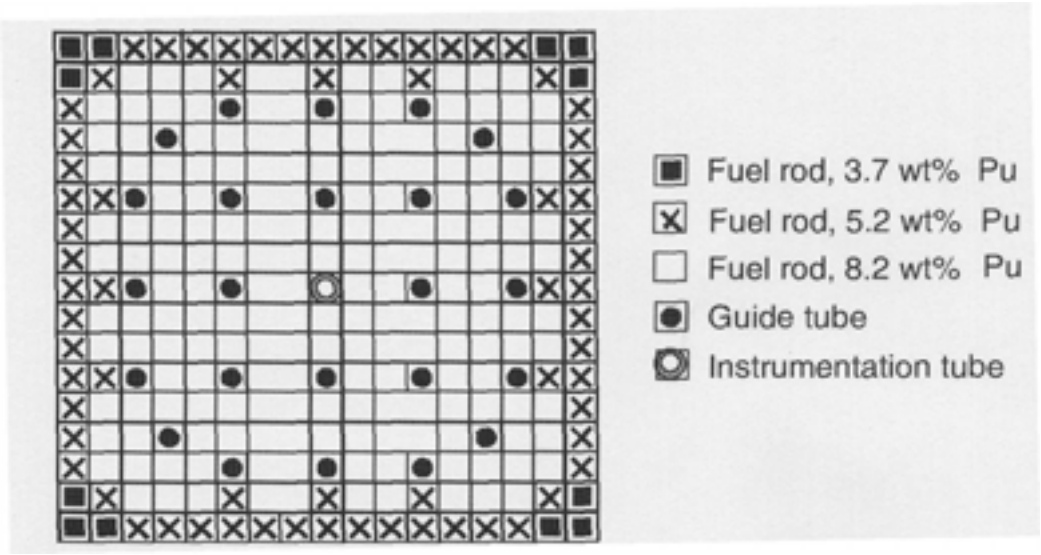

Figure 1.1: Example of a PWR MOX fuel assembly design of 17×17-24 type with a fuel assembly average plutonium content of 7.2 wt%, from IAEA (2003).

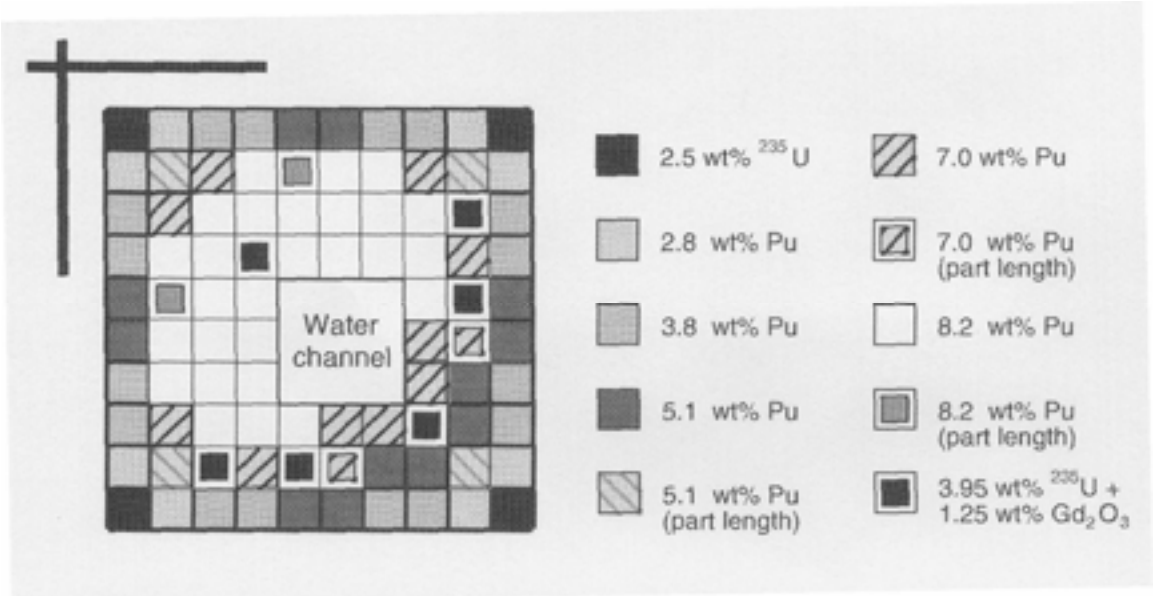

Figure 1.2: Example of a BWR MOX fuel assembly design of 10×10-9Q type with a fuel assembly average plutonium content of 5.4 wt%, from IAEA (2003).

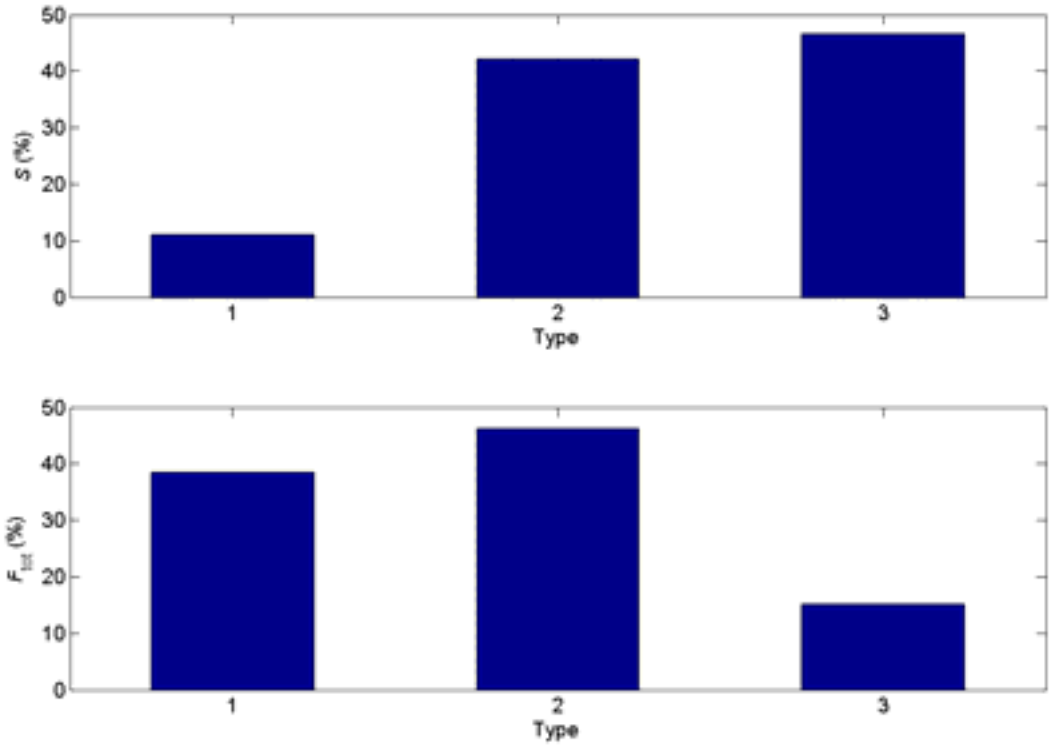

Figure 2.1: Distribution of unirradiated ADU MIMAS MOX in different types of agglomerates after Garcia et. al (2000). Here S is the surface fraction and F_{tot} is the fraction of total Pu. Type 1, 2, 3 denote the Pu-rich, the coating phase and the U-rich agglomerates.

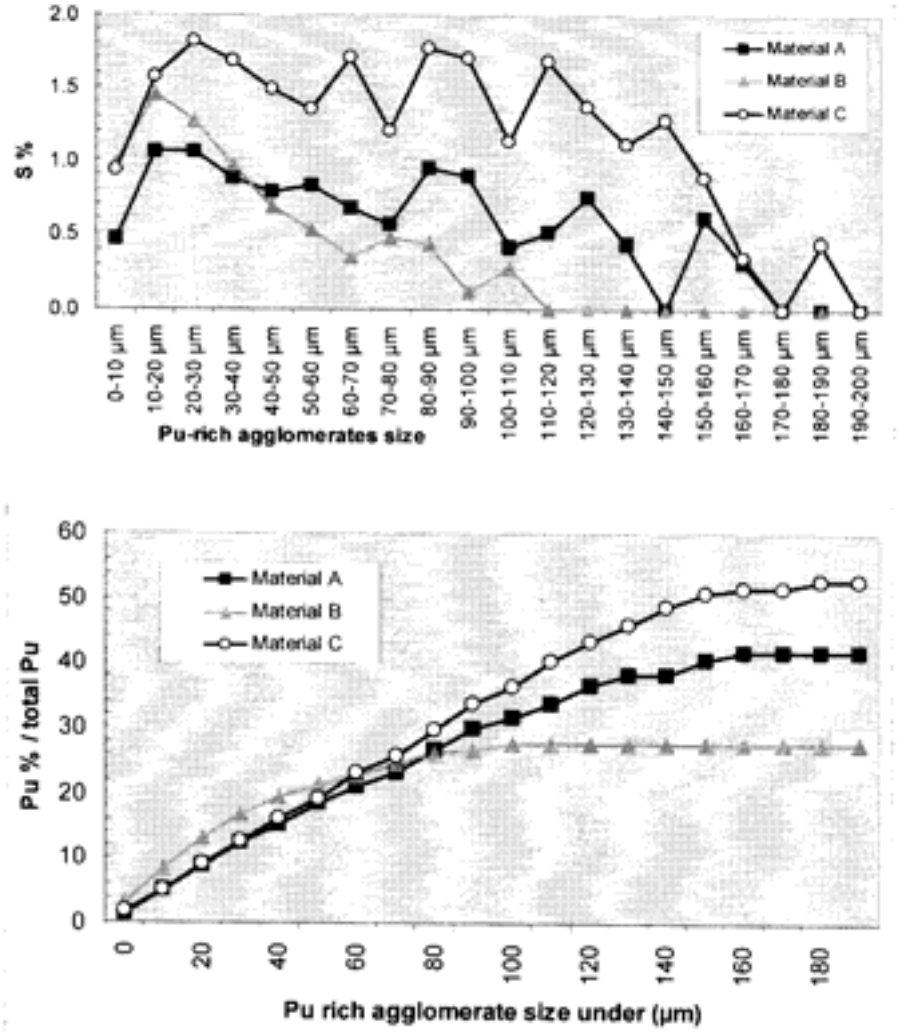

Figure 2.2: Plutonium rich particle size spectra and cumulative plutonium percentage relative to the total plutonium content in un-irradiated MIMAS MOX, from Oudinet et al. (2004).

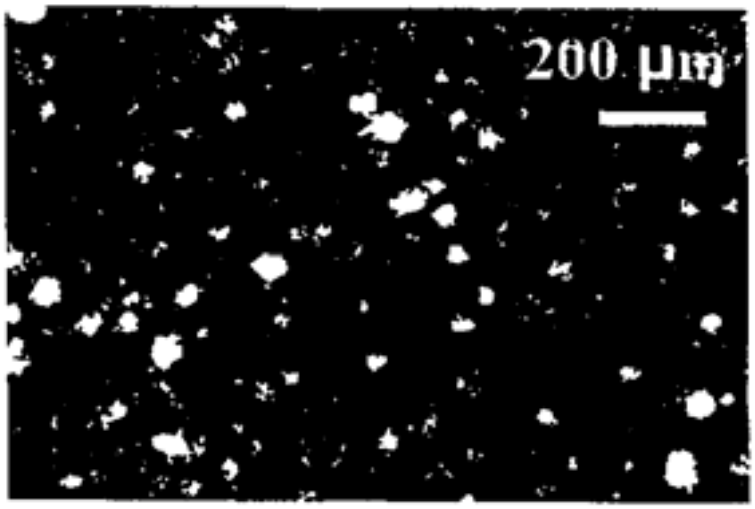

Figure 2.3: Image of Pu particle distribution in unirradiated MIMAS MOX fuel, from Vandzande (2000).

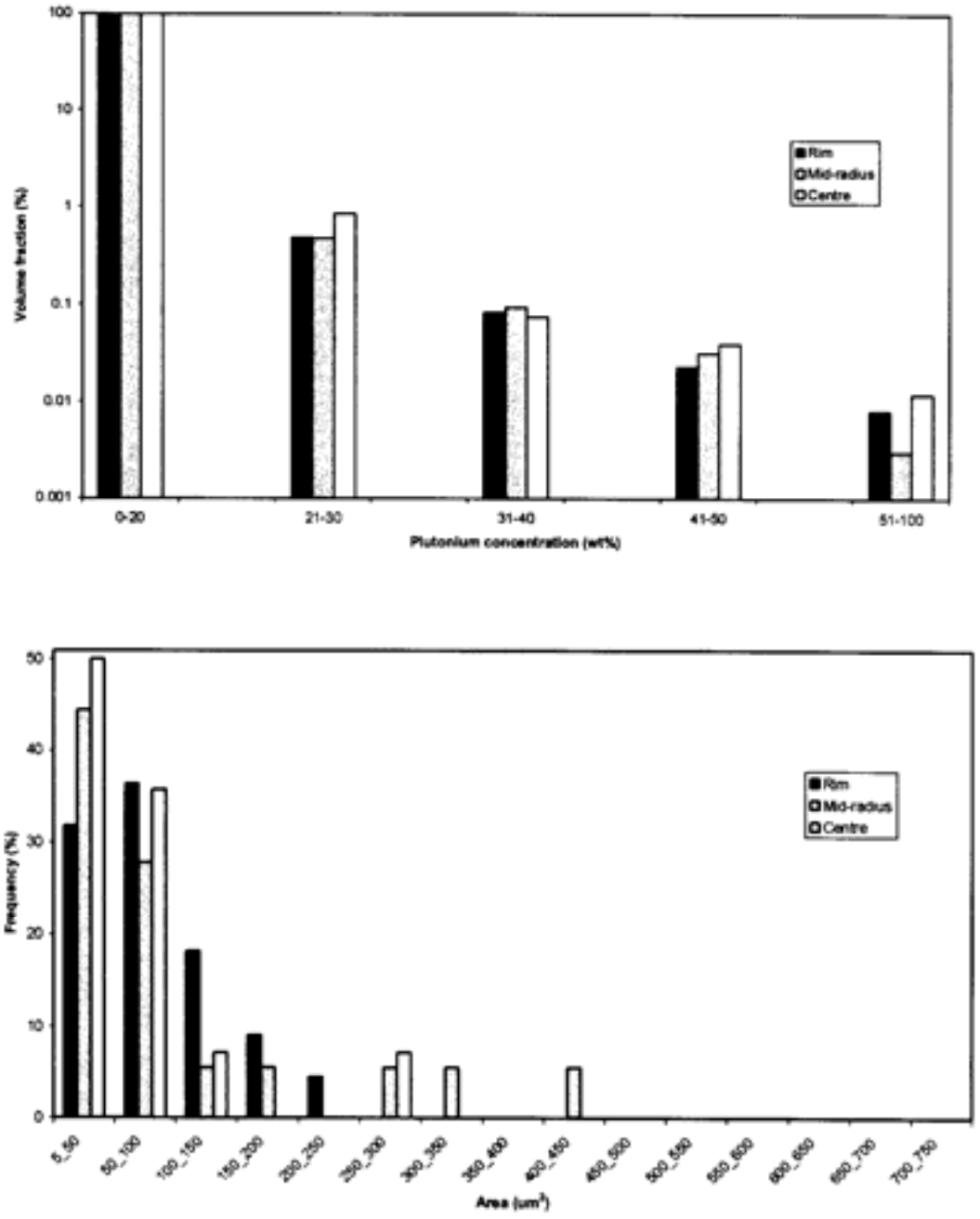

Figure 2.4: Pu particle distribution in unirradiated SBR MOX, from Ivison et al. (2000).

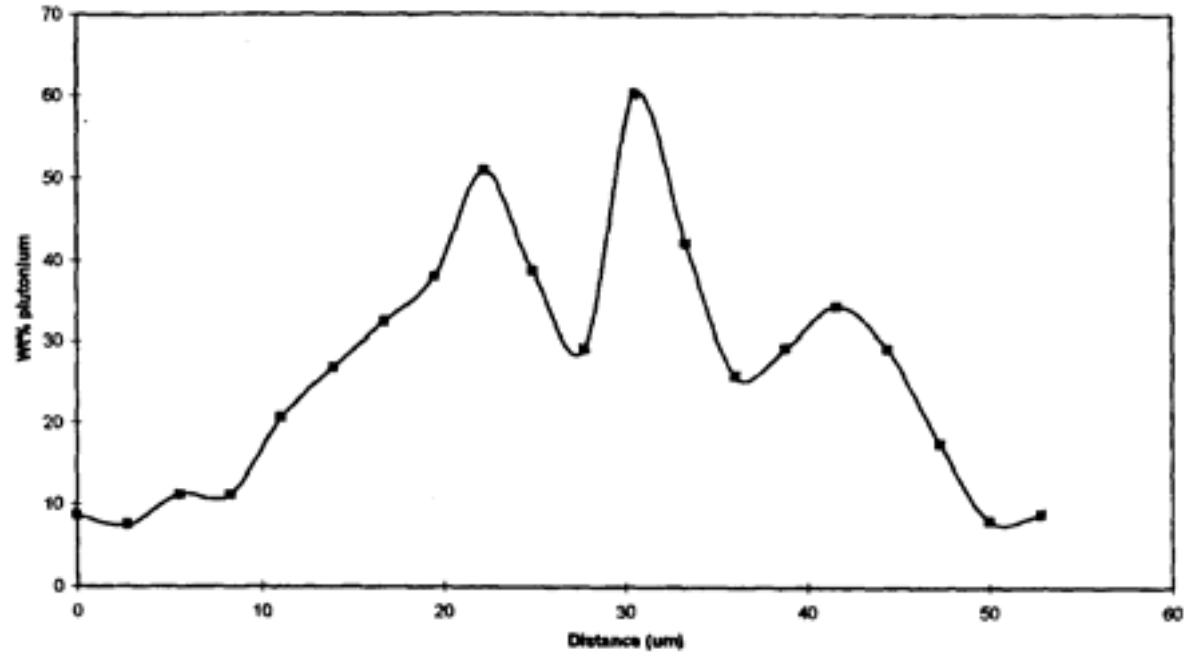

(a)

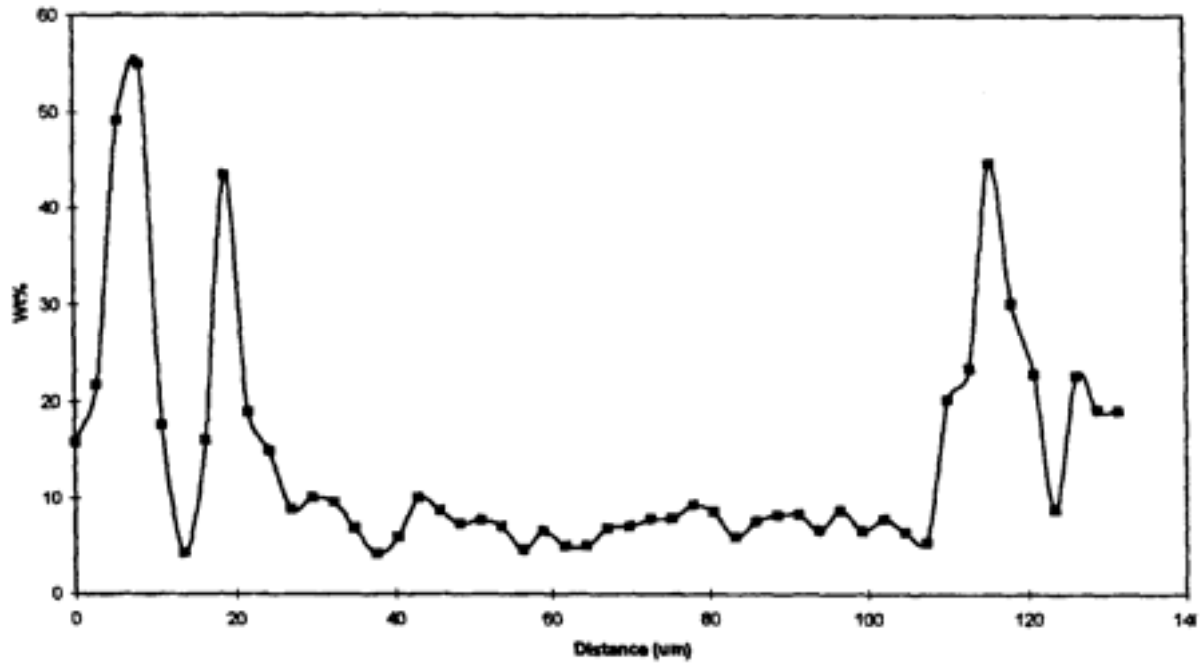

(b)

Figure 2.5: Plutonium concentration profiles in unirradiated SBR MOX fuel: (a) within a Pu-rich agglomerate, (b) between two Pu-rich agglomerates, after (Ivison and Fisher, 1999).

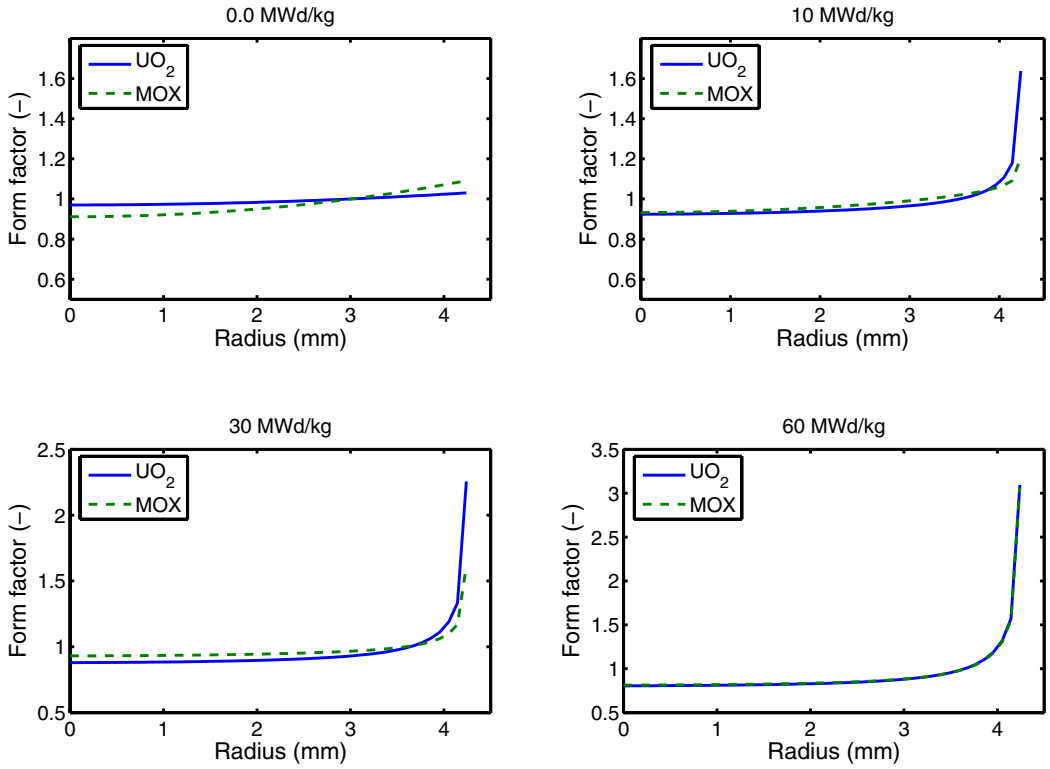

Figure 3.1: Radial power/burnup distribution across fuel pellet at different pellet average burnups calculated using the TUBRNP model: UO_2 fuel (^{235}U =4 wt%) versus MOX fuel with mean Pu content of 5.4 wt% and isotope distribution listed in Table 3.1 and pellet design data in Table 3.5.

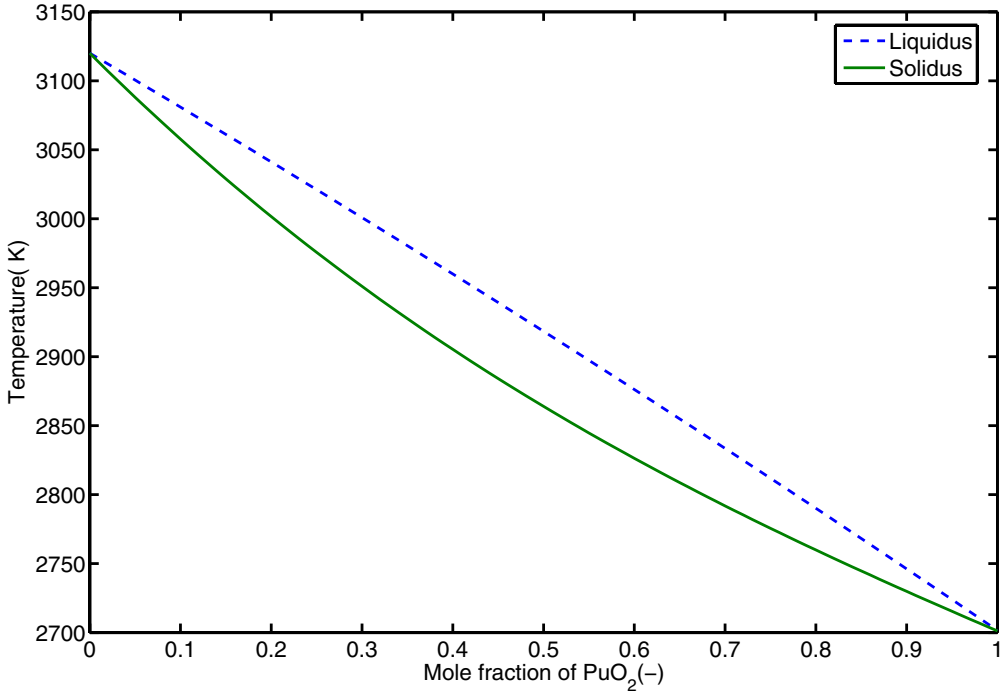

Figure 3.2: Solidus and liquidus lines of UO_2-PuO_2 system calculated using correlations by Adamson et al. (1985).

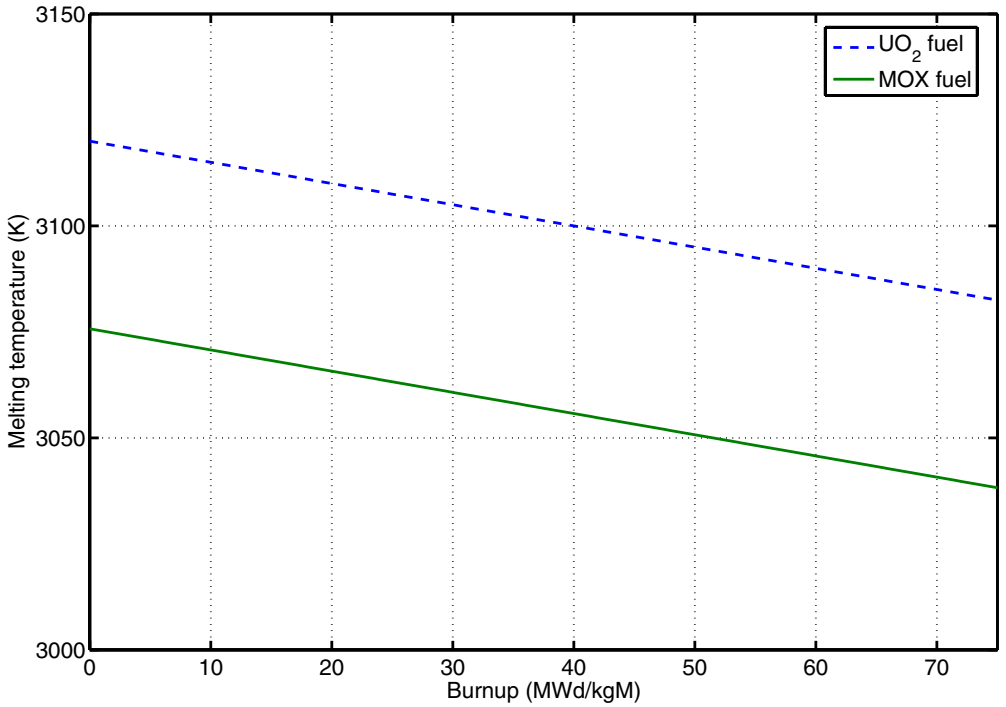

Figure 3.3: Melting temperature as a function of local burnup for UO_2 and MOX fuel, calculated using correlations by Adamson et al. (1985).

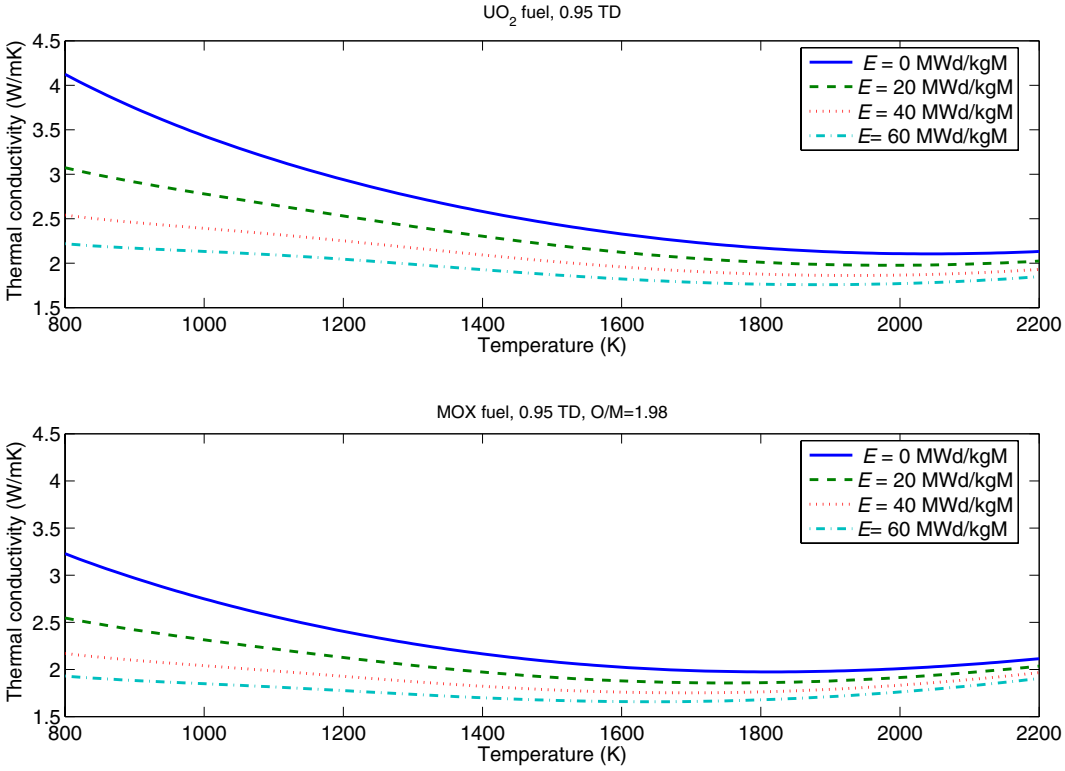

Figure 3.4: Thermal conductivity as a function of temperature at different burnups (E) for UO_2 and MOX fuel, calculated using FRAPCON-3 correlations (Lanning et al., 2005).

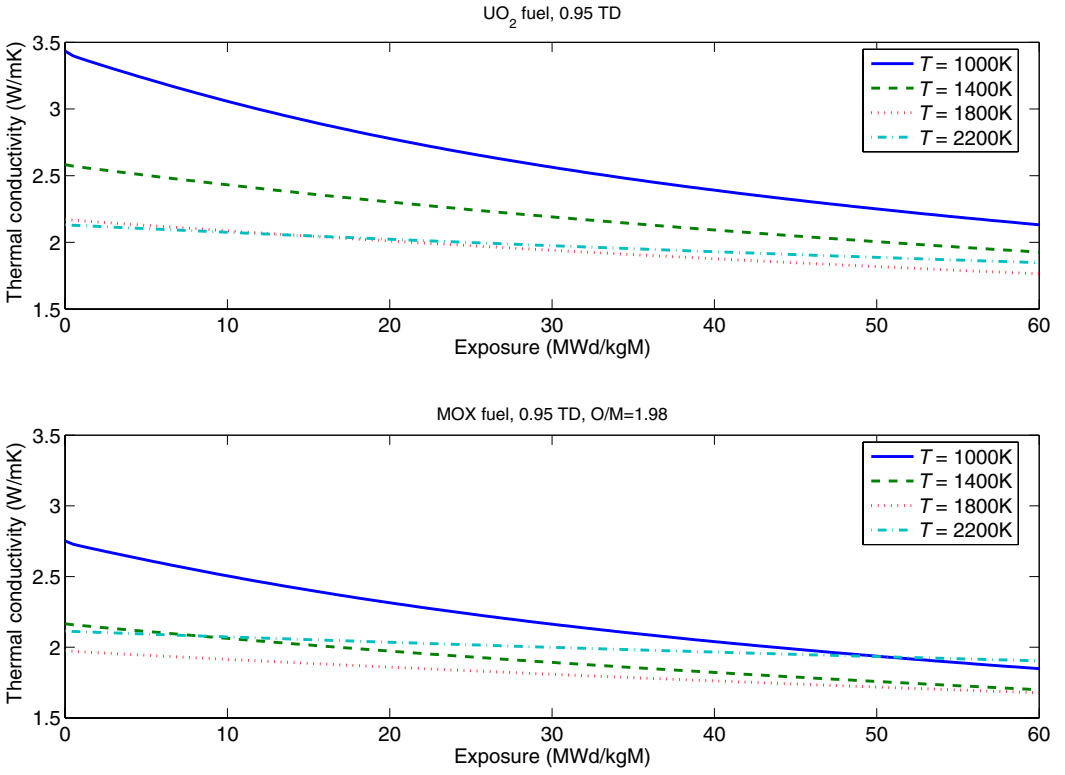

Figure 3.5: Thermal conductivity as a function of exposure (burnup) at different temperatures for UO_2 and MOX fuel, calculated using FRAPCON-3 correlations (Lanning et al., 2005).

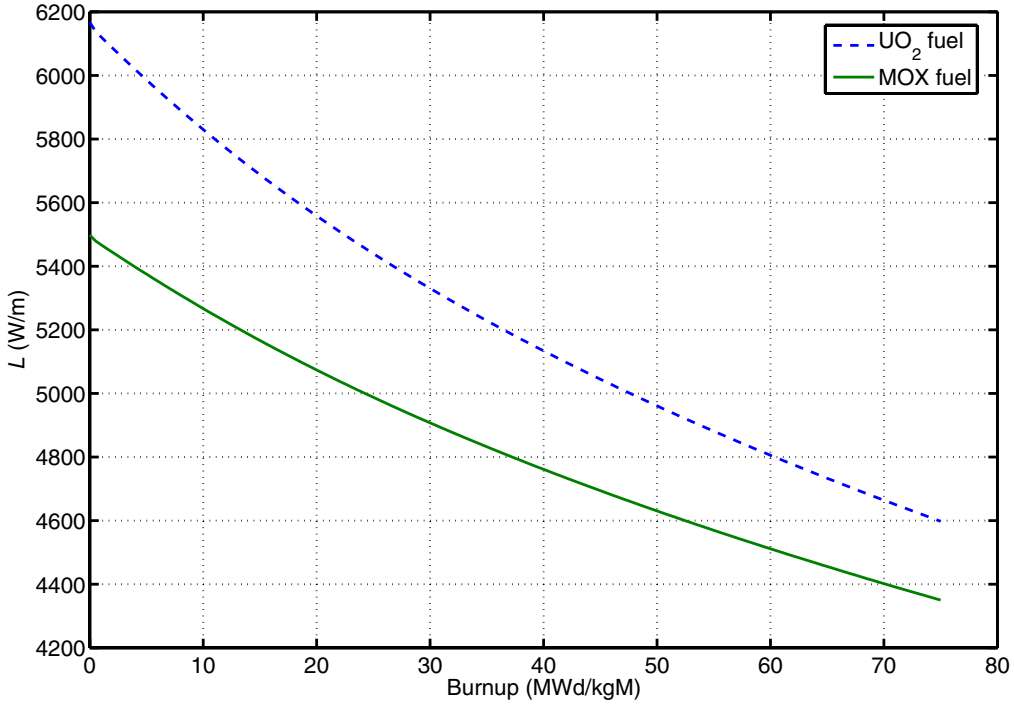

Figure 3.6: The decline of the linear thermal power to melt the fuel pellet centreline with burnup for a 0.95 dense (5% porosity) and O/M=1.98 MOX fuel and equivalent UO_2 fuel.

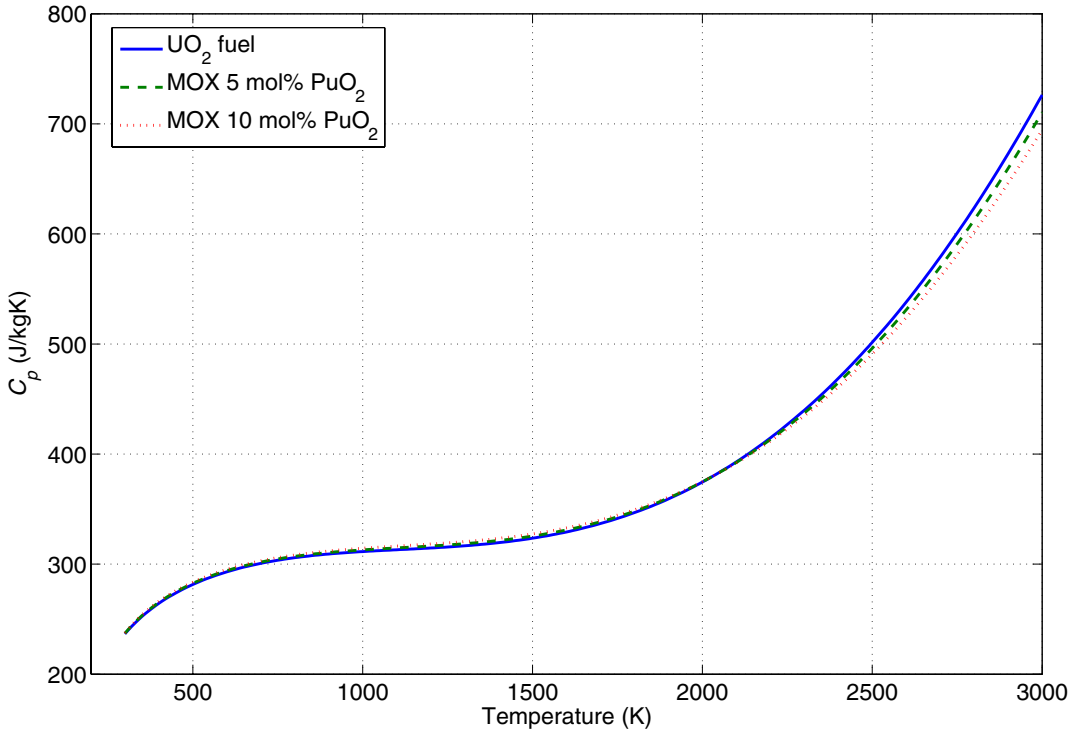

Figure: 3.7 The heat capacity C_p of MOX fuel calculated using the empirical correlations of Fink for UO_2 and PuO_2 and Eq. (3.2).

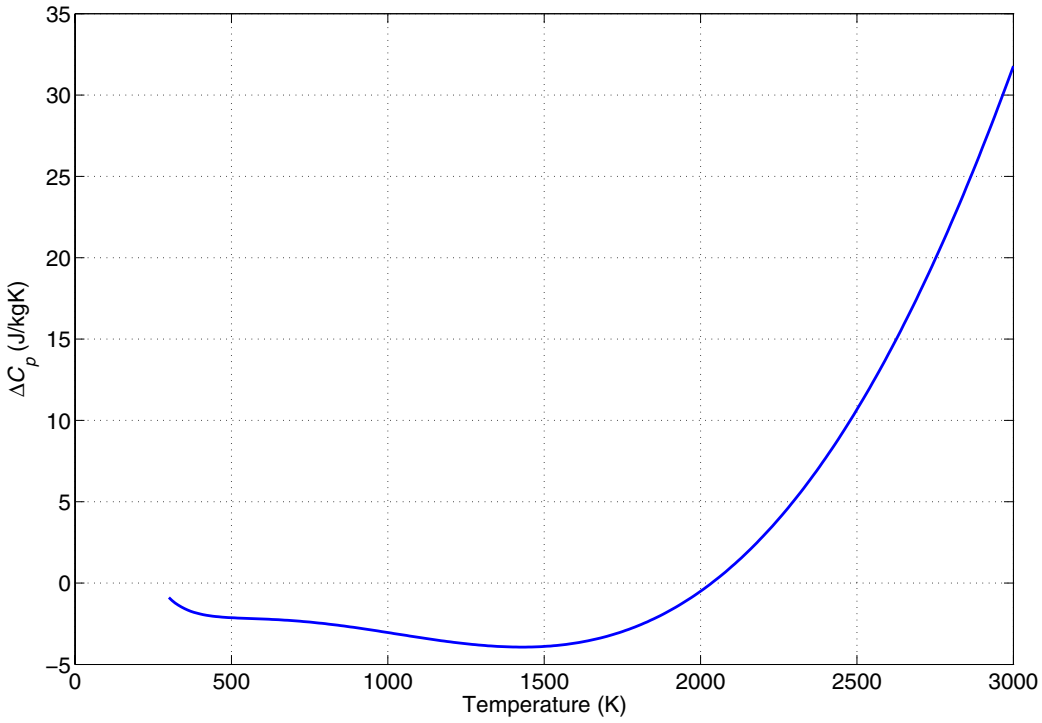

Figure 3.8: The difference between the heat capacity of UO_2 and MOX fuel (10 mol% PuO_2) ΔC_p calculated using the empirical correlations of Fink for UO_2 and PuO_2 and Eq. (3.2).

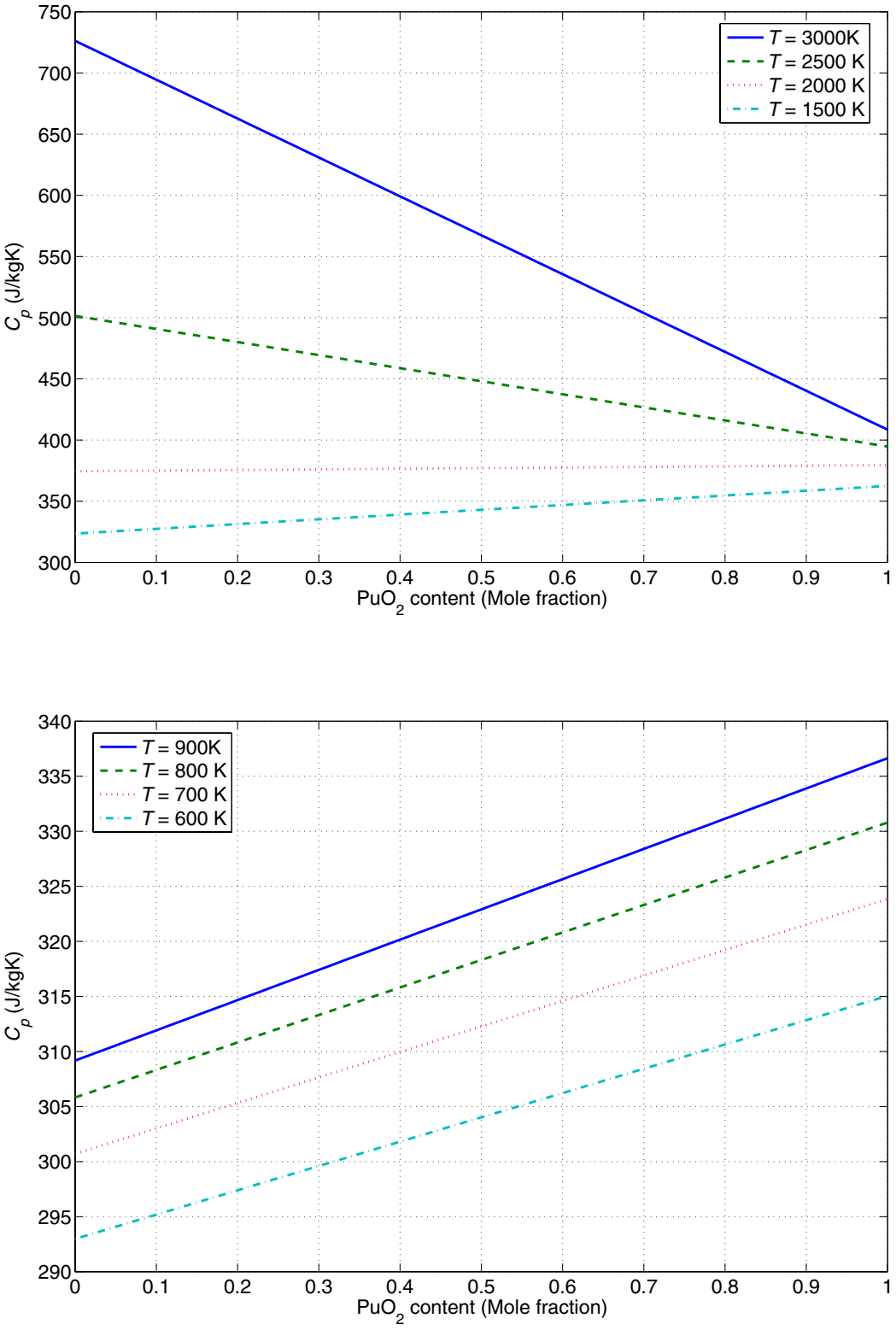

Figure 3.9: The PuO_2 content dependence heat capacity of MOX fuel calculated using the empirical correlations of Fink for UO_2 and PuO_2 and Eq. (3.2) in; high temperature region (upper panel) and low temperature region (lower panel).

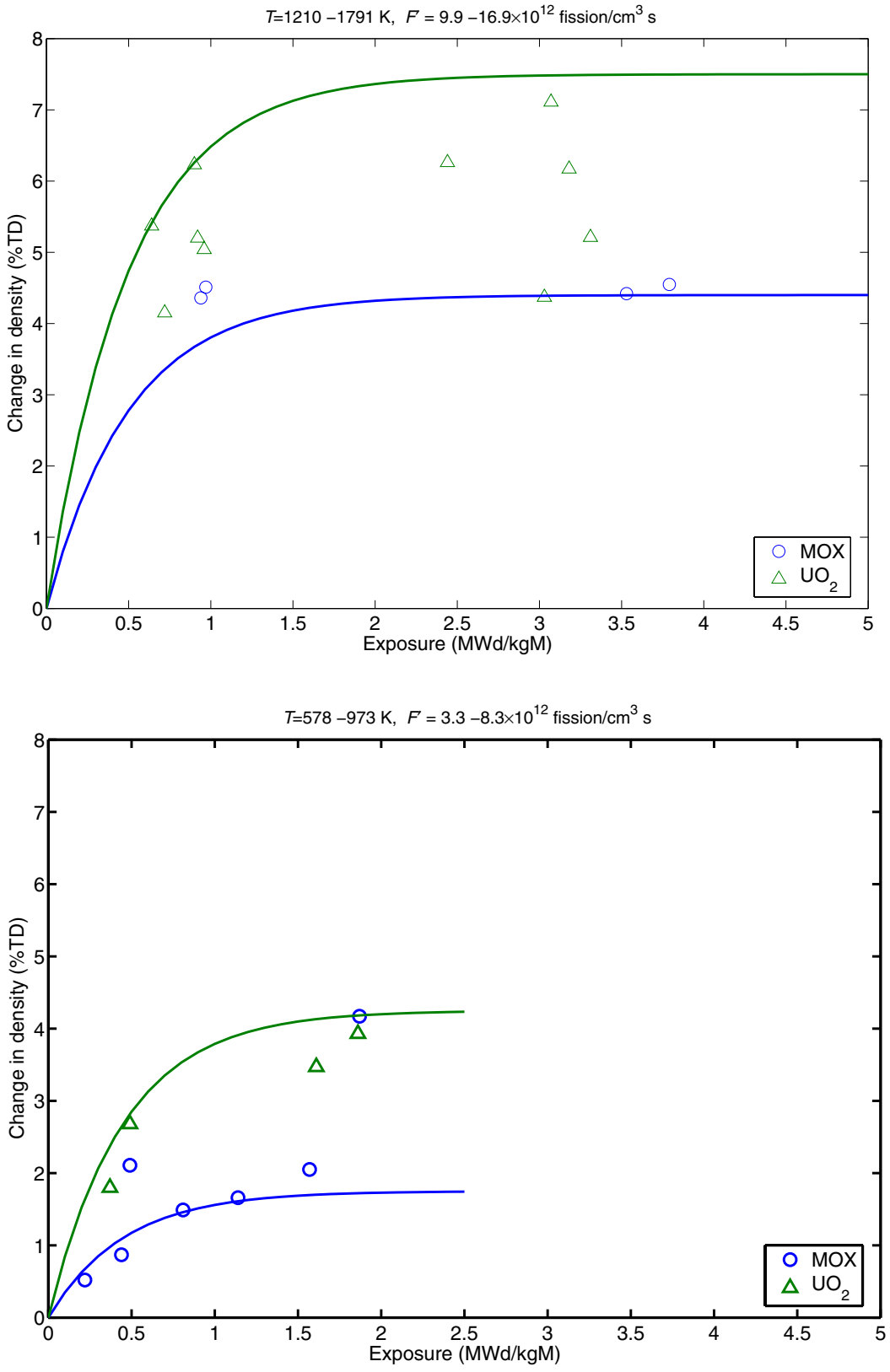

Figure 4.1: The effect of burnup on the densification behaviour of unstable UO_2 and MOX fuels. The symbols are measured values reported by Freshley et al. (1979), while the curves are calculated using the correlation function (4.1). Upper panel: high temperature & high fission rate. Lower panel: Low temperature & low fission rate

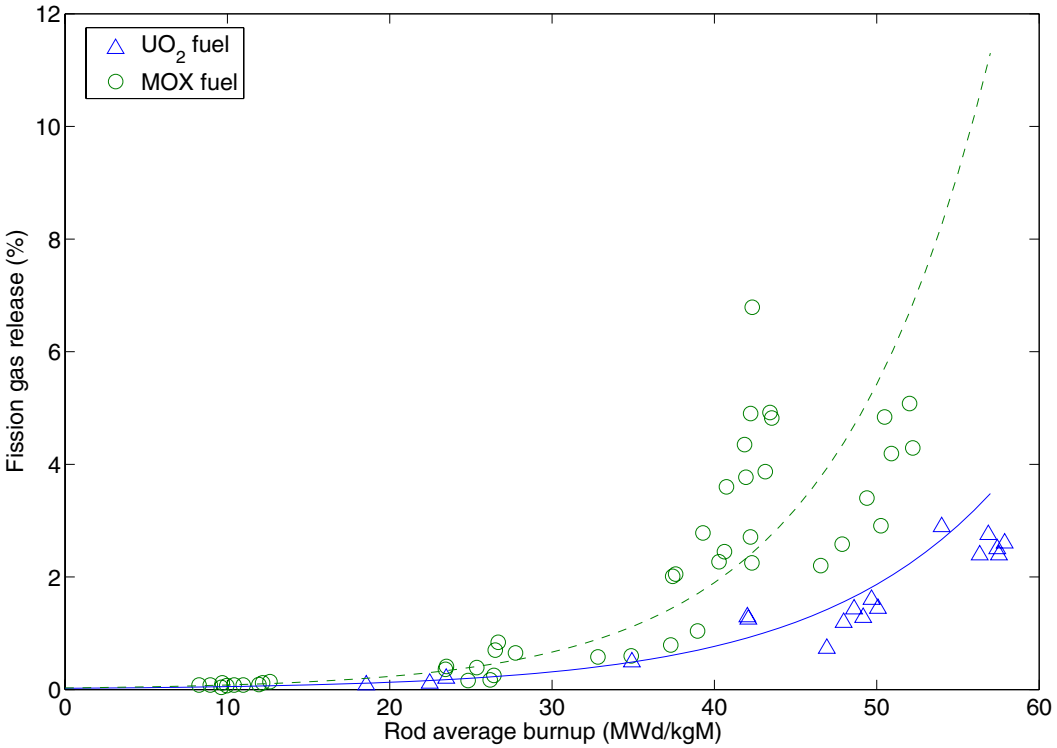

Figure 4.2: Fission gas release fraction as a function of burnup for UO_2 and MOX fuel rods measured in PWRs (Blanpain et al., 2000 and IAEA, 2003). The lines are exponential function fits to the respective data.

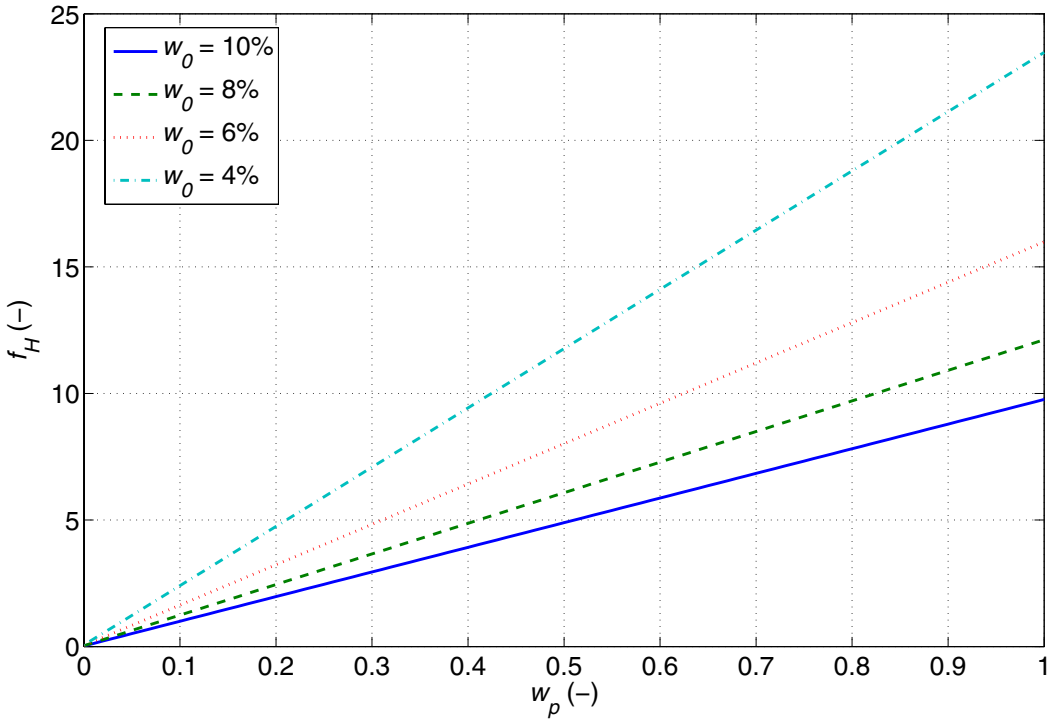

Figure 4.3: Fission rate peaking factor f_H in PuO_2 agglomerates with content w_p for different average PuO_2 concentrations w_0 in MOX fuel, calculated according to equation (4.5).

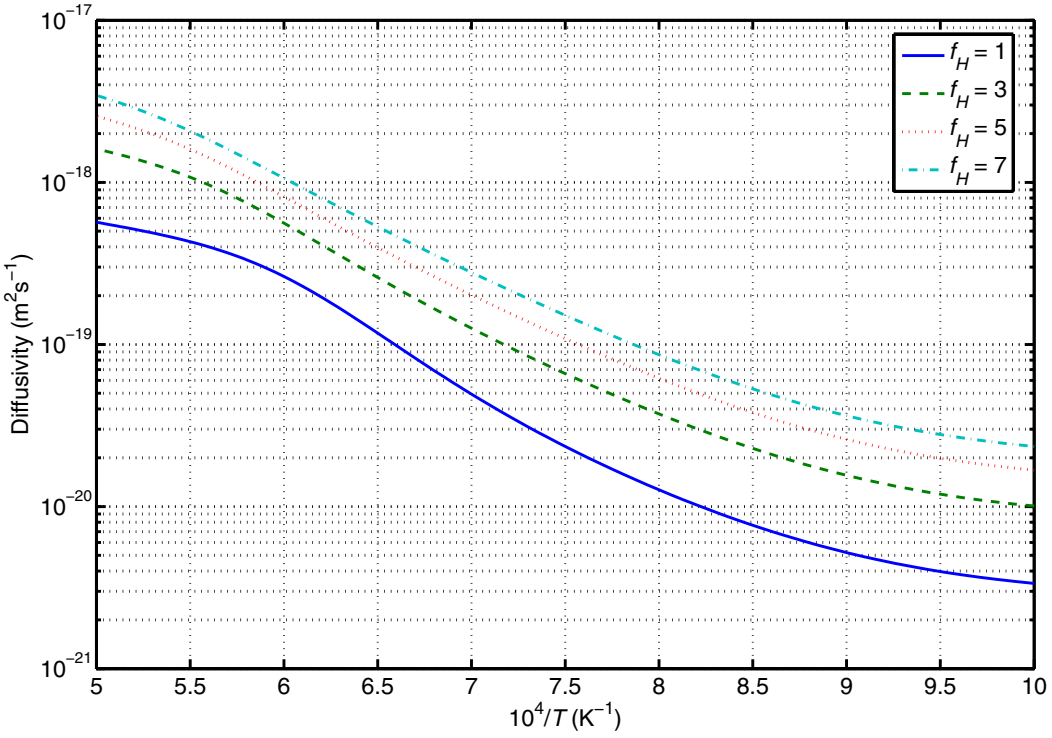

Figure 4.4: Fission gas diffusivity in MOX fuel for different fission rate peaking factors f_H (cf. Fig 4.3) as a function of temperature in the range of 1000 to 2000 K. The fission rate used in this calculation is fixed at $\dot{F} = 1.38\times10^{19}$ fissions/m^3/s.

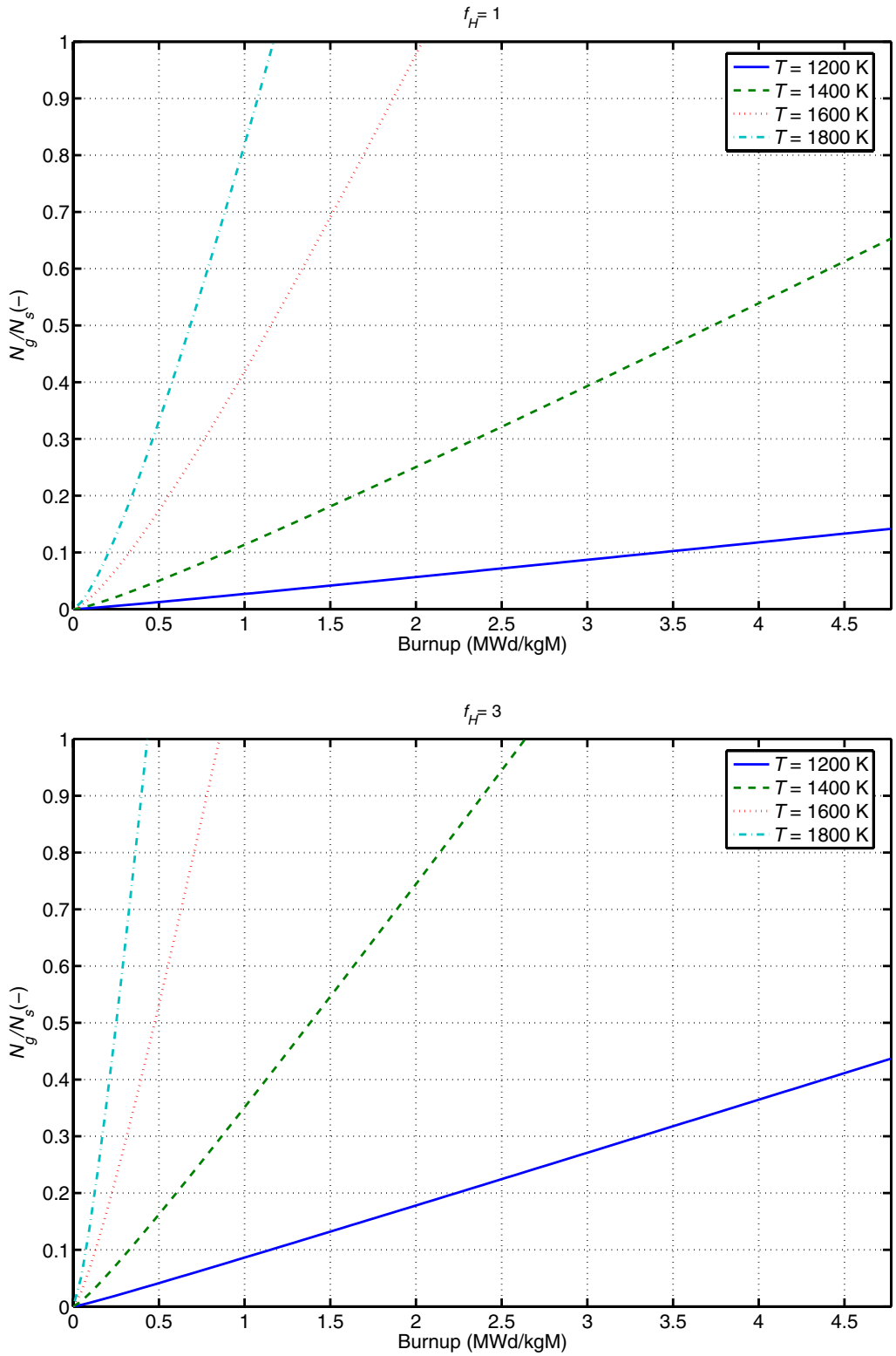

Figure 4.5: Calculated ratio of fission gas density within grain boundary N_g to gas density at saturation N_s at different temperatures versus pellet average burnup. (Top panel) Fission rate peaking factor $f_H = 1$ (UO_2 fuel), (Bottom panel) $f_H = 3$ (MOX fuel).

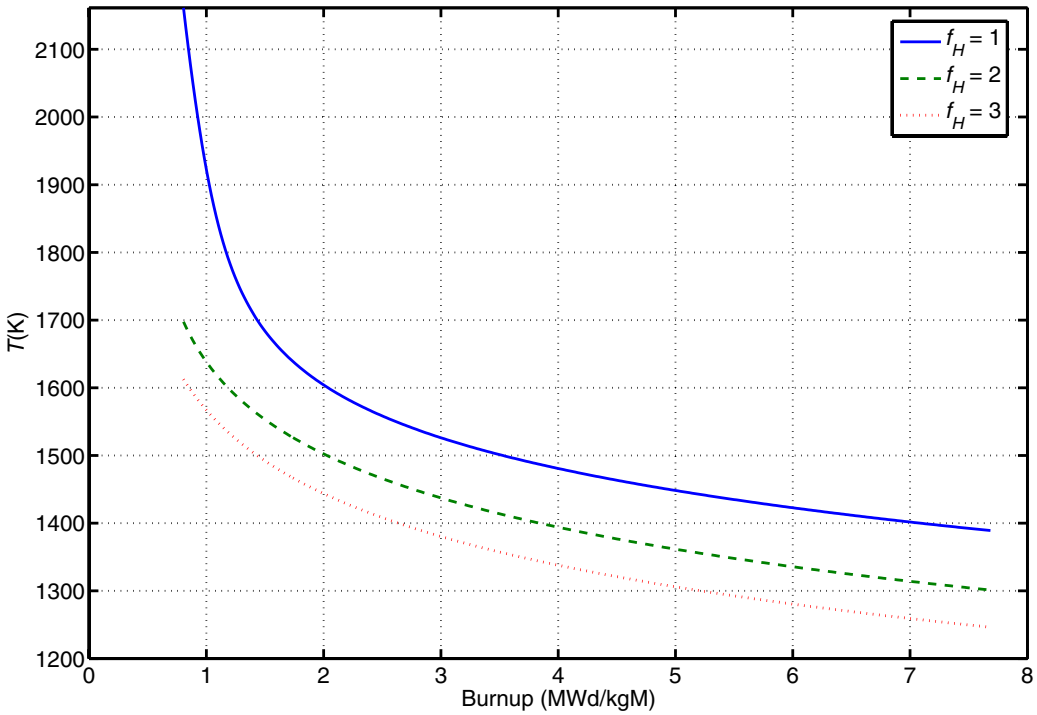

Figure 4.6: Calculated temperature versus burnup for the onset of thermal fission gas release (grain boundary gas saturation, cf. Fig. 4.5) for different fission rate peaking factors f_H (heterogeneity factor, cf. Fig 4.3).

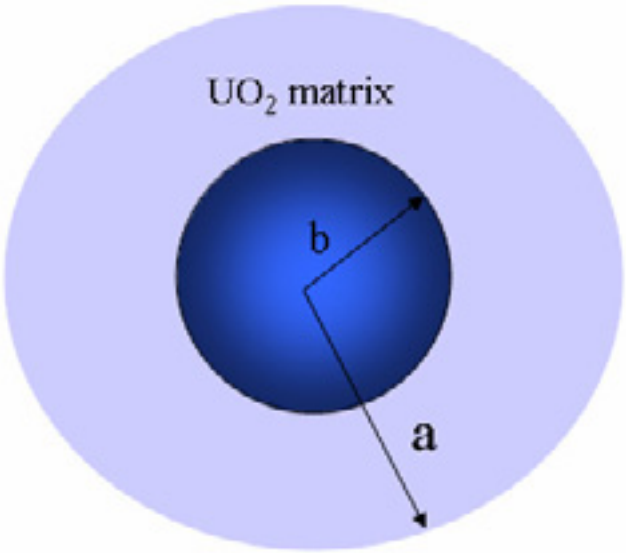

Figure 4.7: Spherical cell model for the PuO_2/UO_2 system. The PuO_2 spot (dark sphere) is embedded in a UO_2 spherical shell (matrix).

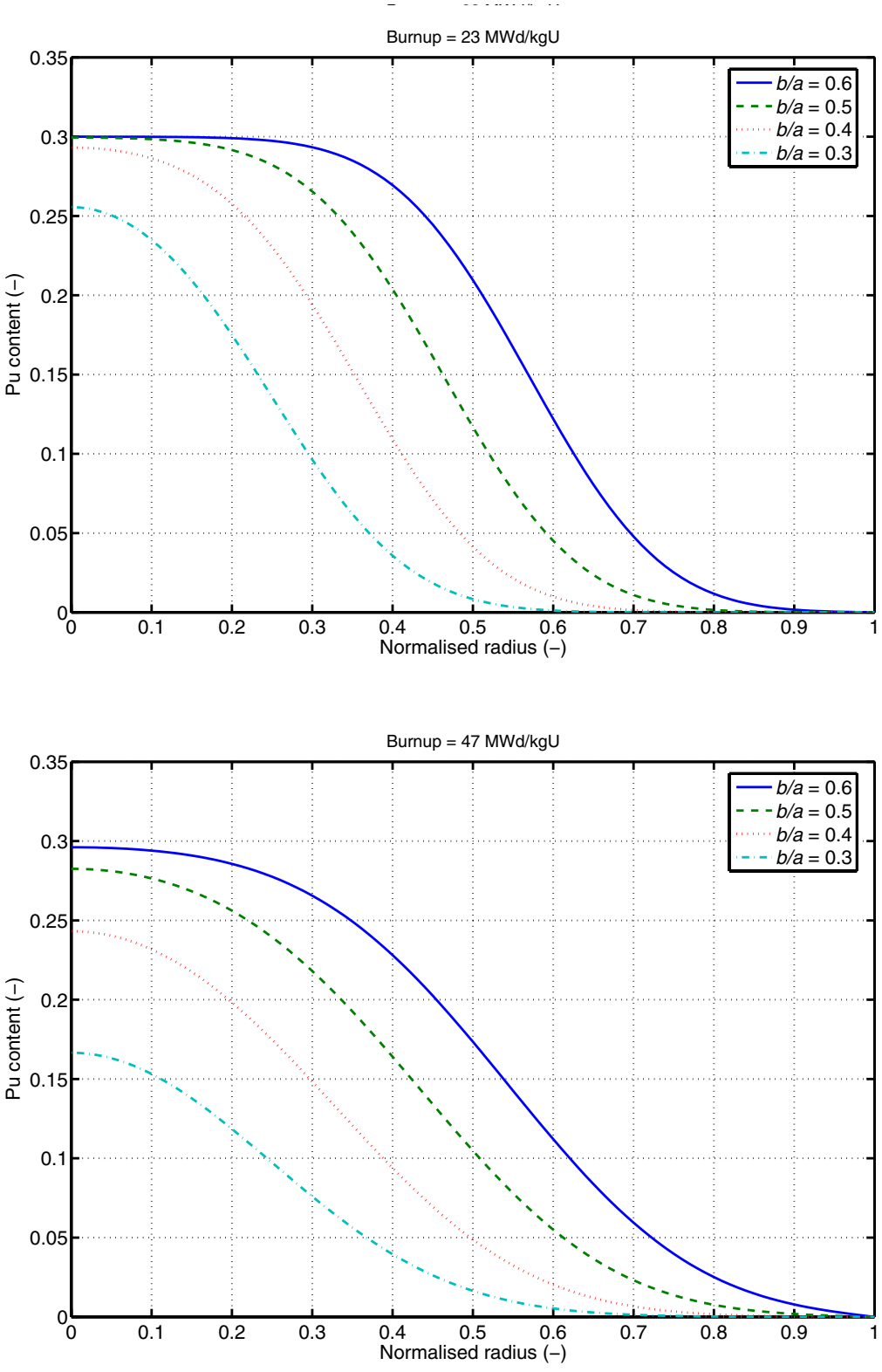

Figure 4.8: Calculation of Pu distribution caused by Pu/U inter-diffusion in MOX fuel with $C_p = 0.30$ *and a=84 μm, using the spherical cell model depicted in Fig. 4.7.*

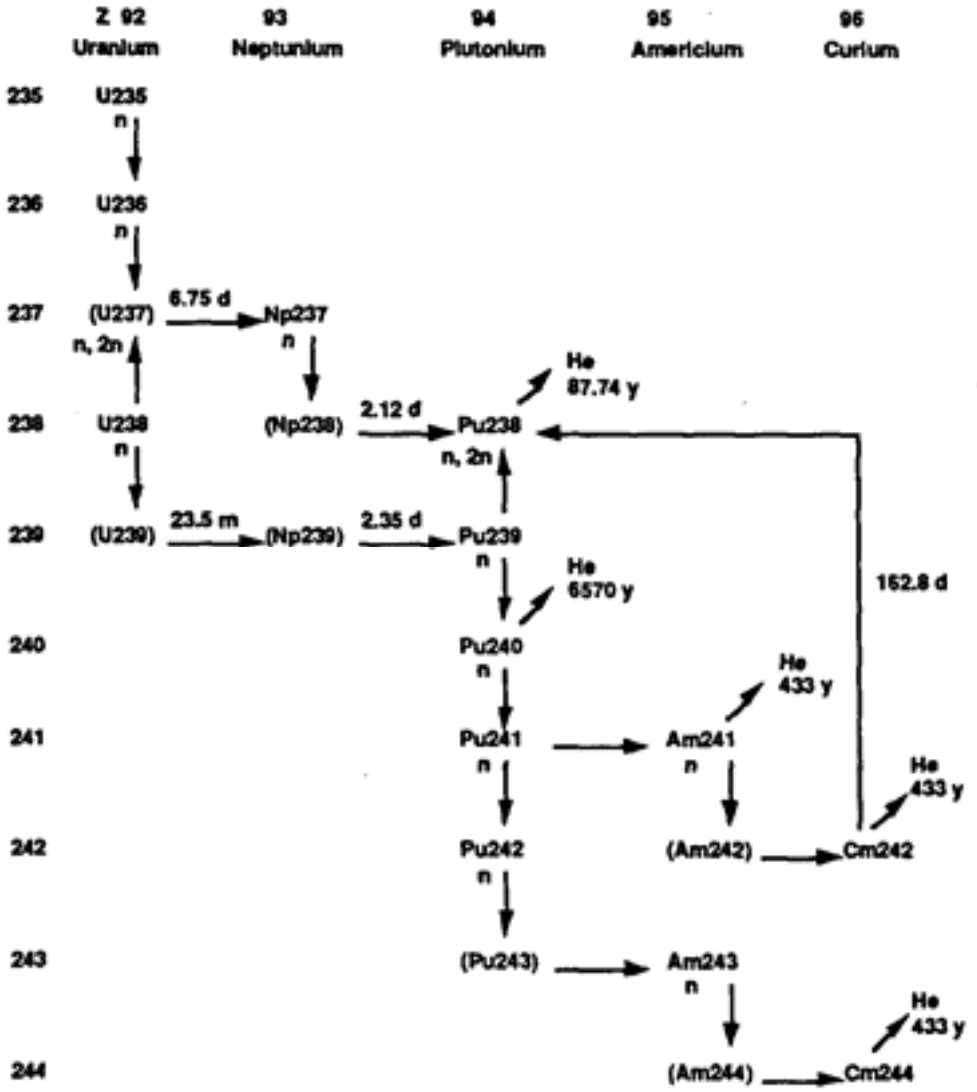

Figure 4.9: Production of helium in nuclear fuel through a chain of actinides.

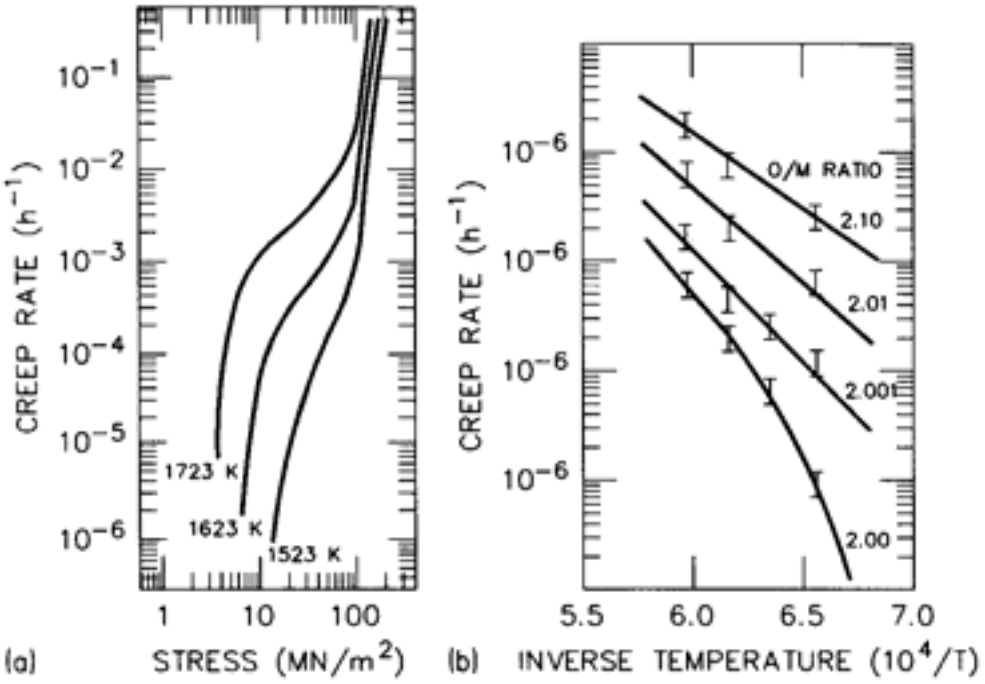

Figure 4.10: Creep rate of UO_2 as a function of stress, temperature and oxygen content. After Burton and Reynolds (1975).

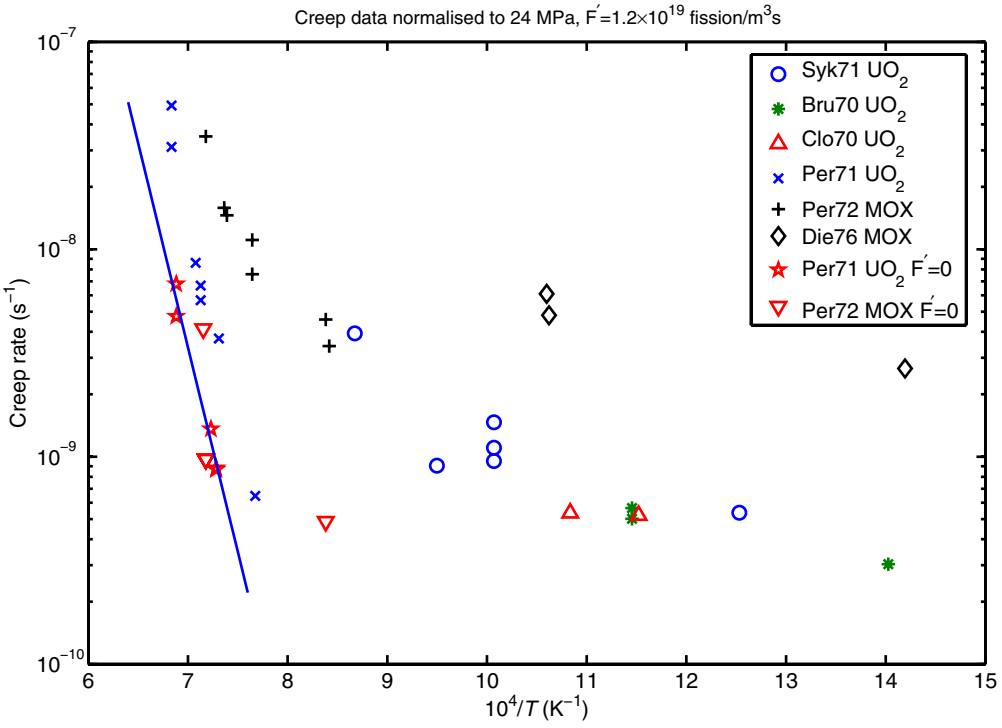

Figure 4.11: Fuel creep data measured directly in various investigations: Syk71 (Sykes & Sawbridge 1971), Bru70 (Brucklacher & Dienst 1970), Clo70 (Clough 1970), Per71 (Perrin 1971), Per72 (Perrin 1972), Die76 (Dienst 1976). The line is an Arrhenius function fit (thermal creep only) to the stars.

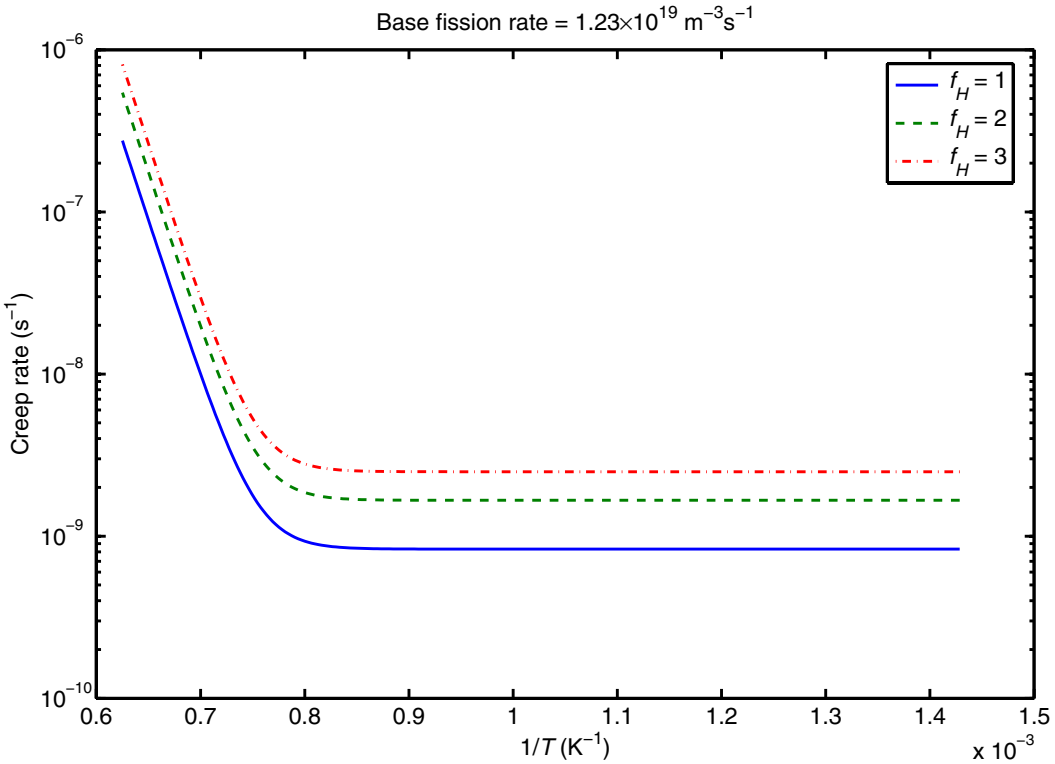

Figure 4.12: Calculation of fuel creep rate using the SRV correlation for the stress level of 24 MPa and base fission rate of 1.23×10^{19} $m^{-3}s^{-1}$ the latter scaled with heterogeneity factors f_H.

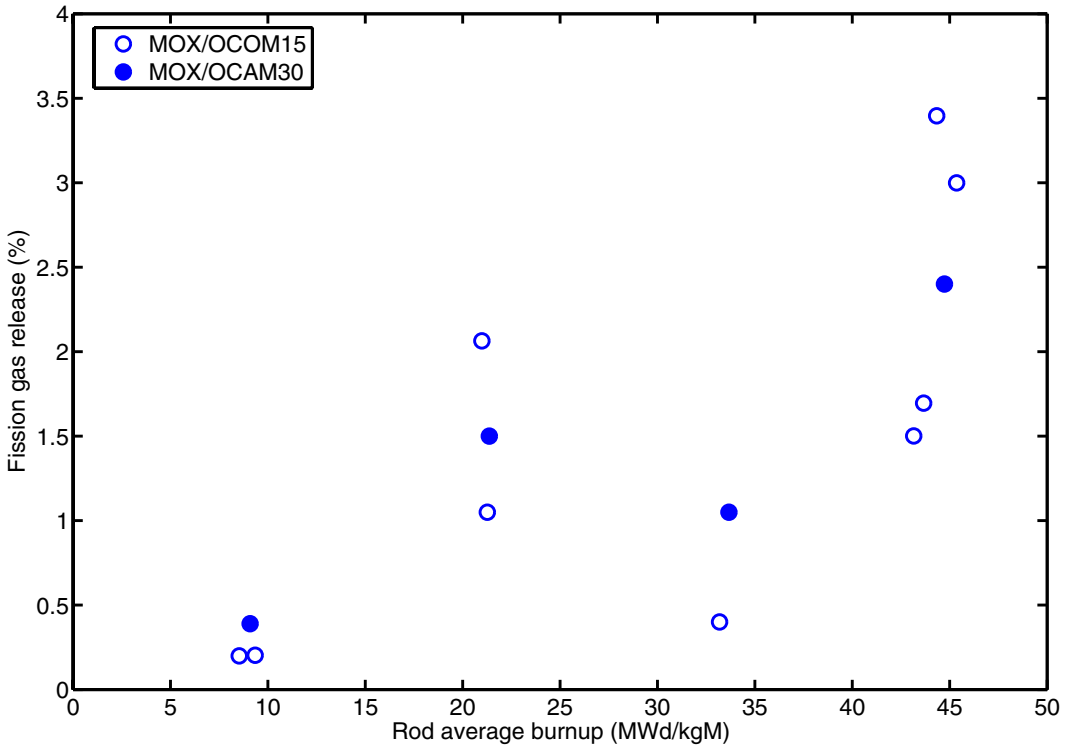

Figure 5.1: Percentage of fission gas release determined by puncturing of MOX/OCOM fuel rods irradiated in a commercial PWR, after Walker et al. (1995).

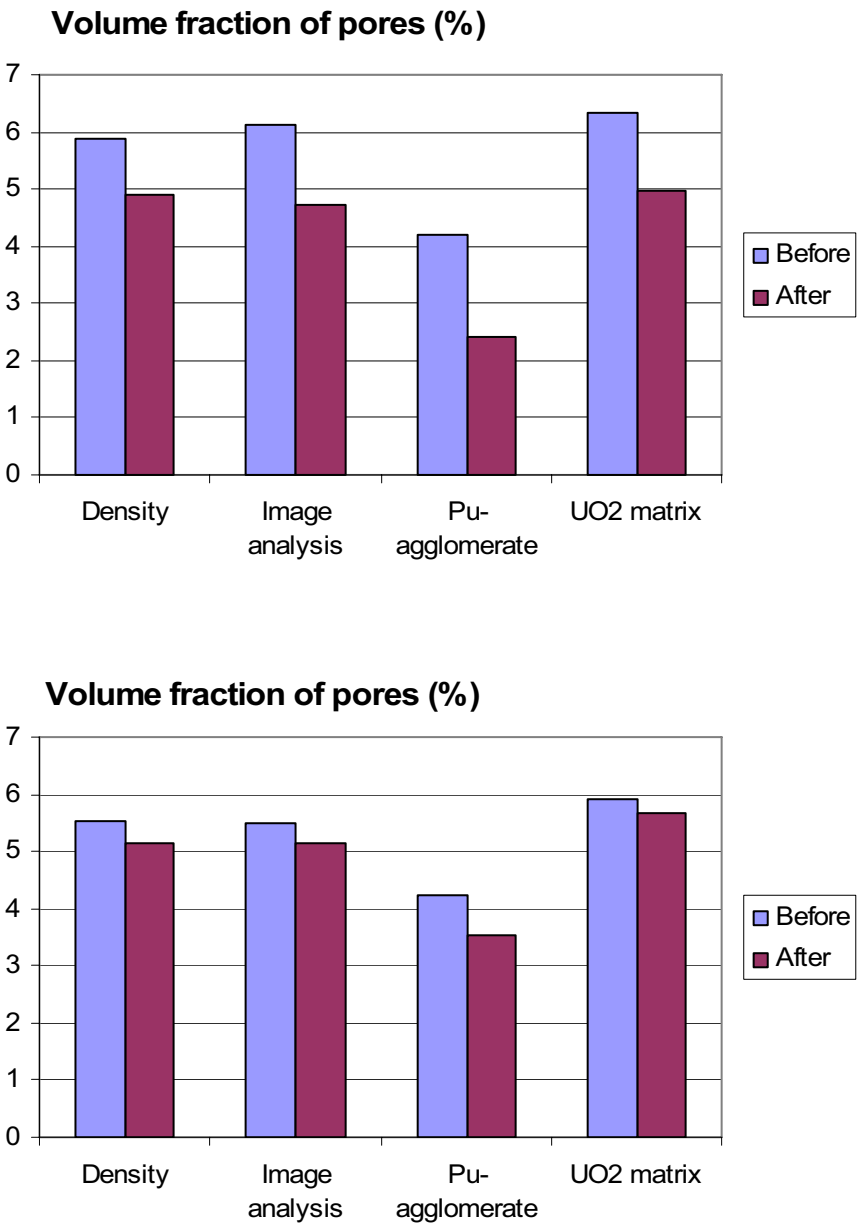

Figure 5.2: Change in volume of pores as a result of densification in MOX/MIMAS fuels: (Upper panel) Before and after irradiation (10 MWd/kg), ADU type fuel, (Lower panel) Before and after sintering (24h/1700 ℃), AUC type fuel. In the abscissa the label Density denotes that measurement is done by hydrostatic density technique, Garcia et al. (2000).

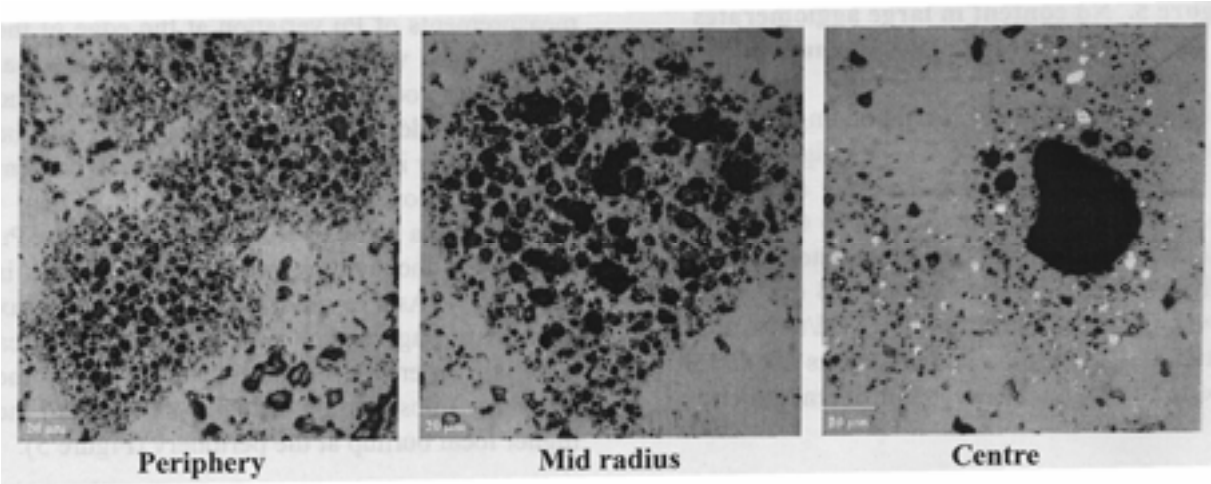

Figure 5.3: Optical micrographs of MIMAS/AUC Pu rich agglomerates across fuel pellet at a pellet average burnup of 55 MWd/kg by Guérin et al. (2000).

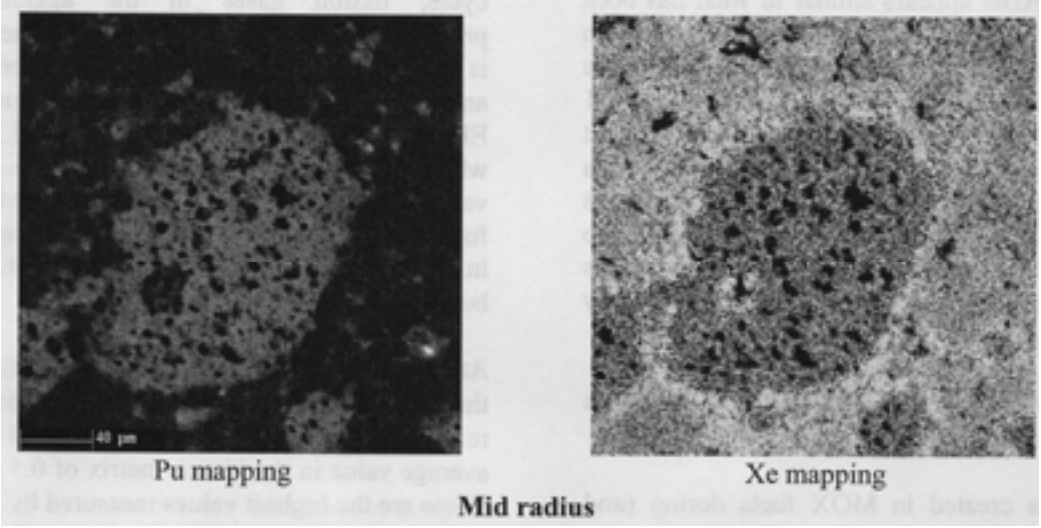

Figure 5.4: X-ray images of MIMAS/AUC Pu rich agglomerates at mid-pellet position at a pellet average burnup of 55 MWd/kg by Guérin et al. (2000). The white lines seen on the Xe mapping demarcate the Pu rich boundary.

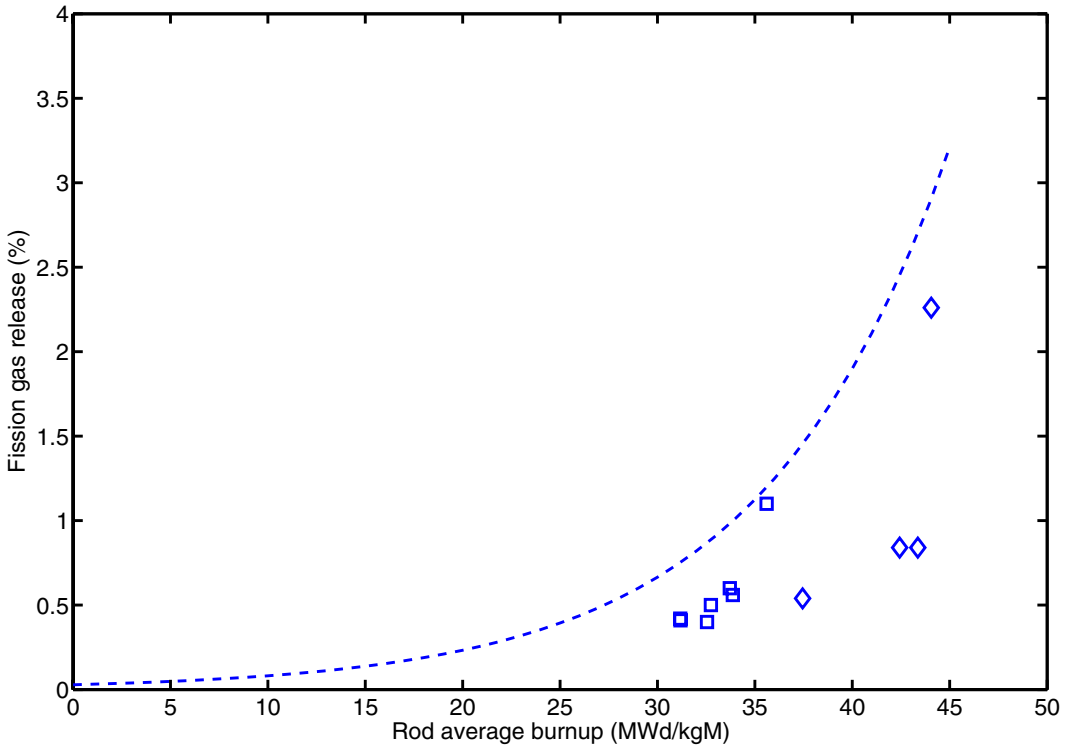

Figure 5.5: Percentage of fission gas release determined by puncturing of MOX/SBR fuel rods irradiated in a commercial PWR, after White et al. (2001) and Cook et al. (2003).The trend line is the correlation fit to MOX/MIMAS fuel presented in Fig. 4.2.

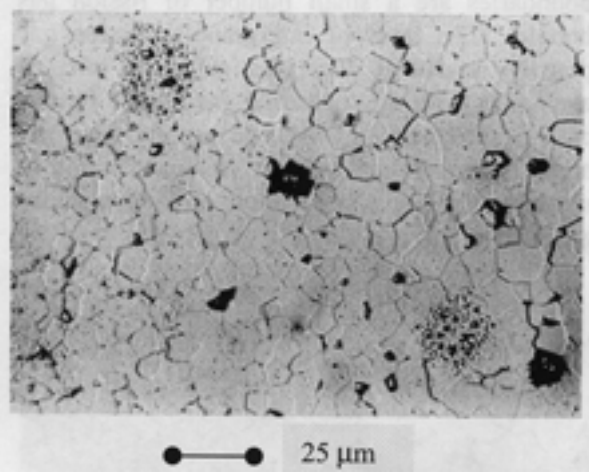

Figure 5.6: Optical micrograph of SBR fuel pellet edge of a rod irradiated in PWR normal operating conditions to a burnup of 35.6 MWd/kg, from Cook et al. (2000). Notice the two dense clusters of pores and fission products, which is a signature of Pu-rich agglomerates in MOX/SBR fuel.

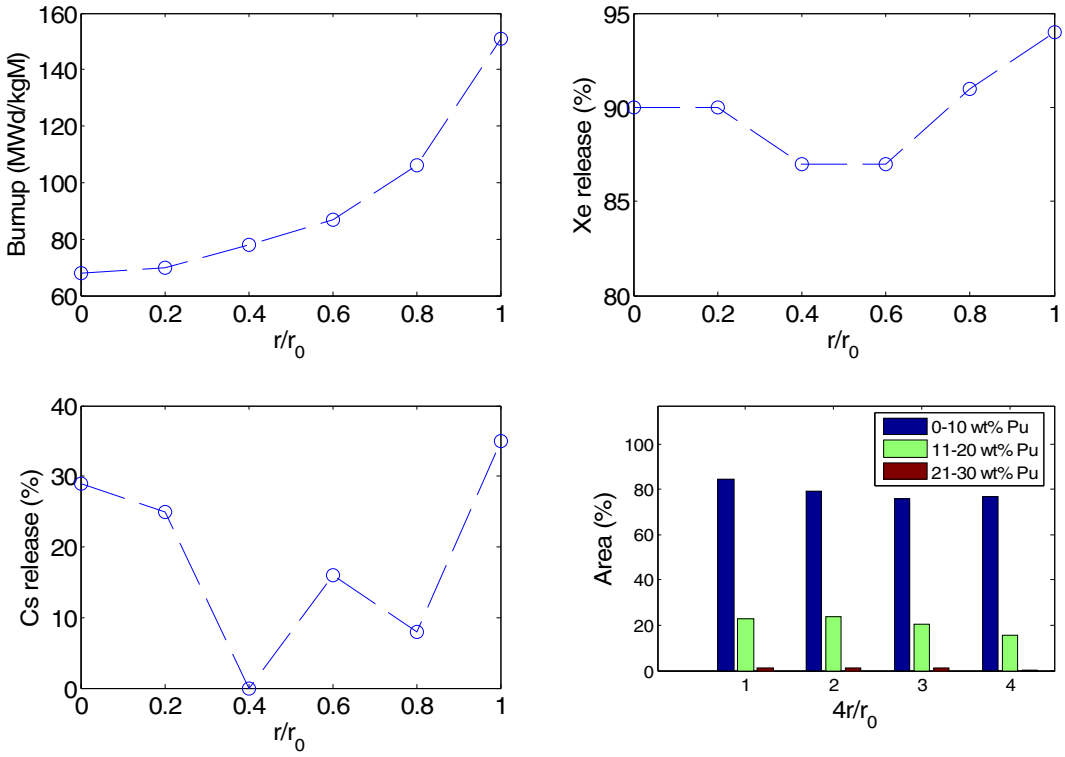

Figure 5.7 Burnup, Xe and Cs release, and Pu content of plutonium rich agglomerates across SBR fuel pellet radius, of a rod irradiated in PWR normal operating conditions to a burnup of 35.6 MWd/kg, after Cook et al. (2000).

REFERENSGRUPP 4 KÄRNBRÄNSLEFORSKNING

Gunnar Rönnberg **OKG Aktiebolag** **Tel: 0491-787686**
E-post: gunnar.ronnberg@okg.sydkraft.se **572 83 OSKARSHAMN** **Fax: 0491-787850**

2 slutrapporter

Björn Andersson **Westinghouse Atom AB** **Tel: 021-**
E-post: bjorn.andersson@se.westinghouse.com **721 63 VÄSTERÅS** **Fax: 021-347733**

Fredrik Winge **Barsebäck Kraft AB** **Tel: ? 046-724459**
E-post: fredrik.winge@ringhals.se **Box 524** **Fax: 046-775793**
246 25 LÖDDEKÖPINGE

Kjell Pettersson **Skeppargatan 84** **Tel:** +46 70 7470677
E-post: kjellp@chello.se **114 59 Stockholm** **Fax: 08-207681**

Håkan Pettersson **Vattenfall Bränsle AB** **Tel: 08-7395328**
E-post: hakan@fuel.vattenfall.se **162 87 Stockholm** **Fax: 08-178640**

Gunnar Wikmark **Studsvik Nuclear AB** **Tel: 0155-221620**
E-post: gunnar.wikmark@studsvik.se **611 82 Nyköping**

SKI –personer (adress SKI , 106 58 Stockholm)

Jan In de Betou
Karen Gott
Jan-Erik Lindbäck

Gustaf Löwenhielm **alla slutrapporter och kallelse**
Lars Skånberg **kallelse**
Lennart Carlsson **kallelse**

www.ski.se

STATENS KÄRNKRAFTINSPEKTION
Swedish Nuclear Power Inspectorate

POST/POSTAL ADDRESS SE-106 58 Stockholm
BESÖK/OFFICE Klarabergsviadukten 90
TELEFON/TELEPHONE +46 (0)8 698 84 00
TELEFAX +46 (0)8 661 90 86
E-POST/E-MAIL ski@ski.se
WEBBPLATS/WEB SITE www.ski.se